OPTIMAL BURNED AREA AND FIRE DETECTION ALGORITHMS USING MODIS AND LANDSAT DATA: CASE STUDY OF UPPER NORTHERN REGION, THAILAND

Suphatphong Ruthamnong

A Thesis Submitted in Partial Fulfillment of the Requirements for the Degree of Doctor of Philosophy in Geoinformatics

Suranaree University of Technology

Academic Year 2016

ขั้นตอนวิธีที่เหมาะสมสำหรับการตรวจจับไฟและพื้นที่ถูกเผาไหม้โดยใช้ข้อมูลโมดิสและแลนด์แซท: กรณีศึกษาบริเวณภาคเหนือตอนบนของประเทศไทย

นายสุภาสพงษ์ รู้ทำนอง

วิทยานิพนธ์นี้เป็นส่วนหนึ่งของการศึกษาตามหลักสูตรปริญญาวิทยาศาสตรดุษฎีบัณฑิต
สาขาวิชาภูมิสารสนเทศ
มหาวิทยาลัยเทคโนโลยีสุรนารี
ปีการศึกษา 2559

OPTIMAL BURNED AREA AND FIRE DETECTION ALGORITHMS USING MODIS AND LANDSAT DATA: CASE STUDY OF UPPER NORTHERN REGION, THAILAND

Suranaree University of Technology has approved this thesis submitted in partial fulfillment of the requirements for the Degree of Doctor of Philosophy.

Thesis Examining Committee

S. Dasananda

(Assoc. Prof. Dr. Songkot Dasananda)

Chairperson

(Assoc. Prof. Dr. Suwit Ongsomwang)

Member (Thesis Advisor)

(Dr. Vivarad Phonekeo)

Member

(Asst. Prof. Dr. Sunya Sarapirome)

Member

(Assoc. Prof. Dr. Sura Pattanakiat)

Member

(Prof. Dr. Sukit Limpijumnong)

Vice Rector for Academic Affairs and Innovation

(Prof. Dr. Santi Maensiri)

Dean of Institute of Science

สุภาสพงษ์ รู้ทำนอง : ขั้นตอนวิธีที่เหมาะสมสำหรับการตรวจจับไฟและพื้นที่ถูกเผาไหม้โดยใช้ข้อมูลโมดิสและแลนด์แซท: กรณีศึกษาบริเวณภาคเหนือตอนบนของประเทศไทย (OPTIMAL BURNED AREA AND FIRE DETECTION ALGORITHMS USING MODIS DATA: CASE STUDY OF UPPER NORTHERN REGION, THAILAND) อาจารย์ที่ปรึกษา : รองศาสตราจารย์ ดร.สุวิทย์ อ๋องสมหวัง, 148 หน้า.

การวิเคราะห์การถดถอยโลจิสติกแบบเรียงลำดับ/ วิธีการตรวจจับไฟและพื้นที่ถูกเผาไหม้ / โมดิส L1B และจุดความร้อนจากโมดิส / แลนด์แซท / ภาคเหนือตอนบนของประเทศไทย

ไฟป่าเป็นปัญหาสำคัญอย่างหนึ่งที่ส่งผลกระทบต่อระบบนิเวศและสุขอนามัยของมนุษย์ ภาคเหนือตอนบนของประเทศไทยเป็นพื้นที่ที่ได้รับผลกระทบอย่างมากต่อการเกิดไฟป่า การศึกษานี้มีวัตถุประสงค์เฉพาะเพื่อ (1) ระบุดัชนีเชิงคลื่นที่เหมาะสมสามอันดับแรกในการประเมินพื้นที่ถูกเผาไหม้ และ (2) ระบุขั้นตอนวิธีที่เหมาะสมสำหรับการตรวจจับไฟและพื้นที่ถูกเผาไหม้ โดยใช้ข้อมูลโมดิสและแลนด์แซท มีระเบียบวิธีวิจัยหลักประกอบด้วย (1) ประเมินดัชนีเชิงคลื่นจากโมดิสที่เหมาะสมในการตรวจจับพื้นที่ถูกเผาไหม้ (2) ระบุขั้นตอนวิธี (algorithm) ที่เหมาะสมในการตรวจจับพื้นที่ถูกเผาไหม้ และ (3) ระบุขั้นตอนวิธีที่เหมาะสมในการตรวจจับไฟ

การระบุดัชนีเชิงคลื่นที่เหมาะสมสามอันดับแรกในการตรวจจับพื้นที่ถูกเผาไหม้ เริ่มจากการคำนวณค่าดัชนีเชิงคลื่นของข้อมูลโมดิส Level 1B (NDVI MSAVI BAI BAIM NBR GEMI MIRBI NDSWIR NDWI NMDI SMI และ CSI) และใช้ค่าข้อมูลดังกล่าวมาเปรียบเทียบกับพื้นที่ถูกเผาไหม้และค่าความรุนแรงของการเผาไหม้ (burn severity) จากข้อมูลแลนด์แซท (Landsat) โดยใช้ค่าเบี่ยงเบน (deviance) จากการวิเคราะห์การถดถอยโลจิสติกแบบเรียงลำดับ ผลการศึกษา พบว่า ดัชนีเชิงคลื่นจากโมดิสในการตรวจจับพื้นที่ถูกเผาไหม้ที่เหมาะสมสามอันดับแรก คือ CSI BAI และ NDSWIR ดัชนีเหล่านี้ถูกนำไปใช้ต่อในการทดสอบขั้นตอนวิธีที่เหมาะสมสำหรับในการตรวจจับพื้นที่ถูกเผาไหม้ โดยใช้เทคนิคการกำหนดค่าขีดแบ่ง (threshold technique) และวิธีต้นไม้การตัดสินใจ (decision tree) พร้อมทั้งประเมินค่าความถูกต้อง (ความถูกต้องโดยรวม สัมประสิทธิ์แคปปาของความสอดคล้อง อัตราการตรวจจับพื้นที่ถูกเผาไหม้ และอัตราการจำแนกเกินจริง) โดยใช้ข้อมูลพื้นที่ถูกเผาไหม้ที่สกัดจากซอฟต์แวร์การจัดทำแผนที่พื้นที่ถูกเผาไหม้ (Burned Area Mapping Software: BAMS) ทั้งนี้ จากการประเมินความถูกต้องและค่าความเชื่อมั่น พบว่า เทคนิคการกำหนดค่าขีดแบ่งโดยใช้ค่าดัชนีเชิงคลื่น BAI จากข้อมูลโมดิส Level 1B เป็นขั้นตอนวิธีที่เหมาะสมในการใช้ตรวจจับพื้นที่ถูกเผาไหม้

การระบุขั้นตอนวิธีที่เหมาะสมสำหรับการตรวจจับไฟ ใช้ข้อมูลจุดความร้อนจากโมดิส (MODIS hotspot) ในปี พ.ศ. 2557 และข้อมูลจุดความร้อนจากโมดิสที่ได้จากการจำแนกโดยใช้ต้นไม้การตัดสินใจจาก 13 ปัจจัย มาทดสอบและประเมินความถูกต้องบนฐานการแปลตีความด้วยสายตา (visual interpretation) จากข้อมูลภาพ Landsat และข้อมูลการสำรวจภาคสนามของกรมป่าไม้ ผลลัพธ์ พบว่า ความถูกต้องของจุดความร้อนจากโมดิสมีค่าความถูกต้องระหว่างร้อยละ 97.49 และ 98.07 ในขณะที่จุดความร้อนจากโมดิสที่ได้จากการจำแนกโดยใช้ต้นไม้การตัดสินใจที่ดีที่สุด โดยใช้ตัวเกณฑ์ 3 ตัว (ระยะห่างจากจุดสำรวจไฟ ความสูงของพื้นที่ และความชัน) มีค่าความถูกต้องระหว่างร้อยละ 62.47 และ 63.84 ดังนั้นจึงสรุปได้ว่าข้อมูลจุดความร้อนจากโมดิส (อัลกอริทึม MOD14/ MYD14) เป็นขั้นตอนวิธีที่เหมาะสมในการใช้ตรวจจับไฟ

จึงสรุปได้ว่าข้อมูลดัชนีเชิงคลื่น BAI จากข้อมูลโมดิส Level 1B สามารถใช้ประเมินพื้นที่ถูกเผาไหม้หลังฤดูไฟป่าได้ ในขณะที่ข้อมูลจุดความร้อนจากโมดิส สามารถประยุกต์ใช้เฝ้าระวังการเกิดไฟป่ารายวัน สำหรับการปฏิบัติงานประจำของหน่วยงานที่เกี่ยวข้องได้

สาขาวิชาการรับรู้จากระยะไกล ลายมือชื่อนักศึกษา____________

ปีการศึกษา 2559 ลายมือชื่ออาจารย์ที่ปรึกษา____________

ลายมือชื่ออาจารย์ที่ปรึกษาร่วม____________

SUPHATPHONG RUTHAMNONG : OPTIMAL BURNED AREA AND FIRE DETECTION ALGORITHMS USING MODIS AND LANDSAT DATA: CASE STUDY OF UPPER NORTHERN REGION, THAILAND. THESIS ADVISOR : ASSOC. PROF. SUWIT ONGSOMWANG, Dr. rer. Nat. 148 PP.

ORDINAL LOGISTICS REGRESSION ANALYSIS / BURNED AREA AND FIRE DETECTION ALGORITHMS / MODIS Level 1B DATA AND MODIS HOTSPOT/ LANDSAT/ UPPER NORTHERN REGION OF THAILAND

Forest fire is one of the serious problems effecting on ecosystem and human health. The Upper Northern region of Thailand is the most affected areas by forest fires. The specific objectives of the study are (1) to identify an optimal top three spectral indices for burned area evaluation; and (2) to identify the algorithms for burned area and fire detection using MODIS and Landsat data. Main components of research methodology consisted of (1) optimum top three MODIS spectral indices for burned area detection evaluation, (2) optimum burned area detection algorithm identification and (3) optimum algorithms for fire detection identification.

For an optimal top three spectral indices for burned area detection identification, MODIS Level 1B data were firstly used to calculate spectral indices, (NDVI, MSAVI, BAI, BAIM, NBR, GEMI, MIRBI, NDSWIR, NDWI, NMDI, SMI, and CSI) and their values were then compared with the extracted burned area and its severity from Landsat data using deviance value of the ordinal logistics regression. As results, it was found that optimum top three MODIS spectral indices for burned area

detection were CSI, BAI, and NDSWIR. These spectral indices were further used to identify optimum burned area detection algorithm using threshold technique and decision tree classification and theirs results were assessed accuracy (overall accuracy, Kappa hat coefficient, burn detection rate and false alarm rate) with the burned areas from Landsat data extraction using Burned Area Mapping Software (BAMS). As results of accuracy assessment and validation, thresholding technique with BAI from MODIS Level 1B spectral index was an optimum algorithm to detect burned area.

To identify an optimal fire detection algorithm, MODIS hotspot data in 2014 and the MODIS hotspot data with decision tree classification with 13 factors were here examined and evaluated accuracy based on visual interpretation of Landsat imageries and ground fire records of Royal Forest Department. The results showed that overall accuracy of MODIS hotspot varied between 97.49% and 98.07%. Meanwhile, MODIS hotspot with the best decision tree classification using three criteria (distance from fire ground survey, elevation, and slope) can provide overall accuracy between 62.47% and 63.84%. Therefore, it can be concluded that MODIS hotspot (MOD14/MYD14 algorithm) was an optimal algorithm to detect forest fire.

In conclusion, BAI from MODIS Level 1B spectral index can be used to estimate burned area after fire season while MODIS hotspot data can be daily applied to monitor forest fire occurrence as routine work of the concerned agencies.

School of Remote Sensing — Student's Signature ____________

Academic Year 2016 — Advisor's Signature ____________

Co-advisor's Signature ____________

ACKNOWLEDGEMENTS

I would like to express my sincere appreciation to Assoc. Prof. Dr. Suwit Ongsomwang, thesis advisor, for his valuable suggestions and critical comments which greatly improved the quality of the work done in this thesis.

I would like to thank Dr. Vivarad Phonekeo, Asst. Prof. Dr. Sunya Sarapirome, Assoc. Prof. Dr. Songkot Dasananda, Assoc. Prof. Dr. Sura Pattanakiat, and Dr. Pantip Piyatassananon and for their guidance and valuable contributions through the progress report discussions.

Thanks to the GISTDA, for providing Landsat 5 TM satellite images of the study area, Forest Fire Control Division, Protected Areas Regional Office 15 (Chiang Rai), and its staffs for providing valuable background information on the forest fire in the study area and experience in the field surveys.

I would also like to thank School of Remote Sensing, Institute of Science, Suranaree University of Technology, for giving the opportunity to pursue a Ph.D. program in Geoinformatics. Moreover, thanks to all my friends in SUT for kindly cooperation on this project.

Thanks are also extended to Kamphaeng Phet Rajabhat University, Assoc. Prof. Suwit Wongboonmak and Asst. Prof. Wallop Thong-on, for giving the opportunity and supporting during the study.

Finally, I wish to thank my parents (Mr. Son Ruthamnong and Mrs. Saengwian Ruthamnong), my daughter, my son, and my wife (Mrs. Wilailak Ruthamnong) for their support and encouragement throughout my study.

Suphatphong Ruthamnong

CONTENTS

Page

ABSTRACT IN THAI I

ABSTRACT IN ENGLISH III

ACKNOWLEDGEMENTS V

CONTENTS VII

LIST OF TABLES XI

LIST OF FIGURES XIV

LIST OF ABBREVIATIONS.. XIX

CHAPTER

I INTRODUCTION.. 1

1.1 Background and significance of the study 1

1.2 Research objectives 4

1.3 Scope of the study 5

1.4 Limitation of the study 6

1.5 Definition of technical terms 6

1.6 Study area 8

1.7 Benefit of the study 11

II RELATED CONCEPTS AND LITERATURE REVIEWS 12

2.1 Planck's law 12

2.2 Wien's displacement law... 13

CONTENTS (Continued)

Page

2.3 Fire spectral signature 14

2.4 MODIS characteristic, algorithm, hotspot and caveat 18

2.4.1 MODIS characteristics 18

2.4.2 MODIS fire detection algorithm 21

2.3.3 Hotspot 29

2.3.4 Caveats of the hotspot 32

2.5 Spectral indices for burned area detection and its algorithm 33

2.5.1 Spectral indices for burned area detection 38

2.5.2 MODIS burned area product and its algorithm 38

2.5.3 LANDSAT burned area extraction and its algorithm 37

2.6 Literature reviews 45

2.6.1 Fire and burned area detection algorithm development and its applications 45

2.6.2 Validation of MODIS hotspot data 51

III RESEARCH METHODOLOGY 53

3.1 Equipment 53

3.2 Research methodology 54

3.2.1 Data collection and preparation 54

3.2.2 Evaluation of the optimal top three burned area spectral indices 62

CONTENTS (Continued)

Page

3.2.3 Development of an optimal burned area and fire detection algorithm 66

3.2.3.1 Development of an optimal burned area detection algorithm 67

3.2.3.2 Development of an optimal fire detection algorithm 70

IV RESULTS AND DISCUSSION 72

4.1 Optimal top three burned area spectral indices evaluation 71

4.1.1 Burned area extraction 71

4.1.2 Burn severity classification 85

4.1.3 Spectral indices calculation 90

4.1.4 Ordinal logistic regression analysis 95

4.1.5 Optimal top three burned area spectral indices identification 98

4.2 An optimum burned area detection algorithm identification 99

4.2.1 Burned area detection algorithm testing using thresholding technique 99

4.2.2 Burned area detection algorithm testing by decision tree classification 106

4.2.3 Optimal burned area detection algorithm identification 108

CONTENTS (Continued)

Page

4.3 An optimal algorithms for fire detection development 112

4.3.1 Fire detection based on MODIS hotspot algorithm 112

4.3.2 Fire detection based on MODIS hotspot with decision tree classification 124

4.3.3 Optimal fire detection algorithm.. 132

V CONCLUSION AND RECOMMENDATIONS 133

5.1 Conclusions 133

5.1.1 Optimal top three spectral indices for burned area evaluation 133

5.1.2 Optimal burned area detection algorithm identification 134

5.1.3 Optimal fire detection algorithm identification 135

5.2 Recommendations 136

REFERENCES 138

CURRICULUM VITAE 148

LIST OF TABLES

Table **Page**

1.1 The statistics of forest fire occurrences in Thailand, year 2012-2014 3

1.2 The statistics of forest fire occurrences in the Upper Northern region of Thailand, year 2012-2014 4

1.3 Area and population in each province of Upper Northern region, Thailand .. 10

1.4 Climate data in 2014 of Upper Northern region of Thailand.......................... 10

2.1 The specification of MODIS sensor 19

2.2 MODIS spectral characteristics 20

2.3 MODIS channels used in fire detection algorithm 24

2.4 The characteristics of selected spectral indices for burned area detection 34

3.1 List of hardware and software.. 53

3.2 List of dataset used for the study 56

3.3 List of used Landsat 5 TM and Landsat 8 OLI/TIRS data............................. 57

3.4 List of used MODIS L1B data 59

3.5 List of 12 selected spectral indices for ordinal logistic regression analysis ... 65

3.6 Confusion matrices for burned area/fire detection and its calculation 68

4.1 Threshold values extraction using supervised training area of two-phase algorithm 76

4.2 Decision tree structure for burned area extraction of no-pair Landsat data 78

LIST OF TABLES (Continued)

Table **Page**

4.3 Area and percentage of burned area for 12 Landsat scenes 78

4.4 Accuracy assessment of burned area extraction in 2014 by BAMS 85

4.5 Area and percentage of burn severity classification 87

4.6 Selected MODIS data according to Landsat data used for burn severity classification 90

4.7 Basic descriptive statistical data of original spectral indices data of 12 MODIS scenes 95

4.8 Basic descriptive statistical data of normalized spectral indices of 12 MODIS scenes 95

4.9 Deviance values of each spectral index and its rank...................................... 97

4.10 Total score value and ranking of spectral indices for optimal top three burned area spectral indices identification... 98

4.11 Descriptive statistics of top three spectral indices over 560 burned grids 100

4.12 Accuracy assessment of burned area detection using thresholding technique with BAI 101

4.13 Accuracy assessment of burned area detection using thresholding technique with CSI... 102

4.14 Accuracy assessment of burned area detection using thresholding technique with NDSWIR 103

4.15 Accuracy comparison of two burned area detection algorithms................... 109

LIST OF TABLES (Continued)

Table **Page**

4.16 Pairwise Z test of Kappa hat coefficient value for burned area extraction between thresholding technique and decision tree classification 109

4.17 Accuracy comparison of two burned area detection algorithms for algorithm validation 110

4.18 Comparison of detected/extracted burn area based on MODIS L1B and Landsat-8 data with three different approaches 112

4.19 Basic statistical data of MODIS hotspot data by year between 2010 and 2014 of Upper Northern of Thailand. 113

4.20 Basic statistical data of MODIS hotspot data by month between 2010 and 2014 of Upper Northern of Thailand 114

4.21 Basic statistical data of MODIS hotspot data by period of time between 2010 and 2014 of Upper Northern of Thailand 114

4.22 Basic Statistic data of MODIS hotspot attribute data 114

4.23 Summary of accuracy assessment of MODIS hotspot 123

4.24 Overall accuracy comparison by various combination biophysical factors of decision tree classification 130

LIST OF FIGURES

Figure **Page**

1.1 Map of the study area 9

2.1 Typical spectral reflectance signatures of pure charcoal, green vegetation and dry vegetation 16

2.2 Spectral signatures of the burned/unburned areas as recorded from the (a) IKONOS (b) ASTER (c) LANDSAT TM and (d) MODIS 17

2.3 The apparent temperature of the pixel at 3.96 μm, as observed by MODIS, for a single fire as a function of the fraction of the pixel covered by the fire and its temperature 22

2.4 Fire pixels detection using MODIS 31

2.5 Burned Area Mapping Software (BAMS) 39

2.6 Flow chart for the burned area mapping section (a) seeds, (b) second stage result, (c) seeds and second stage result superimposed, (d) result. Note that some of the burned areas fulfilling only the second stage criteria are not kept as they do not contain a burned seed 44

2.7 Fire detection process using HJ-IRS 50

3.1 Workflow of research methodology framework 55

3.2 Example of false color composite of MODIS data. 58

3.3 Example of false color composite of MODIS data. 59

LIST OF FIGURES (Continued)

Figure **Page**

3.4 Example of MODIS hotspot distribution over study area: Date 29 March 2014... 61

3.5 Distribution ground fire record by RFD during fire season in 2014............... 61

3.6 Schematic workflow of an optimal top three burned area spectral indices evaluation component. 63

3.7 Schematic workflow of identification algorithm for burned area and fire detection using MODIS data component.. 66

4.1 Appearance of burned area with major land cover in various locations on color composite image of Landsat-8: Band 7, 5, and 3 (RGB)....................... 73

4.2 Development of fire: (a) pre-fire: (25 February 2014), (b) active fire: (13 March 2014), and post-fire: (29 March 2014) 74

4.3 MODIS hotspot data as ancillary data overlaid on Landsat data (13 March 2014) for visual interpretation 74

4.4 Example of burned area extraction using BAMS: (a) small patch and (b) large patch 77

4.5 Multi-temporal burned area comparison between 13 March 2014 and 29 March 2014 77

4.6 Distribution of burned area for 12 Landsat scenes... 79

4.7 Burned area extraction and burn severity with 1 sq.km grid size 86

4.8 Distribution of burn severity for 12 Landsat scenes 88

4.9 Spectral indices from MODIS scene 2014057.0350.005: 26 February 2014 . 91

LIST OF FIGURES (Continued)

Figure **Page**

4.10 Spectral indices from MODIS scene 2014064.0400.005: 5 March 2014 93

4.11 Accuracy assessment and Kappa hat coefficient of burned area detection using thresholding technique with BAI... 104

4.12 Accuracy assessment and Kappa hat coefficient of burned area detection using thresholding technique with CSI 104

4.13 Accuracy assessment and Kappa hat coefficient of burned area detection using thresholding technique with NDSWIR... 104

4.14 Distribution of burned and unburned area detection (a) reference burned area, (b) BAI, (c) CSI and (d) NDSWIR.. 105

4.15 Decision tree structure for burned and unburned areas detection based on spectral indices.. 107

4.16 Distribution of burned and unburned area detection (a) reference burned area and (b) decision tree classification 108

4.17 Distribution of burned and unburned area detection by thresholding technique with BAI spectral index.. 111

4.18 Distribution of burned and unburned area detection by decision tree classification with BAI and CSI spectral indices... 111

4.19 MODIS hotspot distributions, Upper Northern of Thailand: (a) 2010 (b) 2011 (c) 2012 (d) 2013 and (e) 2014... 115

4.20 Distribution of brightness temperature of Band 21/22 from MODIS hotspot Upper Northern of Thailand between 2010 and 2014...................... 116

LIST OF FIGURES (Continued)

Figure **Page**

4.21 Distribution of brightness temperature of Band 31 from MODIS hotspot Upper Northern of Thailand between 2010 and 2014.................................. 116

4.22 Distribution of fire confidence from MODIS hotspot Upper Northern of Thailand between 2010 and 2014 117

4.23 Distribution of fire radiative power from MODIS hotspot Upper Northern of Thailand between 2010 and 2014 117

4.24 Distribution of difference of brightness temperature from MODIS hotspot Upper Northern of Thailand between 2010 and 2014 118

4.25 Distribution of hotspot over Landsat 8 image (a) Scene LC81300472014 088 and (b) scene LC81310472014079 119

4.26 Distribution of fire record by ground survey of RFD over Landsat 8 image (a) Scene LC81300472014088 and (b) scene LC81310472014079 120

4.27 An example of fire record and its attribute by ground survey of RFD 121

4.28 Distribution true and False MODIS hotspot over Landsat image scene, LC81300472014088 122

4.29 Distribution true and False MODIS hotspot over Landsat image scene, LC8 1310472014079... 122

4.30 An example of MODIS hotspot validation by visual interpretation over Landsat data as true hotspot (red colored point) and false hotspot (yellow colored point) in various locations.. 123

LIST OF FIGURES (Continued)

Figure **Page**

4.31 Biophysical factor maps 124

4.32 Optimum decision tree to classify true and false MODIS hotspot using distance from fire ground survey, elevation and slope 129

4.33 True and false hotspot classification using decision tree with three biophysical factors of MODIS hotspot over Landsat scene LC8130047 2014088.. 131

4.34 True and false hotspot classification using decision tree with three biophysical factors of MODIS hotspot over Landsat scene LC8 131047 2014079.. 132

LIST OF ABBREVIATIONS

ASTER	=	Advanced Spaceborne Thermal Emission and Reflection Radiometer
AVHRR	=	Advanced Very High Resolution Radiometer
BAI	=	Burned Area Index
BAIM	=	Burned Area Index Modified
BAMS	=	Burned Area Mapping Software
BT21/22	=	Brightness Temperature in Channel 21 or 22
BT31	=	Brightness Temperature in Channel 31
CSI	=	Char Soil Index
CSIT	=	Char Soil Index Thermal
DEM	=	Digital Elevation Model
DMSP	=	Defense Meteorological Satellite Program
DNP	=	Department of National Park Wildlife and Plant Conservation
DWR	=	Department of Water Resources
EVI2	=	Enhanced Vegetation Index 2
FC	=	Fire Confidence
FIRMS	=	Fire Information for Resources Management System
FRP	=	Fire Radiative Power

ABBREVIATIONS (Continued)

GEMI	=	Global Environment Monitoring Index
GEMI3	=	Global Environment Monitoring Index 3
GIS	=	Geographic Information System
GISTDA	=	Geo-Informatics and Space Technology Development Agency
GPS	=	Global Positioning System
LAADS	=	Level 1 and Atmosphere Archive and Distribution System
LANCE	=	Land Atmosphere Near real-time Capability for EOS
LDD	=	Land Development Department
MASTER	=	MODIS/ASTER airborne
MIR	=	Middle Infrared
MIRBI	=	Mid InfraRed Burn Index
MOD14	=	MODIS Active Fire Product LEVEL 2 TERRA
MYD14	=	MODIS Active Fire Product LEVEL 2 AQUA
MODIS	=	Moderate Resolution Imaging Spectroradiometer
MSAVI	=	Modified Soil Adjusted Vegetation Index
NASA	=	National Aeronautics and Space Administration
NBR	=	Normalized Burn Ratio
NBRT	=	Normalized Burn Ratio Thermal

ABBREVIATIONS (Continued)

NDSWIR	=	Normalized Difference Shortwave Infrared
NDVI	=	Normalized Difference Vegetation Index
NDVIT	=	Normalized Difference Vegetation Index Thermal
NDWI	=	Normalized Difference Water Index
NIR	=	Near Infrared
NMDI	=	Normalized Multi-band Drought Index
NOAA	=	National Oceanic and Atmospheric Association’s
NSEv1	=	NIR-SWIR-Emissivity Version 1
NSEv2	=	NIR-SWIR-Emissivity Version 1
NSTv1	=	NIR-SWIR-Temperature Version 1
NSTv2	=	NIR-SWIR-Temperature Version 2
OLI/ TIRS	=	Operational Land Imager and Thermal Infrared Sensor
REF2	=	MODIS Reflectance in Channel 2
RFD	=	Royal Forest Department
RTSD	=	Royal Thai Survey Department
SAVI	=	Soil Adjusted Vegetation Index
SAVIT	=	Soil Adjusted Vegetation Index Thermal
SMI	=	SWIR-MIR Index
SPSS	=	Statistical Package for the Social Sciences
SUT	=	Suranaree University of Technology

ABBREVIATIONS (Continued)

SWIR	=	Short Wave Infrared
TIR	=	Thermal Infrared
TM	=	Thematic Mapper
USGS	=	United States Geological Survey
UTM	=	Universal Transverse Mercator
VI3	=	Vegetation Index 3
VI6T	=	Vegetation Index 6 Thermal
WGS 1984	=	World Geodetic System 1984

CHAPTER I

INTRODUCTION

1.1 Background and significance of the study

Forest fire is one of the serious problems effecting on ecosystem and human health. In Thailand, forest fires occur annually during the dry season from November to April with its peak in March. Fires, which are mostly classified as surface fire, mainly take place in dry dipterocarps forest, mixed deciduous forest, and forest plantations. Almost all forest fires in Thailand are man-made, primarily started by rural settlers who live in or adjacent to the forests. The main activities that cause forest fires include the gathering of non-timber products, spreading of agricultural debris burning, hunting, and carelessness (Akaakara, 2000). The Upper Northern region of Thailand is the most affected areas by forest fires, both in terms of occurrence statistics and the impact of fire and smoke. In addition, most of the burned areas are a mountainous land and situate nearby neighboring countries, namely Myanmar and Laos. Moreover, it is difficult to assess by ground survey. The statistics of forest fire occurrences between 2012 and 2014 in Thailand and the Upper Northern region are summarized as shown in Tables 1.1 and 1.2, respectively (Department of National Park Wildlife and Plant Conservation: DNP, 2015).

Remote sensing is high-efficient tool for detecting and monitoring forest fires. A large number of studies have demonstrated the value of remote sensing to quantify fire occurrences and the areas affected by fire. Remote sensing provides two principal options to infer on fires including spectral and thermal information. MODIS hotspot has great potential for monitoring fire dynamics because the data freely deliver and nearly real time information from a maximum of four satellite overpasses each day and with a data record that spans more than a decade (Kaufman et al., 1998; Justice et al., 2002; Giglio, Descloitres, Justice, and Kaufman, 2003; Justice et al., 2006; Giglio, 2010) However, hotspots have some caveats such as the textural component of the detection algorithm causes problems with false detections in areas where the canopy cover exhibits strong differences in surface temperatures. Cloud cover obstructs fire detection and may lead to high errors of omission (undetected fires). The size of a particular fire cannot be calculated from hotspot data and no distinction can be made between large fires and small fires. The hotspots do not allow distinguishing, if one or more fires are actively flaming within a pixel on the same day and burned areas cannot be derived from the hotspots (Giglio et al., 2003; Giglio, Csiszar, and Justice, 2006; Miettinen, Langner, and Siegert, 2007; Schroeder et al., 2008; Giglio, 2010; Aragao and Shimabukuro, 2010).

Currently, the use of spectral indices to detect burned area and fire is a well-known method. This method includes the following indices:

(1) Vegetation indices: NDVI (Tucker, 1979), SAVI (Huete, 1988), GEMI (Pinty and Verstraete, 1992), VI3 (Kaufman and Remer, 1994), MSAVI (Qi, Chehbounidi, Huete, Kerr, and Sorooshian, 1994), and EVI2 (Jiang, Huete, Didan, and Miura, 2008);

(2) Thermal spectral indices: NBRT, VI6T (Holden, Smith, Morgan, Rollins, and Gessler, 2005), CSIT, NDVIT, SAVIT (Smith et al., 2007), and NSEv1, NSEv2, NSTv1, and NSTv2 (Veraverbeke, Harris, and Hook, 2011); and

(3) Specific indices for burned area: NDWI (Gao, 1996), MIRBI (Trigg and Flasse, 2001), BAI (Chuvieco, Martín, and Palacios, 2002), NDSWIR (Gerard et al., 2003), NBR (Key and Benson, 2005), BAIM (Martin, Gómez, and Chuvieco, 2005), CSI (Holden et al., 2005), GEMI (Barbosa et al., 2006), NMDI (Wang, Qu, and Hao, 2008), and SMI Index (Veraverbeke et al., 2011).

However, the results of accuracy assessment are significant difference depend on the variation of the study area. In addition, an optimal method is not identified to detect burned area and fire in practice. Therefore, this study aims to evaluate the effectiveness of different spectral indices with assessing burn severity and identify burned area and fire detection using MODIS and Landsat data with a case study of the Upper Northern region of Thailand. The result of the study can enhance the efficiency and compatibility of burned area and fire detection methods. Moreover, it's lead to support the forest fire management in Thailand.

Table 1.1 The statistics of forest fire occurrences in Thailand, year 2012-2014.

Region	2012		2013		2014	
	Number of fires	**Damaged areas (Rai)**	**Number of fires**	**Damaged areas (Rai)**	**Number of fires**	**Damaged areas (Rai)**
1) Northern	2,686	21,397	3,274	31,641	2,793	25,661
2) North-East	844	9,828	1,574	19,622	772	10,984
3) Center and East	311	3,927	355	4,078	438	5,206
4) Southern	154	12,747	54	3,177	204	8,872
Total	**3,995**	**47,899**	**5,257**	**58,516.9**	**4,207**	**50,723**

Note 1 Rai equals 1,600 sq. m.

Source: DNP (2015).

Table 1.2 The statistics of forest fire occurrences in the Upper Northern region of Thailand, year 2012-2014.

Region	2012		2013		2014	
	Number of fires	**Damaged areas (Rai)**	**Number of fires**	**Damaged areas (Rai)**	**Number of fires**	**Damaged areas (Rai)**
1) Chiang Mai	865	6,264	1,361	14,541	937	9,044
2) Mae Hong Son	413	2,499	508	2,955	429	2,919
3) Lamphun	219	1,557	166	1,449	238	1,959
4) Chiang Rai	181	922	98	690	91	905
5) Lampang	242	1,463	310	1,994	375	1,746
6) Phayao	76	317	38	194	36	327
7) Phrae	158	1,470	147	1,011	111	927
8) Uttaradit	48	336	53	316	41	303
9) Nan	29	311	123	1,260	88	972
Total	**2,231**	**15,139**	**2,804**	**24,410**	**2,346**	**19,102**

Note 1 Rai equals 1,600 sq. m.

Source: DNP (2015).

1.2 Research objectives

The ultimate goal of the study is to identify optimal burned area and fire detection algorithms using MODIS and Landsat data. The specific objectives of the study are:

(1) to identify an optimal top three spectral indices for burned area evaluation; and

(2) to identify the algorithms for burned area and fire detection using MODIS and Landsat data.

1.3 Scope of the study

Scope of this study can be summarized as follow:

(1) For an optimal top three spectral indices for burned area evaluation, MODIS Level 1B data (2010-2014) are firstly used to calculate index values (NDVI, MSAVI, BAI, BAIM, NBR, CSI, GEMI, MIRBI, NDSWIR, NDWI, NMDI, and SMI). After that, the calculated spectral index values are then compared with an extracted burned area with their severity from Landsat data in the same date using ordinal logistics regression for deviance values calculation. Finally, minimal deviance values from 12 selected spectral indices are ranked to identify top three spectral indices as optimal spectral indices for burned area detection.

(2) For an optimal burned area detection algorithm identification, MODIS Level 1B data in 2014 are firstly used to extract burned area based on the optimal top three spectral indices using thresholding technique and decision tree classification. All products are used to assess accuracy with the burned areas from Landsat data extraction, RFD fire report, and field survey. The algorithm which provides the best overall accuracy and Kappa coefficient values with pair-wise Z-test is selected as an optimal burned area detection algorithm.

(3) For an optimal fire detection algorithm identification, MODIS hotspot data in 2014 (MOD14/MYD14 algorithm) and the MODIS hotspot data with decision tree are firstly extracted and then overall accuracy are performed based on Landsat data, RFD fire report, and field survey. Herein, ancillary data of 13 biophysical factors include elevation, slope, NDVI, distance from stream, distance from water body, distance from road, distance from village, distance from fire ground survey, distance from agricultural area, distance from shifting cultivation, distance from

evergreen forest, distance from deciduous forest, and distance from degraded forest are used to construct decision tree structure.

1.4 Limitation of the study

Limitation of the study is listed below.

(1) There are many spectral indices for burned area detection. Therefore, the study carefully selected only 12 spectral indices based on the reviewing of the past and present research works.

(2) For MODIS data acquisition, free available data from Level 1 and Atmosphere Archive and Distribution System (LAADS) and Fire Information for Resources Management System (FIRMS) are compiled during fire season between 2010-2014 for burned area and fire detection algorithm identification. At the same time, Landsat data from USGS are downloaded (www.glovis.usgs.gov) at least one dataset per month for burned area and its severity extraction.

(3) For this research, burned area and fire detection are focused on the fire phenomena during the fire season (February to April).

1.5 Definition of technical terms

Definition of technical terms in the study is listed below.

(1) Hotspot or called MODIS hotspot or active fire. It represents locations of fire pixel in 1 km^2, which is flagged by the MOD14/MYD14 fire and thermal anomalies algorithm, in this study the hotspots collected from NASA/LANCE-FIRMS.

(2) Burned area. In the study, burned areas which are disturbed by fire are extracted using two data sources: MODIS and Landsat data. For MODIS data, selected spectral indices are used to calculate and identify burned using two selected techniques (thresholding technique and decision tree). While, Landsat data are used to extract and identify burned area using Burned Area Mapping Software (BAMS).

(3) Burn severity and its classification. Burn severity is here defined as percentage of the identified burned area by Landsat over MODIS grid (1 km). The classifications of burn severity are as follows:

Percentage of burned area within 1 km MODIS grid	Severity classes
0%	None
1-25%	Low
25-50%	Moderate
50-75%	High
75-100%	Very high

(4) An optimal top three burned area spectral indices. The optimal burned area spectral indices are identified based on the ranking of the deviance values using ordinal logistics regression analysis. Herein, the top three ranking indices with minimal deviance values are selected and used as an optimal top three burned area spectral indices.

(5) An optimal burned area and fire detection algorithm. The optimal algorithms are justified based on accuracy assessment and Z statistics pair-wise comparison. For an optimal burned area detection algorithm, the selected spectral indices and their modification are used for these justifications. Meanwhile, MODIS

hotspot and modified MODIS hotspot with decision tree are used to identify an optimal fire detection algorithm.

(6) Fire season. In this study, fire season is here considered between February and April in each year.

1.6 Study area

The study area covers 9 provinces in the Upper Northern region of Thailand, defined by the National Geographical Committee in 1978 with six-region classification system. There are Mae Hong Son, Chiang Rai, Chiang Mai, Phayao, Lam Pang, Lamphun, Phrae, Nan, and Uttaradit provinces. It is located between latitudes 17° 09' 18″ N and 20° 28' 23″ N and between longitudes 97° 20' 36″ E and 101° 02' 26″ E. The elevation ranges from 40 to 2,565 m above mean sea level (Figure 1.1). It covers area of 96,293.05 km^2. In 2014, population is about 6,169,843 (Table 1.3).

Upper Northern region of Thailand is geographically characterized by several mountain ranges, which continue from the Shan Hills in bordering Myanmar and Laos, and the river valleys which cut through them. In the western part, it is bounded by the Salween River and the Mekong in the eastern part. The study site consists of four major basins, namely Ping, Wang, Yom, and Nan, which tributary of the Chao Phraya River, in the central part run from north to south. The basins cut across the mountains of two great ranges, the Thanon Thong Chai Range in the western part and the Phi Pan Nam in the eastern part (Wikipedia, 2014).

The climate is divided into three distinct seasons; summer is from February to April, the rainy season is from May to October, and winter is from November to

January, with cooler winters than the other regions. The statistics of climate data in 2014 show that mean annual temperature is about 26.37 °C, mean relative humidity is about 74.33%, mean pressure is approximately 1,009.43 mbar, annual rainfall is about 1,105.96 mm, and number of rainy days is 122 days (Table 1.4).

A large part of Upper Northern region of Thailand is covered by mountains and hills with forests. Minority ethnic hill tribe villages dotted many parts of the hills. The land use and land cover type in 2011 of Land Development Department (LDD) shows 62.79% covered by forest land, and 21.83% is agricultural land. The majority of forest type is deciduous forest (60.59%) and evergreen forest (34.99%).

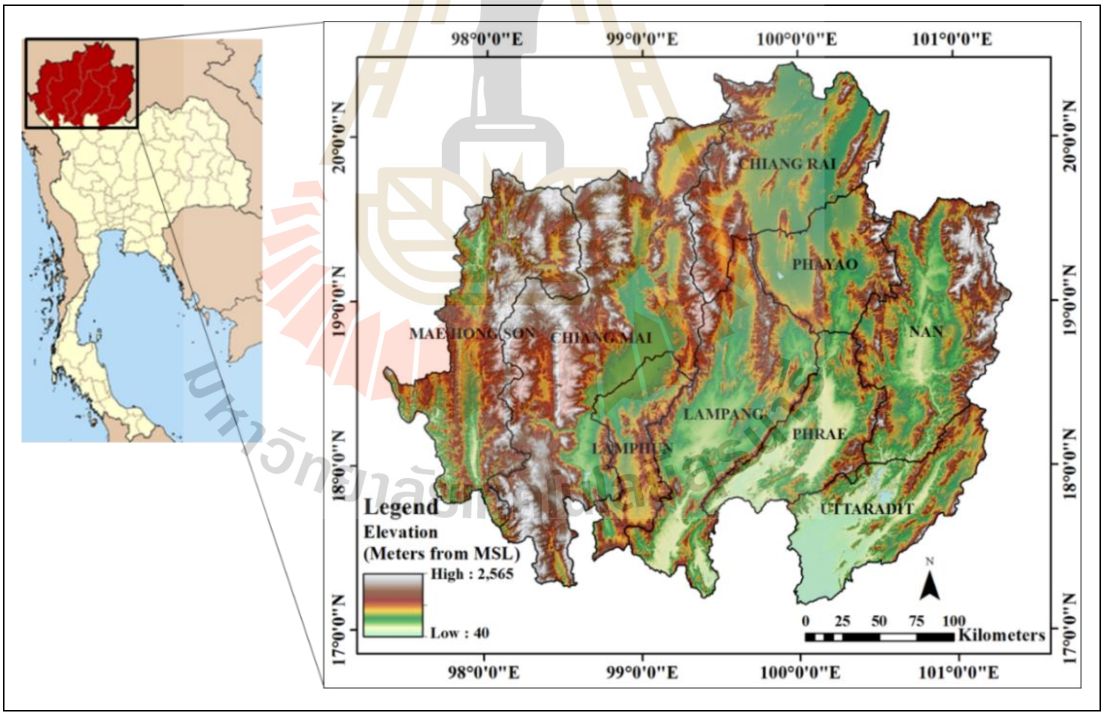

Figure 1.1 Map of the study area.

Table 1.3 Area and population in each province of Upper Northern region, Thailand.

Province	Area (km^2)	Population (31 December 2014)	Population (31 December 2013)
(1) Chiang Mai	22,110.49	1,678,284	1,666,888
(2) Chiang Rai	11,560.21	1,207,699	1,204,660
(3) Lampang	12,524.62	753,013	754,862
(4) Phayao	6,154.05	484,454	486,744
(5) Nan	12,254.60	478,264	477,912
(6) Uttaradit	7,922.38	460,400	460,995
(7) Phrae	6,467.54	454,083	456,074
(8) Lamphun	4,490.51	405,468	405,268
(9) Mae Hong Son	12,808.65	248,178	246,549
Total	**96,293.05**	**6,169,843**	**6,159,952**

Source: Department of Provincial Administration (2014).

Table 1.4 Climate data in 2014 of Upper Northern region of Thailand.

Province	Mean of temperature (celsius)	Mean of relative humidity (%)	Mean of pressure (mbar)	Mean of rainfall (mm)	Number of rainy days (day)
(1) Chiang Mai	26.7	70.0	1,010.0	1,064.4	112.0
(2) Chiang Rai	25.0	76.0	1,009.2	1,470.0	128.0
(3) Lampang	26.7	74.0	1,010.1	1,145.8	110.0
(4) Phayao	25.5	76.0	1,009.2	1,141.5	97.0
(5) Nan	26.5	76.0	1,009.4	1,048.0	114.0
(6) Uttaradit	27.8	72.0	1,009.2	1,224.9	110.0
(7) Phrae	26.6	77.0	1,009.4	1,046.1	112.0
(8) Lamphun	26.5	72.0	1,009.1	788.0	101.0
(9) Mae Hong Son	26.0	76.0	1,009.3	1,024.9	124.0
Average	**26.37**	**74.33**	**1,009.43**	**1,105.96**	**112**

Source: National Statistical Office (2014).

1.7 Benefit of the study

The main benefits of the study can be summarized in the following lists.

(1) To understand in detail of spectral indices for burned areas detection, especially an optimal of spectral indices for burned area detection in Upper Northern region of Thailand.

(2) To obtain optimal algorithms for burned area and fire detection using MODIS and Landsat data in Upper Northern region of Thailand.

CHAPTER II

RELATED CONCEPTS AND LITERATURE REVIEWS

Related theories and concepts include (1) Plank's law, (2) Wien's displacement law, (3) fire spectral signature, (4) MODIS characteristic, algorithm, hotspot and caveat, (5) spectral indices for burned area detection and its algorithm, and (6) literature reviews are described in this chapter.

2.1 Planck's law

Planck's radiation law defines the behavior of the energy emitted by a surface as a function of wavelength and temperature. For any external surface of a body, if its temperature is higher than 0 K or -273.14 °C, it emits electromagnetic radiation in relation to the body temperature and the physical-chemical-geometric characteristics of its surface, while it reflects, absorbs or transmits the electromagnetic radiation coming from an external source. The two main sources of electromagnetic energy are the sun and the earth.

Electromagnetic radiation is defined by wavelength (λ) and radiation frequency (v), they have a inversely proportional relelationship as:

$$\lambda = \frac{c}{\nu}, \tag{2.1}$$

where c is light speed in a vacuum (m.s^{-1}), λ is wavelength (m), and v is radiation frequency (s^{-1}).

The propagation of the light, or electromagnetic radiation can be considered at constant speed in the vacuum space about 300,000 km s^{-1}. The general law of electromagnetic emission was enunciated by Planck in December 1900 as:

$$Q = h\nu, \tag{2.2}$$

where Q is quantum of energy of the radiation (J), h is Plank's constant (6.626×10^{-34} J s), and v is radiation frequency (Gomarasca, 2004).

2.2 Wien's displacement law

According to the Wien's displacement law, the hotter a surface is the peak of its temperature curve shifts to the shorter wavelengths, and the colder a surface is, its peak temperature shifts to the longer wavelengths. Wien's displacement law can be expressed as:

$$\lambda_{max} = \frac{2{,}898}{T}, \tag{2.3}$$

where λ_{max} is the wavelength at which the radiation is maximum, and it is expressed in µm, T is the absolute temperature in Kelvin, and 2,898 is the Wien's displacement constant.

With the help of Wien's displacement formula, it is possible to know the wavelength at which the radiation peaks if the temperature of the blackbody is known (Gomarasca, 2004). For example when the temperature is 750 K (fire condition) then the maximum temperature on applying Wien's displacement law would be at band 3.9 µm. But, if the temperature is 300 K (normal non fire condition) the maximum temperature would be at band 9.7 µm. Therefore, the spectral range 3.9 and 9.7 µm are often used for fires detection.

2.3 Fire spectral signature

Wildfire generates various types of remotely sensed signal as a result of the biomass combustion process. Some fire effects, such as heat and smoke last for relatively short periods of time. Others, like the char residue left on the surface, and especially the altered vegetation structure are more persistent (Pereira, 1999).

(1) Heat

Temperatures of 1,000 K and 600 K can be assumed as representative of typical flaming and smouldering combustion phases of vegetation fires, respectively (Lobert and Warnatz, 1993). According to Wien‘s displacement law, the peak emission of radiance for flames and smouldering surfaces would be located in the middle infrared (MIR), between 3-5 µm. For an ambient temperature of 290 K (17 °C), the peak of radiance emission is located at approximately 10 µm. Fire detection from remote sensing exploits this behavior, and typically relies on some combination of brightness temperature measured in the 3-5 µm and 10-12 µm regions.

(2) Smoke

Biomass burning in wildfires is not fully efficient, due to high fuel moisture, insufficient oxygenation of the reaction zone, inefficient heat transfer, etc. The more efficient phase of flaming combustion yields products such as char (partially oxidized wood) coexists with less efficient smouldering combustion, the phase that takes place behind the active flame front and yields substantial amounts of smoke. Since the objective is to detect and map fire effects at the land surface, smoke is seen as an atmospheric disturbance that interferes with this objective. (Jacob, 1999).

The perturbation caused by smoke aerosol to observation of the land surface from satellite can be quantified calculating the aerosol transmittance, which increases strongly with wavelength. Smoke aerosol transmittance is very low in the visible spectral domain, which becomes inadequate to monitor the land surface when biomass burning emissions are present in the atmosphere in significant amounts. Under such circumstances burned area mapping is better accomplished using near infrared (NIR 0.7-1.2 µm) and shortwave infrared (SWIR 1.4-2.5 µm) spectral data (Justice et al., 2006; Pereira, Mota, Calado, Oliva, and González-Alonso, 2011).

(3) Charcoal

The magnitude and direction of spectral changes caused by the surface charring depends on the condition of the vegetation prior to burning. In ecosystems dominated by herbaceous vegetation (e.g., savannas, steppe, and grasslands), there is a marked annual phenological cycle, and the aboveground plant parts typically are dead and dry at the time fires occur. The major spectral change is a sharp decrease in surface reflectance over the entire 0.4-3.0 µm region, i.e. from bright dry grass to charred soil surface. In contrast, in most forests and shrub lands, the aboveground vegetation is alive and green during the fire season. In this case, the drop in NIR reflectance tends to be smaller than in savannas, steppes, and grasslands. Spectral reflectance changes in the SWIR are more complex, because tall, dense vegetation is dark and replacing this kind of land cover by a charcoal layer may not darken the surface much further. When a bright soil background is exposed as a result of the fire-induced erosion, SWIR surface reflectance may display a small increase (Pereira et al., 2011). Spectral signatures of charcoal, green vegetation, and dry vegetation is shown in Figure 2.1.

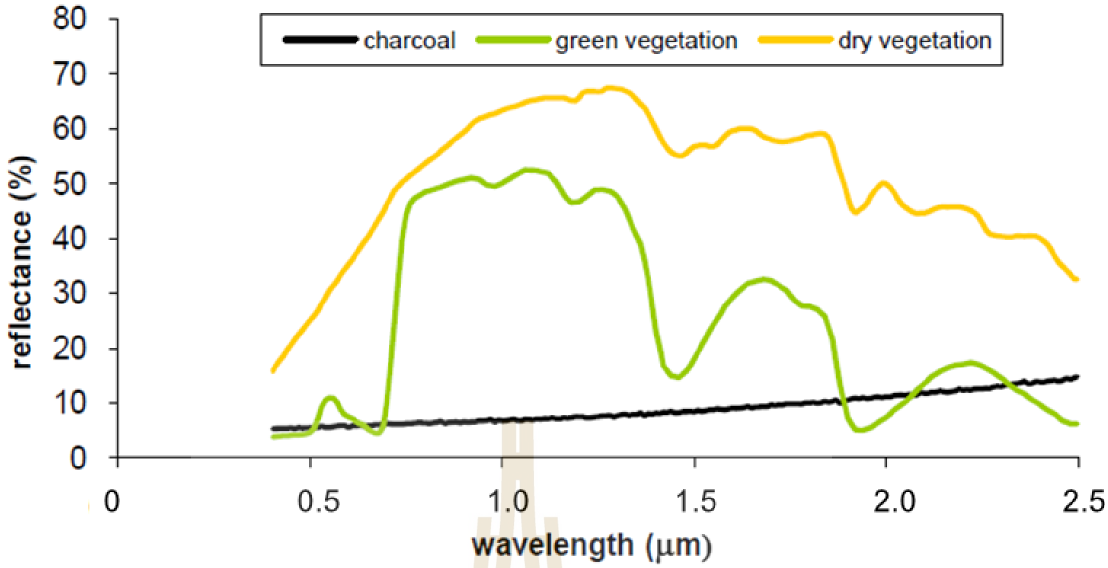

Source: Pereira et al. (2011).

Figure 2.1 Typical spectral reflectance signatures of pure charcoal, green vegetation and dry vegetation.

(4) Burned area

Fire alters the vegetation structure by consuming leaves, twigs and fine branches. The resulting spectral changes last longer than those caused by the deposition of ash and charcoal. Persistence of the burned area signal is a function of vegetation type, net primary productivity and plant succession dynamics, and may range from a few weeks in tropical grasslands to decades in boreal forests. Modifications of the three dimensional structure of vegetation affects its shading pattern, while consumption of photosynthetically active plant parts eliminates the greenness signal. The soil background exposed by vegetation removal will also contribute to the overall spectral signal of the fire burned area (Pereira et al., 2011).

In the visible area of spectrum (0.4-0.7 μm) a multispectral behavior of burned areas can be seen depending on the type of the affected vegetation, severity of burning, and others. A strong decrease in reflectance of burned surfaces is observed in near infrared (0.78-0.90 μm). The destruction of the leaf cell structure, which reflects large quantities of the incident solar radiation, is responsible for the reduction of the spectral signal of burned surfaces. In contrast, an increase in reflectance of burned surfaces is observed in middle infrared because of the water content (Koutsias, Pleniou, Nioti, and Mallinis, 2010). The spectral signatures of the burned and unburned areas as recorded from the difference sensor are shown in Figure 2.2.

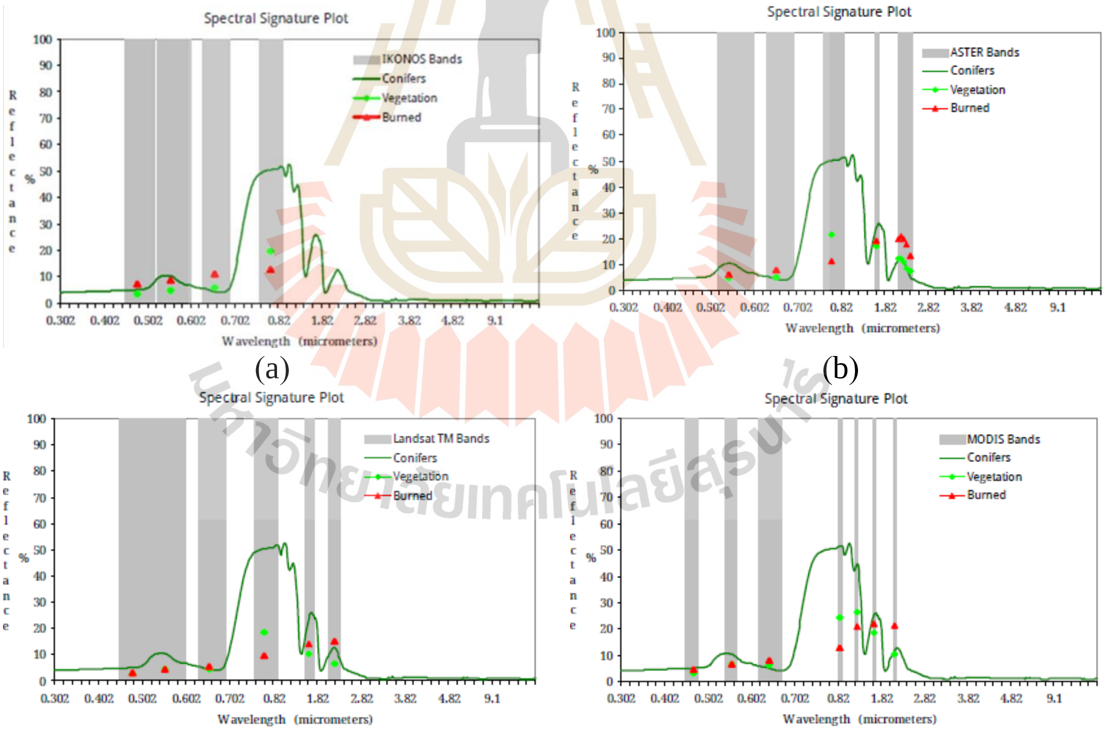

(c) (d)

Source: Koutsias et al. (2010).

Figure 2.2 Spectral signatures of the burned/unburned areas as recorded from the (a) IKONOS (b) ASTER (c) LANDSAT TM and (d) MODIS.

2.4 MODIS characteristic, algorithm, hotspot and caveat

There are a number of satellite instruments that have been used to detect fires from space. Among these are the visible and low light sensors of the Defense Meteorological Satellite Program (DMSP), the Advanced Very High Resolution Radiometer (AVHRR) onboard the National Oceanic and Atmospheric Association's (NOAA) satellites, the visible and infrared spin-scan radiometer on board the Geostationary Operational Environmental Satellite (GOES), the thematic mapper on board the Landsat satellites, and more recently the Moderate Resolution Imaging Spectroradiometer (MODIS) sensor onboard the NASA's Earth Observation Satellites (EOS). In this study characteristic of MODIS and its application in fire detection is here emphasized.

2.4.1 MODIS characteristics

The MODIS instruments on board AQUA and TERRA provide global coverage of the Earth's surface in high radiometric sensitivity (12 bits). Data collected from the MODIS instruments span over 36 spectral bands, ranging from the visible (0.4 μm) to the long wave infrared (14.4 μm). The MODIS design combines high resolution data from the visible and near infrared channels (250-500 m) with the moderate resolution of its infrared channels (1 km). MODIS is the first sensor that included fire monitoring capabilities in its design. Up to date MODIS is one of the most important data sources for global mapping of both fire locations and burned areas. MODIS sensors are mounted aboard two satellites, the Terra spacecraft launched in December 1999 and the Aqua spacecraft launched in May 2002.

The orbit of the Terra satellite goes from north to south across over Thailand and study area around 10.00-11.00 AM and 10.00-11.00 PM for nighttime, and Aqua passes south to north over Thailand around 01.00-02.00 PM day time and 01.00-02.00 AM night time. (NASA FIRMS, 2015). The specification and spectral characteristic of MODIS are shown in Tables 2.1 and Table. 2.2 (NASA, 2012).

Table 2.1 The specification of MODIS sensor.

Structure	Specification
Orbit:	705 km, Terra and Aqua,
	Sun-synchronous, near-polar, and circular
Scan rate:	20.3 rpm, cross track
Swath dimensions:	2,330 km (cross track) by 10 km (along track at nadir)
Telescope:	17.78 cm diam. off-axis
	A focal (collimated), with intermediate field stop
Size:	1.0 x 1.6 x 1.0 m
Weight:	228.7 kg
Power:	162.5 W (single orbit average)
Data rate:	10.6 Mbps (peak daytime)
	6.1 Mbps (orbital average)
Quantization:	12 bits
Spatial resolution:	250 m (bands 1-2)
	500 m (bands 3-7)
	1,000 m (bands 8-36)
Design life:	6 years

Source: NASA (2012).

Table 2.2 MODIS spectral characteristics.

Primary Use	Band	Bandwidth	Spectral Radiance (W/m^2 -µm-sr)
Land/cloud/aerosols boundaries	1	620 - 670 nm	21.8
	2	841 - 876 nm	24.7
Land/cloud/aerosols properties	3	459 - 479 nm	35.3
	4	545 - 565 nm	29.0
	5	1,230 - 1,250 nm	5.4
	6	1,628 - 1,652 nm	7.3
	7	2,105 - 2,155 nm	1.0
Ocean color/phytoplankton/ biogeochemistry	8	405 - 420 nm	44.9
	9	438 - 448 nm	41.9
	10	483 - 493 nm	32.1
	11	526 - 536 nm	27.9
	12	546 - 556 nm	21.0
	13	662 - 672 nm	9.5
	14	673 - 683 nm	8.7
	15	743 - 753 nm	10.2
	16	862 - 877 nm	6.2
Atmospheric water vapor	17	890 - 920 nm	10.0
	18	931 - 941 nm	3.6
	19	915 - 965 nm	15.0
Surface/cloud temperature	20	3.660 - 3.840 µm	0.45 (300K)
	21	3.929 - 3.989 µm	2.38 (335K)
	22	3.929 - 3.989 µm	0.67 (300K)
	23	4.020 - 4.080 µm	0.79 (300K)
Atmospheric temperature	24	4.433 - 4.498 µm	0.17 (250K)
	25	4.482 - 4.549 µm	0.59 (275K)
Cirrus clouds/water vapor	26	1.360 - 1.390 µm	6.00
	27	6.535 - 6.895 µm	1.16 (240K)
	28	7.175 - 7.475 µm	2.18 (250K)
Cloud properties	29	8.400 - 8.700 µm	9.58 (300K)
Ozone	30	9.580 - 9.880 µm	3.69 (250K)
Surface clound temperature	31	10.780 - 11.280 µm	9.55 (300K)
	32	11.770 - 12.270 µm	8.94 (300K)
Cloud top altitude	33	13.185 - 13.485 µm	4.52 (260K)
	34	13.485 - 13.785 µm	3.76 (250K)
	35	13.785 - 14.085 µm	3.11 (240K)
	36	14.085 - 14.385 µm	2.08 (220K)

Source: NASA (2012).

MODIS used to generate a range of products that capture the location of a fire, its emitted energy, the flaming and smouldering ratio, and an estimate of the area burned (Giglio et al., 2003; Justice et al., 2006; Davies, Ilavajhala, Wong, and Justice, 2009). In addition, it is especially suitable for fire monitoring because it provides a high temporal revisiting rate with four daily satellite overpasses resulting in up to four hotspots observations per day. The MODIS fire products allow producing dense and historical time series of fire occurrences that can be used to assess the multi-temporal characteristics of fire occurrences and the seasonality of fire. Furthermore, the real time data may allow characterizing the effectiveness and efficiency because of the long data record with daily observations, the MODIS fires may also permit calculating the seasonality, timing, and inter-annual variation of fires (Giglio, Werf, Randerson, Collatz, and Kasibhatla, 2006).

2.4.2 MODIS fire detection algorithm

The fire detection of MODIS is based on heritage algorithms developed for the AVHRR and TRMM VIRS (Tropical Rainfall Measuring Mission with Visible and Infrared Scanner). (Kaufman et al., 1998; Justice et al., 2002; Giglio et al., 2003; Justice et al., 2006). The MODIS fire detection and characterization techniques are fully automated for the production of daily, global fire information. In order to detect the presence of fire in a non-interactive fashion, a set of detection criteria different for the day and night fire observations are prescribed. These multispectral criteria are based on the apparent temperature of the fire pixel and the difference between the fire pixel and its background temperature (Justice et al., 2006).

Based on a review of fire properties by Lobert and Warnatz (1993) flaming temperature can be anywhere between 800 K and 1,200 K and as hot as

1,800 K. Smoldering should be under 850 K and above 450 K. The actual range is probably smaller. Therefore, on the assumption that the flaming temperature is 1,000 K ± 200 K and the smoldering temperature is 600 K ± 100 K.

In addition, in a given fire pixel, it may have areas that are not burned, areas that are smoldering and areas that are in flames. Justice et al. (2006) stated that the 4 μm channel is sensitive to both flaming and smoldering. Figure 2.3 shows the effect of fire size and temperature on the apparent temperature of the pixel at 4 μm. This channel is sensitive to fires as small as 10^{-4} of the fire pixel.

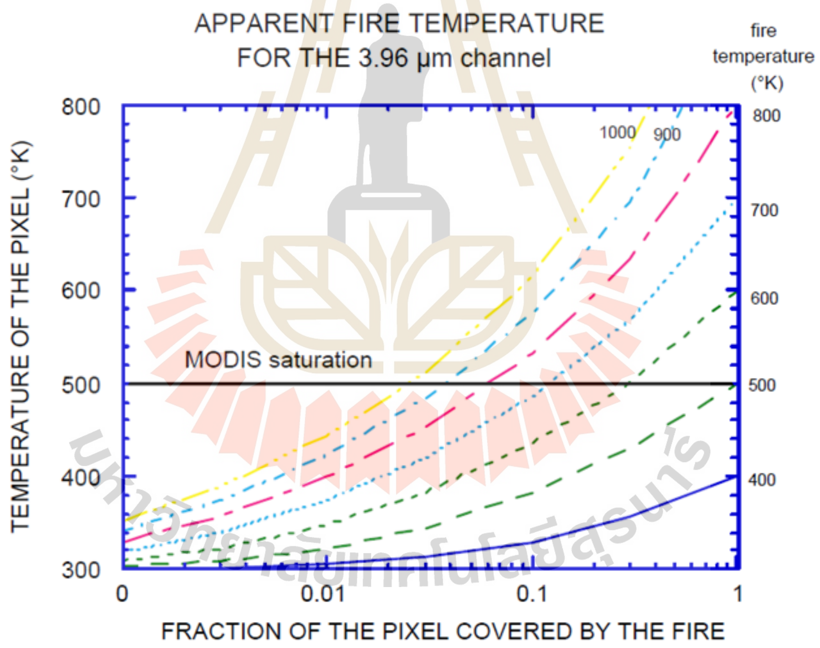

Source: Justice et al. (2006).

Figure 2.3 The apparent temperature of the pixel at 3.96 μm, as observed by MODIS, for a single fire as a function of the fraction of the pixel covered by the fire and its temperature.

Fire detection algorithm is performed using a contextual algorithm that exploits the strong emission of mid infrared radiation from fires. The algorithm examines each pixel of the MODIS swath, and ultimately assigns to each one of the following classes: missing data, cloud, water, non-fire, fire, or unknown. The algorithm uses brightness temperatures derived from the MODIS 4 µm and 11 µm channels, denoted by T4 and T11, respectively. The MODIS instrument has two 4 µm channels, numbered 21 and 22, both of which are used by the detection algorithm. Channel 21 saturates at nearly 500 K; channel 22 saturates at 331 K. Since the low-saturation channel (22) is less noisy and has a smaller quantization error, T4 is derived from this channel whenever possible. However, when channel 22 saturates or has missing data, it is replaced with the high saturation channel (21) to derive T4. T11 is computed from the 11 µm channel (channel 31), which saturates at approximately 400 K for the Terra MODIS and 340 K for the Aqua MODIS. The 12 µm channel (channel 32) is used for cloud masking and brightness temperatures for this channel are denoted by T12 (Justice et al., 2002; Giglio et al., 2003; Justice et al., 2006). The 250 m resolution red and near infrared channels, aggregated to 1 km, are used to reject false alarms and mask clouds. These reflectance are denoted by ρ0.65 and ρ0.86, respectively. The 500 m resolution of 2.1 µm band, also aggregated to 1 km, is used to reject water-induced false alarms; the reflectance in this channel is denoted by ρ2.1 (Justice et al., 2002; Giglio et al., 2003; Justice et al., 2006). A summary of all MODIS bands used in fire detection algorithm is shown in Table 2.3.

Table 2.3 MODIS channels used in fire detection algorithm.

Channel	Wavelength (μm)	Purpose
1	0.65	Sun glint and coastal false alarm rejection; cloud masking.
2	0.86	Bright surface, sun glint, and coastal false alarm rejection; cloud masking.
7	2.1	Sun glint and coastal false alarm rejection.
21	4.0	High-range channel for fire detection.
22	4.0	Low-range channel for fire detection.
31	11.0	Fire detection, cloud masking.
32	12.0	Cloud masking.

Source: Giglio et al. (2003).

To avoid false detection under MODIS fire detection algorithm, Justice et al. (2006) stated that all pixels for which T4 < 315 K (305 K at night) or ΔT = T4 - T11 < 10 K (3 K at night) or ρ0.86 > 0.3 (daytime only) should be immediately eliminated as possible fires (potential fire pixels). For absolute fire detection, the algorithm requires that at least one of two conditions is satisfied. These are

(1) T4 > 360 K (330 K at night), and

(2) T4 > 330 K (315 K at night) and ΔT > 25 K (10 K at night).

If either of these absolute criteria is not met, the algorithm pursues a relative fire detection in which the fire is distinguished from the mean background values by three standard deviations in T4 and ΔT as

T4 > mean (T4) + 3stddev (T4), and

ΔT > median (ΔT) + 3stddev (ΔT).

The mean, median, and standard deviations (denoted by “mean”, “median”, and “stddev” above) are computed for pixels within an expanding grid centered on the candidate fire pixel until a sufficient number of cloud, water, and fire-free pixels are identified. A "sufficient number" is defined as 25% of all background pixels, with a minimum of six. Water pixels are identified with an external water mask, and cloud pixels are identified with the MODIS cloud mask product (MOD35). Fire-free background pixels are identified as those pixels for which $T4 < 325$ K (315 K at night) and $\Delta T < 20$ K (10 K at night). If either standard deviation is below 2 K, a value of 2 K is used instead.

The background window is allowed to grow up to 21X21 pixels in size. If this limit is reached and the previous criteria regarding the minimum number of valid background pixels are not met, the relative detection tests cannot be used. If the absolute tests do not indicate that an active fire is present in this situation, the algorithm flags the detection result as unknown.

Combining all tests into a single expression, a pixel is classified as a fire pixel in daytime if the following conditions are satisfied:

$\{T4 > \text{mean}(T4) + 3\text{stddev}(T4) \text{ or } T4 > 330 \text{ K}\}$, and

$\{\Delta T > \text{median}(\Delta T) + 3\text{stddev}(\Delta T) \text{ or } \Delta T > 25 \text{ K}\}$, or

$T4 > 360$ K.

For the nighttime algorithm they become as:

$\{T4 > \text{mean}(T4) + 3\text{stddev}(T4) \text{ or } T4 > 315 \text{ K}\}$, and

$\{\Delta T > \text{median}(\Delta T) + 3\text{stddev}(\Delta T) \text{ or } \Delta T > 10 \text{ K}\}$, or

$T4 > 330$ K.

Finally, for daytime observations when sun glint may cause false detections, a fire pixel is rejected if the MODIS 250 m red and near infrared channels have a reflectance above 30% and it lies within 40° of the specular reflection position.

Although the original MODIS fire detection algorithm of Kaufman et al. (1998) and Justice et al. (2002) are functioning reasonably well, they have two significant problems limiting the overall quality of the product. Firstly, persistent false detections occurred in some deserts and sparsely vegetated land surfaces, particularly in northern Ethiopia, the Middle East, and Central India. Not unexpectedly, most of these were caused by the algorithm's absolute threshold tests. Secondly, relatively small (yet generally obvious) fires were frequently not detected. In response to these problems, Giglio et al. (2003) have developed a replacement version of contextual algorithm that offers superior sensitivity to smaller, cooler fires and have yielded fewer blatant false alarms and now that available on version 5 (Giglio et al., 2003; Giglio, 2010).

Giglio et al. (2003) had improved some aspect of the MODIS original algorithm. Their algorithm is starting from cloud and water remark. Daytime pixels are considered to be cloud-obscured if the following condition is satisfied:

$$(\rho 0.65 + \rho 0.89 > 0.9) \text{ or } (T12 < 265 \text{ K}), \text{ or}$$

$$(\rho 0.65 + \rho 0.89 > 0.7) \text{ or } (T12 < 285 \text{ K}).$$

Nighttime pixels are flagged as cloud if the single condition T12 < 265 K is satisfied.

Subsequently, the process is identifying the potential fire pixel. It is like the original algorithm, but is changed so that a daytime pixel is identified as a potential fire pixel if T4 > 310 K, ΔT > 10 K, and ρ0.86 < 0.3. For nighttime pixels, the reflective test is omitted and the T4 threshold reduced to 305 K. Pixels failing these preliminary tests are immediately classified as non-fire pixels. There are two logical paths through which fire pixels can be identified. The first consists of a simple absolute threshold test. This threshold must be set sufficiently high so that it is triggered only by very unambiguous fire pixels, i.e. those with very little chance of being a false alarm. The second path consists of a series of contextual tests designed to identify the majority of fire pixels that are less obvious (Giglio et al., 2003).

In this algorithm, the absolute threshold criterion remains identical to one employed in the original algorithm of Kaufman et al. (1998) as:

$$T4 > 360 \text{ K } (320 \text{ K at night}). \tag{2.4}$$

In the next phase of the algorithm to background characterization, which is performed regardless of the outcome of the absolute threshold test, an attempt is made to use the neighboring pixels to estimate the radiometric signal of the potential fire pixel in the absence of fire. Valid neighboring pixels in a window centered on the potential fire pixel are identified and are used to estimate a background value. Within this window, valid pixels are defined as those that (1) contain usable observations, (2) are located on land, (3) are not cloud-contaminated, and (4) are not background fire pixels. Background fire pixels are in turn defined as those having $T4 > 325$ K and $\Delta T > 20$ K for daytime observations, or $T4 > 310$ K and $\Delta T > 10$ K for nighttime observations (Giglio et al., 2003).

If the background characterization was successful, a series of contextual threshold tests are used to perform relative fire detection. These look for the characteristic signature of an active fire in which both the 4 µm brightness temperature (T4) and the 4 - 11 µm brightness temperature difference (ΔT) depart substantially from that of the non-fire background. Relative thresholds are adjusted based on the natural variability of the background. The tests are as following:

$$\Delta T > \Delta\bar{T} + 3.5\ \delta\Delta T, \tag{2.5}$$

$$\Delta T > \Delta\bar{T} + 6K, \tag{2.6}$$

$$T4 > \bar{T}4 + 3\delta 4, \tag{2.7}$$

$$T11 > \bar{T}11 + \delta 11 - 4\ K, \text{ and} \tag{2.8}$$

$$\delta' 4 > 5K. \tag{2.9}$$

where $\bar{T}4$ and $\delta 4$ are the respective mean and mean absolute deviation of T4 for the valid neighboring pixels ($\bar{T}11$ and $\delta 11$), the respective mean and mean absolute deviation of T11 for the valid neighboring pixels ($\Delta\bar{T}$ and $\delta\Delta T$), the respective mean and mean absolute deviation of ΔT for the valid neighboring pixels. The 4 µm brightness temperature mean and mean absolute deviation of those neighboring pixels that were rejected as background fires are also computed and are denoted by $\bar{T}'4$ and $\delta' 4$, respectively.

Of these conditions, the first three isolate fire pixels from the non-fire background. The factor of 3.5 appearing in test Eq. 2.5 is larger than the corresponding factor of 3 in test Eq. 2.7 to help adjust for partial correlation between the ΔT observations. Condition (Eq. 2.8), which is restricted to daytime pixels, is primarily used to reject small convective cloud pixels that can appear warm at 4 µm (due to reflected sunlight) yet cool in the 11 µm thermal channel. It can also help reduce coastal false alarms that sometimes occur when cooler water pixels are unknowingly included in the background window. Any test based on $\delta 11$, however risks rejecting very large fires since these will increase the 11 µm background variability substantially. For example, over a typical land surface $\delta 11 \approx 1$ K, whereas for land pixels spanning a large forest fire, $\delta 11$ will routinely exceed 20 K. For this reason, test Eq. 2.9 will be employed to disable test Eq. 2.8 when the background window appears to contain large fires. This situation is recognized by an elevated value of δ4′; the presence of background fire pixels increases this statistic considerably (Giglio et al., 2003).

In the position to tentatively identify pixels containing active fires, for nighttime fires, in fact this will be an unambiguous, final identification. For daytime pixels, three additional steps are used to help eliminate false alarms caused by sun glint, hot desert surfaces, and coasts or shorelines as followings.

A daytime pixel is tentatively classified as a fire pixel if

{test Eq. 2.4 is true}, or

{test Eq. 2.5 - Eq. 2.7 are true and test Eq. 2.8 or test Eq. 2.9 is true};

otherwise it is classified as non-fire.

A nighttime candidate fire pixel is definitively classified as fire if

{test Eq. 2.4 is true}, or

{test Eq. 2.5 - Eq. 2.7 are true};

otherwise it is classified as non-fire.

For those daytime and nighttime pixels for which the background characterization failed, i.e. an insufficient number of valid neighboring pixels were identified; only test Eq. 2.4 is applied in this step. If not satisfied, the pixel is classified as unknown, indicating that the algorithm was not able to unambiguously render a decision considerably (Giglio et al., 2003; Justice et al., 2006).

2.4.3 Hotspot

The MODIS Rapid Response System was developed to provide near real time imagery from the MODIS instrument for a broad range of users. The Rapid

Response Team produces the MODIS fire location data that identify and characterize actively burning fires (e.g. wildfires and agricultural fires, etc.), and other thermal anomalies (e.g. volcanoes, etc.) at the time of satellite overpass. Fires that do not emit sufficient heat under relatively cloud-free conditions at overpass time are unlikely to go detected. The fire detection algorithms are fully automated and produce daily fire information for the entire globe. The detection criteria are based on the temperature of an each potential fire pixel and the difference between the temperature brightness of the fire pixel and its background temperature (Justice et al., 2006).

The detection algorithm identifies pixels with one or more actively burning fires that are commonly referred to as "hotspot." Each detected fire represents the centre of an (approximately) 1 km pixel that contains one or more hotspots. The actual pixel size varies depending on the location of an observation in the swath. Pixels further away from nadir (exactly vertical from the satellite) will grow larger. The coordinates of the fire in the attribute table does not represent the exact location of the fire, but the centre point of the pixel (Giglio, 2010).

The size of the fire can be much smaller than the pixel size (Figure 2.4). The detection probability of hotspot depends on a number of factors, among others on fire temperature and satellite viewing angle. Hotspot can detect flaming fires (~1000 K) as small as 100 m^2 under ideal conditions with a 50% detection probability, or a 1000-2000 m^2 smouldering fire (~600 K). Detection rates will be higher when the daily peak fire activity will coincide with the time of satellite overpass (Kaufman et al., 1998; Giglio et al., 2003; Hawbaker, Radeloff, Syphard, Zhu, and Stewart, 2008). Also, fires in degraded forests are easier to detect than fires in primary forests, because degraded forests burn hotter due to more dry fuel and the open canopy. Primary forests are often dominated by ground fires with little heat production (Langner and Siegert, 2009). Ultimately, the algorithm assigns to each pixel one of the following classes: missing data, water, cloud, fire, non-fire or unknown (Giglio et al., 2003; Justice et al., 2006).

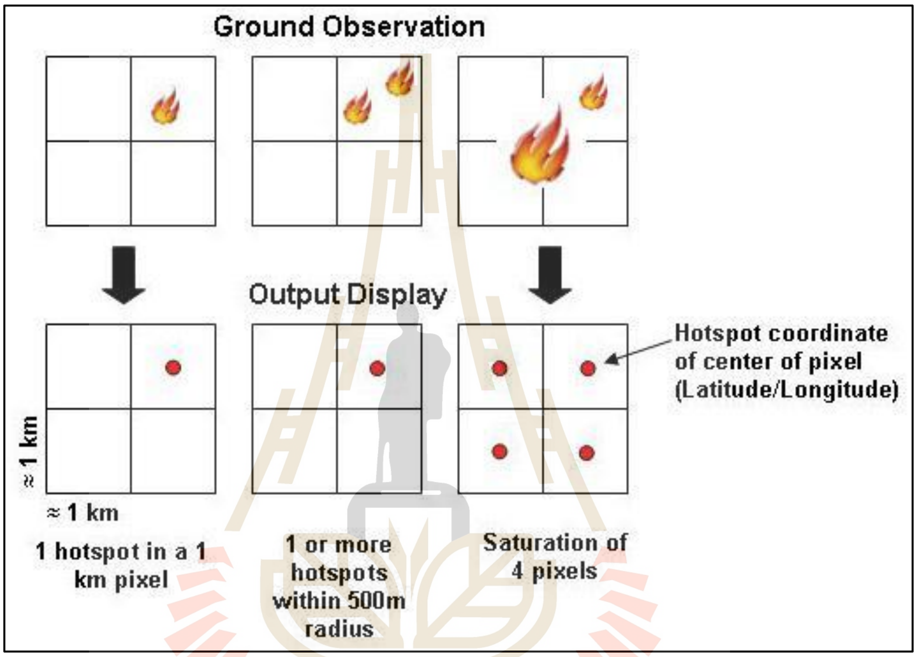

Source: NASA (2013).

Figure 2.4 Fire pixels detection using MODIS.

The hotspots are derived from multiple MODIS channels to detect the thermal anomalies on a per-pixel basis. They produce very sophisticated fire information, which is also based on the algorithms developed by Kaufmann et al. (1998), Justice et al. (2002), and Giglio et al. (2003). hotspots are calculated by the MODIS Rapid Response system and reported by FIRMS with multiple reported fields. These fields include latitude and longitude (center point location), brightness temperature in Kelvin (BT) of either channel 21 or 22, scan and track (actual spatial resolution of the scanned pixel), acquisition date and time of the overpass of the satellite, satellite name (Terra or Aqua), percentage of fire confidence, version of algorithm, and brightness temperature of channel 31. Sometimes that can be called MOD14 then hotspot detected by Terra and MYD14 then detected by Aqua (Justice et al., 2006; Giglio, 2010).

2.4.4 Caveats of the hotspot

Several issues obstruct the use of the MODIS fire products to indicate the location of active small scale fires. For one, the textural component of the detection algorithm causes problems with false detections in areas where the canopy cover exhibits strong differences in surface temperatures. This may be the case where gaps in the forest canopy cover are present that can be due to recent clearings. Another fraction of false detections may be related to recent burning activities where homogenous areas of dark char cause errors of commission, such as in the Amazon (Schroeder et al., 2008).

Cloud cover obstructs fire detection and may lead to high errors of omission (undetected fires). Fire counts are thus likely underestimated, particularly in tropical regions (Giglio et al., 2006b; Schroeder et al., 2008). Clouds are yet also indicative of rain when fire probability is low, which possibly reduces this bias (Aragao and Shimabukuro, 2010).

The size of a particular fire cannot be calculated from the fire hotspot data and no distinction can be made between large fires and small fires. While there is possibly a direct relation between the number of fires detected in a specific area, the size of the area affected, the smoke emitted, and the biomass burnt, the degree of these linkages is unclear from the hotspot. (Aragao and Shimabukuro, 2010).

The hotspot does not allow distinguishing, if one or more fires were actively flaming within a pixel on the same day. Yet, it is often quite likely that more than one fire occurs within a pixel during the burning season, because of the coarse spatial resolution (1 km2) of the fire records (Giglio et al., 2003; Giglio, 2010).

Finally, burned areas cannot be derived from the hotspots, because the actual size and area affected of the fire is unknown. The hotspots data can still be useful to approximate fire affected areas in the absence of high resolution burned area maps (Giglio et al., 2003; Miettinen et al., 2007).

2.5 Spectral indices for burned area detection and its algorithm

2.5.1 Spectral indices for burned area detection

There are many spectral indices that can use for burned area detection. The characteristics of selected spectral indices applied in this study are summarized as shown Table 2.4. It covers index, abbreviation, formula, concept or application, and reference.

Table 2.4 The characteristics of selected spectral indices for burned area detection.

Index	Abbreviation	Formula	Concept or Application	Reference
Normalized Difference Vegetation Index	NDVI	NDVI = (NIR - red)/(NIR + red)	The NDVI is an equation that takes into account the amount of infrared reflected by plants. Live green plants absorb solar radiation, which they use as a source of energy in the process of photosynthesis. The reason NDVI is related to vegetation is that healthy vegetation reflects very well in the near-infrared part of the electromagnetic spectrum. The NDVI value is varies between -1.0 and +1.0. The negative values of NDVI correspond to deep water. Values close to zero (-0.1 to 0.1) generally correspond to barren areas of rock, sand, or snow. Low, positive values represent shrub and grassland (approximately 0.2 to 0.4), while high values indicate temperate and tropical rainforests. The typical range is between about 0.1 to 0.6 (for a very green area). Then, the NDVI is strongly related to above-ground biomass and as a result the index has shown to discriminate reasonably well between burned and unburned areas.	Tucker (1979); Huete et al. (2002)
Global Environment Monitoring Index	GEMI	GEMI = γ(1 -0.25 γ) -((Red -0.125)/(1 - Red)) with γ = (2(NIR2 - Red2) + 1.5NIR + 0.5Red)/(NIR + Red+ 0.5)	The Global Environmental Monitoring Index (GEMI), claimed to be less affected by soil and atmospheric variations than NDVI (Pinty and Verstraete,1992). It has also proved to be more sensitive to burned area discrimination than NDVI (Pereira 1999). in addition the study of Chuvieco et al. (2002) that to compare of grey displays of NDVI, SAVI, and GEMI showed similar patterns for burned area, although a higher contrast with unburned areas is observe d in GEMI.	Pinty and Verstraete (1992); Pereira (1999); Chuvieco et al. (2002)

Table 2.4 (Continued) The characteristics of selected spectral indices for burned area detection.

Index	Abbreviation	Formula	Concept or Application	Reference
Modified Soil Adjusted Vegetation Index	MSAVI	MSAVI = (2NIR + 1 -((/2NIR+ 1)^2 - 8(NIR -red))$^{1/2}$)/2	Qi et al. (1994) developed the MSAVI to more reliably and simply calculate a soil brightness correction factor. The output of MSAVI is a new image layer representing vegetation greenness with values ranging from -1 to +1. Furthermore, MSAVI have been successfully applied in burned land.	Qi et al. (1994)
Normalized Difference Water Index	NDWI	NDWI = (NIR - sSWIR)/(NIR + sSWIR) (Band 6)	The NDWI is defined as the ratio of a near infrared (NIR) channel centered at 0.86 µm and a short wave infrared (SWIR) channel centered at 1.64 µm. NDWI is influenced by both desiccation and wilting in the vegetation canopy, and thus it may be a sensitive indicator for drought monitoring.	Gao, (1996); Wang et al. (2008)
Burned Area Index	BAI	BAI = 1/ ((NIR-0.06)^2+(red-0.1)^2)	The BAI defined by Martin (1998) specifically to discriminate fire affect areas. This index is computed from the spectral distance from each pixel to a reference spectral point, where recently burned areas tend to converge. The BAI emphasizes the charcoal signal in red near infrared (R-NIR) bi-spectral space. Furthermore, the research of Chuvieco et al. (2002) compared the grey displays of NDVI, SAVI and GEMI showed similar patterns for burned areas, although a higher contrast with unburned areas is observed in GEMI. Unlike the other indices, BAI shows the highest values for burned areas, clearly separating before/after situations.	Martin (1998); Chuvieco et al. (2002)

Table 2.4 (Continued) The characteristics of selected spectral indices for burned area detection.

Index	Abbreviation	Formula	Concept or Application	Reference
Mid InfraRed Burn Index	MIRBI	MIRBI = 10 lSWIR - 9.8 sSWIR + 2	The MIRBI make use of the characteristic post-fire reflectance increase in the short wave infrared (SWIR) spectral domain (1.3 to 2.5 µm) in combination with the near infrared (NIR) reflectance drop associated with the vegetation removal.	Trigg and Flasse (2001)
Burned Area Index Modified	BAIM	BAIM = 1/ $((NIR-0.05)^2+(lSWIR-0.2)^2)$	The BAIM is based on the Burned Area Index (BAI), previously proposed by Martin (1998) to map burned areas using NOAA-AVHRR. The utility of the BAIM index has been assessed against other spectral indices (MIRBI, NDVI, NBR) to map burned areas, The research of Martin et al. (2005) using 10-day multi-temporal composites of MODIS data acquired over the Iberian Peninsula in August 2001 and 2003. The BAIM provided the highest discrimination ability among the indices tested, and offered a high accuracy for medium to large fires.	Martin et al. (2005)
Normalized Burn Ratio	NBR	NBR = (NIR - lSWIR)/(NIR + lSWIR)	The NBR combining information on the NIR channel centered at approximately 0.8 µm and a SWIR channel centered at approximately 2.1 µm has been widely used to map burned areas and burn severity. Since the NIR and SWIR spectral bands have the greatest change among reflective spectral bands, with NIR decreasing and SWIR increasing through the fire, the NBR would be most discriminating for burn effects. In addition, the NBR has become accepted as the standard spectral index to assess the burn severity.	Key and Benson (2005)

Table 2.4 (Continued) The characteristics of selected spectral indices for burned area detection.

Index	Abbreviation	Formula	Concept or Application	Reference
Normalized Difference Shortwave Infrared	NDSWIR	NDSWIR = (NIR - sSWIR)/(NIR + sSWIR)	George, Rowland, Gerard, and Balzter (2006) used NDSWIR of MODIS imagery to map burnt areas of boreal forest in Central Siberia. They found that this index was sensitive to canopy moisture and structure. Therefore, immediately after a fire, the SWIR reflectance decreases due to absorption by combustion.	George et al. (2006)
Normalized Multi-band Drought Index	NMDI	NMDI = (NIR -(sSWIR -lSWIR))/(NIR + (sSWIR -lSWIR))	The NMDI has strong signals corresponding to fires. The research of Wang et al. (2008) showed NMDI reveals the highest overall performance and discrimination power compared to NDWI and NBR.	Wang et al. (2008)
SWIR-MIR Index	SMI	(sSWIR -MIR)/(sSWIR + MIR)	SWIR-MIR index (SMI) based on single date short-wave infrared (SWIR) and mid infrared (MIR) reflectance. In contrast with the (d)NBR, SMI index is robust against scattering caused by smoke plumes over fires. In addition, Veraverbeke, Hook, and Hulley, 2012), generated the SMI using MODIS/ASTER showed the SMI is more sensitive to char fractional cover than the NBR. The SMI results in values close to zero for char, whereas all terrain features not affected by fire result in higher SMI values. As the SMI only inputs longer wavelengths that remain unaffected by smoke of the fire, it can be used over large fires.	Veraverbeke et al. (2012)
Char Soil Index	CSI	CSI = NIR/ lSWIR	CSI is defined as the simple ratio between the NIR and lSWIR reflectance. The study of Schepers et al. (2014) to used airborne imaging spectroscopy data from the Airborne Prism Experiment (APEX) sensor to: (1) investigate which spectral regions and spectral indices perform best in discriminating burned from unburned areas; and (2) assess the burn severity of fire in the Kalmthoutse Heide, found that CSI was the best index in dry heath vegetation to assess burn severity.	Schepers et al. (2014)

2.5.2 MODIS burned area product and its algorithm

The MODIS burned area algorithm maps the approximate day of burning using multitemporal land surface reflectance data based on a method described by Roy, Jin, Lewis, and Justice (2005). The algorithm is applied independently to geolocated pixels over a long time-series of reflectance observations. A bi-directional reflectance (BRF) model is inverted against multitemporal reflectance observations to provide predicted reflectances and uncertainties for subsequent observations. A statistical measure of the difference between the observed surface BRF and the predicted BRF at the viewing and illuminating angles of the observation is used to quantify change from a previously observed state. Large discrepancies between predicted and measured values are attributed to change. A temporal constraint is used to differentiate between temporary changes, such as shadows, that are spectrally similar to more persistent fire induced changes. The identification of the date of burning is constrained by the frequency and occurrence of missing observations and to reflect this product, the algorithm is run to report the burn date with an 8 day precision. The burned area product is identified as MCD45A1 and spatial resolution of product equal 500 meter (Roy et al., 2005; Justice et al., 2006).

2.5.3 LANDSAT burned area extraction and its algorithm

Bastarrika et al. (2014); Bastarrika (2014) developed a new supervised burned area mapping software based on Landsat data named BAMS (Burned Area Mapping Software). The tool is built from standard ArcGIS libraries. It computes several of the spectral indexes most commonly use in burned area detection and implements a two-phase supervised strategy to map areas burned between two Landsat multitemporal images. The only input requires from the user is the visual delimitation of a few burned areas, from which burned perimeters are extracted. After the discrimination of burned patches, the user can visually assess the results, and iteratively select additional sampling burned areas to improve the extent of the burned patches. The final result of the BAMS program is a polygon vector layer containing three categories: (a) burned perimeters, (b) unburned areas, and (c) non-observed areas.

The detail of BAMS workflow (Figure 2.5), which includes (1) generation of reflectances, (2) computation of burned area spectral indexes, (3) temporal composites, (4) burned area mapping supervised methodology, and (5) batch process are summarized based on Bastarrika et al. (2014) as followings.

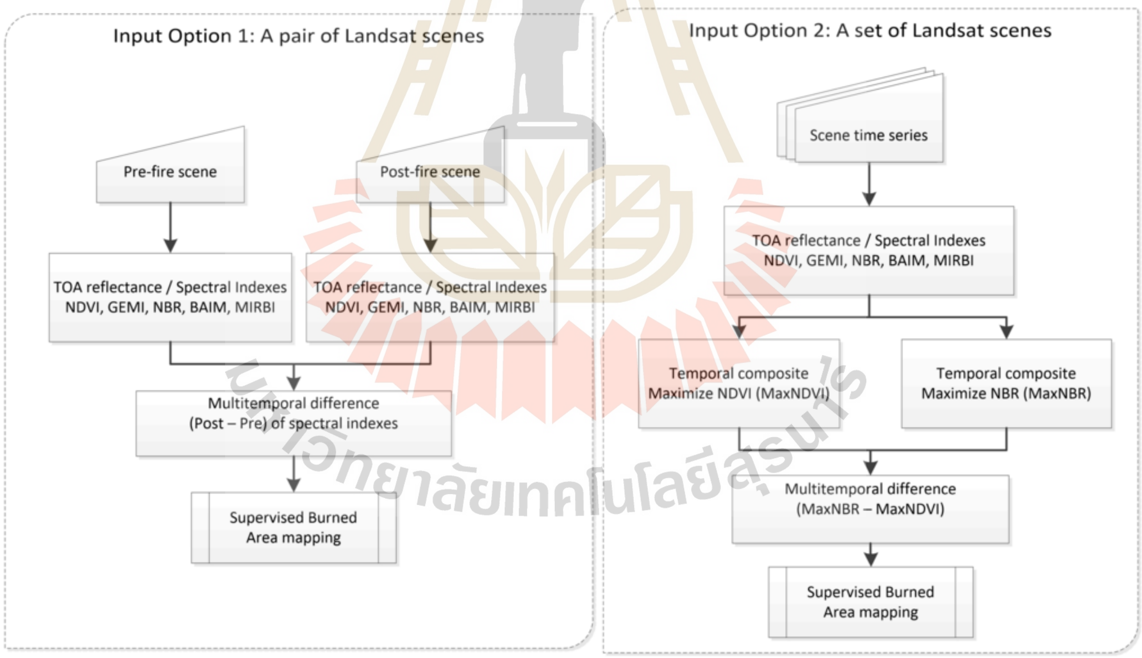

Source: Bastarrika et al. (2014).

Figure 2.5 Burned Area Mapping Software (BAMS).

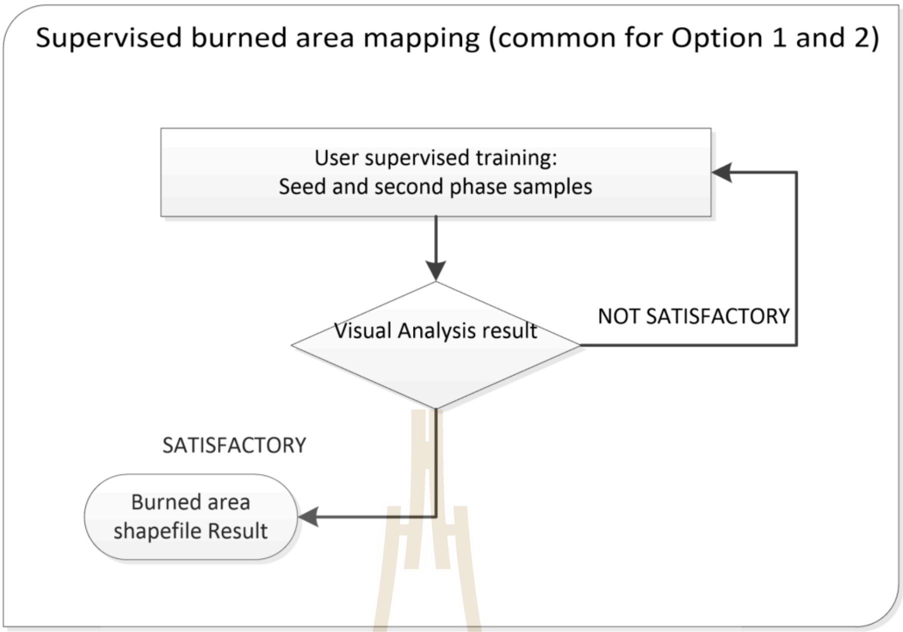

Figure 2.5 (Continued) Burned Area Mapping Software (BAMS).

(1) Generation of reflectances.

Under this step, the program can readily access two data input sources: the USGS Landsat Terrain Correction (Level 1T) GeoTiff format and the USGS Landsat Surface Reflectance Climate Data Record (SRCDR) HDF format. In the case of the former, BAMS converts Raw Digital Numbers (DN) into at-sensor radiance and then into exoatmospheric Top of Atmosphere (TOA) reflectance using the simplified reflectance equation. For Landsat TM and ETM+, the following equation is used:

$$\rho\lambda \ = \ \pi \cdot L\lambda^2 \cdot d^2/(ESUN\lambda \cdot cos\theta s), \quad (2.10)$$

$$L\lambda = G_{rescale} \cdot Q_{cal} + B_{rescale} \quad (2.11)$$

Where:

$\rho\lambda$ = Exoatmospheric Top of Atmosphere reflectance (TOA)

$L\lambda$ = Spectral radiance at the sensors aperture

d = Earth-Sun distance

$ESUN\lambda$ = Mean exoatmospheric solar irradiance

θs = Solar zenith angle

$G_{rescale}$ = Band-specific rescaling gain factor from the metadata

Q_{cal} = Quantized calibrated pixel value (DN)

$B_{rescale}$ = Band-specific rescaling bias factor from the metadata

Reflectance for OLI data is as follows:

$$\rho\lambda = (M\rho \cdot Qcal + A\rho)/cos\theta s, \tag{2.12}$$

where:

$\rho\lambda$ = TOA planetary reflectance, without correction for solar angle.

$M\rho$ = Band-specific multiplicative rescaling factor from the metadata

$Qcal$ = Quantized and calibrated standard product pixel values (DN)

$A\rho$ = Band-specific additive rescaling factor from the metadata

θs = Solar zenith angle

(2) Computation of burned areas spectral indexes

Burned areas are characterized by deposits of char and ash, removal of vegetation cover, and fuel, as well as exposure of the underlying soil. However, the magnitude and direction of spectral changes caused by charcoal and ash deposition depend on the type and condition of the vegetation prior to burning and the degree of combustion. BAMS computes the most common spectral indexes previously suggested in burned area studies. They include:

1. Normalized Difference Vegetation Index (NDVI)

2. Burned Area Index Modified (BAIM)

3. Global Environmental Monitoring Index (GEMI)

4. Normalized Burned Ratio (NBR)

5. Mid-Infrared Burned Index (MIRBI)

These spectral indexes represent the most important bi-spectral spaces for burned area mapping, NIR/SWIR (BAIM and NBR), Long SWIR/Short SWIR (MIRBI), and Red/NIR (GEMI and NDVI). In order to avoid floating variables, the variables NBR, MIRBI, GEMI, and NDVI are saved in 16-bit bands applying a scaling factor of 10,000 while the BAIM is truncated directly to an integer number.

(3) Temporal composites

BAMS makes it possible to produce temporal composites for users who require burned area information for more than two periods (to reconstruct fire history with multiple Landsat scenes, for example). Two temporal composites are created in the process: one minimizes the NBR index, which aims to identify the most affected burned areas observed at each time frame of the series. This criterion will create the post-fire image of the time series. The second criterion maximizes the NDVI index, and aims to identify the time framework when each pixel is less affected by fire. The final composite will be considered as the pre-fire image of the time series.

(4) Burned area mapping supervised methodology

BAMS follows a two-phase burned area strategy, which has produced good results for mapping of burned areas with low and medium spatial resolution. This strategy aims at keeping a balance between commission and omission errors: In the first phase the goal is to reduce the commission errors by using strict criteria, so that only the more clearly burned pixels are retained (seed pixels), even at the cost of omitting some burned pixels within each burned patch. The second phase analyzes the vicinity of the seed pixels, applies a more flexible criterion, and accepts as burned those neighboring pixels with spectral characteristics similar to the seeds. This phase progressively increases the burned area until the whole burned patch is covered and aims at reducing the omission errors.

The two-phase strategy implemented by this tool is simple (see Figure 2.6). To start with, two Boolean rasters are generated, one for the seeds (Figure 2.6a, in red) and another for those pixels that fulfill the second-stage criteria (Figure 2.6b, in orange). From the second-stage criteria raster, groups are created from pixels connected by any of the eight neighboring sides (right, left, above, below, and diagonals). Therefore only those groups that intersected with the seeds are retained (Figure 2.6c, 2.6d). A multi-index approach is taken for the first and second phase. It has shown to be effective in Landsat automatic methodologies. BAMS code makes use of 10 spectral variables (the post-fire BAIM, NBR, MIRBI, GEMI, and NDVI indexes, plus the temporal differences of those five indexes). For the spectral indexes NDVI, GEMI, and NBR, the fire decreases the pre-fire value, so the tool sets a maximum value (the lower the value, the higher the probability of being burned). For BAIM and MIRBI, where the fire increases their pre-fire value, a minimum value is set (a higher value indicates higher probability of being burned). Two independent sets of criteria are defined, one for the seed phase (strict criteria) and another for the second phase (more relaxed). To avoid the impact of isolated pixels, seeds with less than two pixels in the immediate eight neighborhoods are removed. The final burned area is obtained by keeping only burned patches generated by the second-phase raster-intersecting seeds selected in the first phase. Once this raster layer is obtained, it is transformed to an ArcGIS shape vector format.

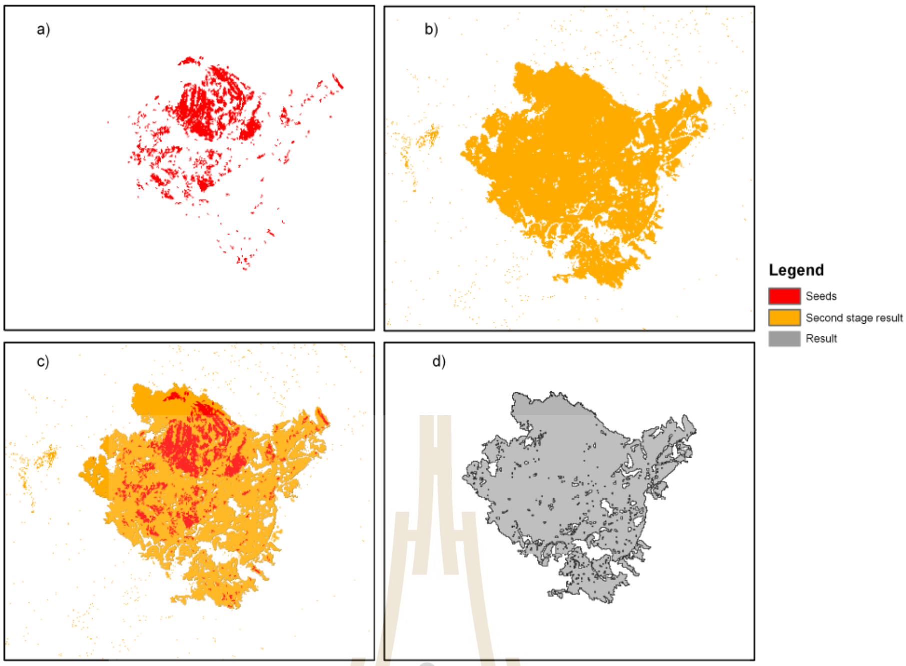

Source: Bastarrika et al. (2014).

Figure 2.6 Flow chart for the burned area mapping section (a) seeds, (b) second stage result, (c) seeds and second stage result superimposed, (d) result. Note that some of the burned areas fulfilling only the second stage criteria are not kept as they do not contain a burned seed.

The crucial point of the algorithm is the selection of threshold values for each of the input spectral indices. These values are extracted from the training polygons identified visually by the user from the post- and/or pre-fire color composites. In opposition to traditional supervised classification methodologies, where both burned and unburned training areas are required, BAMS only needs burned training areas, which makes the training process easier and faster than previous approaches, because the unburned category is always more heterogeneous due to the higher spectral diversity of unburned land covers. Two different burned training polygons have to be sampled to set the threshold values, one for the seeds and the other for the second phase. For each, the minimum of all the samples are retained for MIRBI and BAIM variables, whereas the maximum values are extracted for the rest (NDVI, GEMI, and NBR). It is very important to avoid false positives in this phase, since the burned area thresholds will be set with these values and the results will then be less accurate. The thresholds extracted from the two user-defined training polygons are applied with the logical operation “AND”. The result should be assessed before deciding whether more training areas are needed to complete the burned cartography, by extracting new thresholds from different iterations.

(5) Batch process

If the user needs to process a large number of images, the program could also be run in a batch mode. This option makes it possible to run the process automatically, using a set of thresholds previously defined in the supervised mode with different images.

2.6 Literature reviews

Relevant literature reviews are here categorized into two aspects include fire and burned area detection algorithm development and its application, and validation of MODIS hotspot data.

2.6.1 Fire and burned area detection algorithm development and its applications

Wang et al. (2008) selected satellite-derived indices, NMDI, NDWI, and NBR, for detecting forest fires burning in southern Georgia, USA and southern Greece in 2007. Index performance is evaluated using hotspot data. Satellite images generated from each index are compared with the hotspot map. Performance measures extracted from the statistical analyses using the confusion matrices are used to verify the capacity of the indices for fire detection. For each test case, NMDI has strong signals corresponding to fire accurately. Both, performance evaluations by image comparison and statistical analyses, indicate that fire detection using NMDI is quite accurate. NMDI reveals the highest overall performance and discrimination power compared to NDWI and NBR. The successful application of NMDI for detecting fires in different areas proves that NMDI is not site-specific and is expected to be applicable to different areas for fire detection. Such a capacity can help monitor large-scale fire hazards and is therefore useful to carry out regional and global studies.

Maeda, Formaggio, Shimabukuro, Arcoverde, and Hansen (2009) applied remote sensing and GIS technique to areas with high occurrence of forest fires in the Brazilian Amazon. The aim was to recognize land use changes that could identify areas with high risk of being burnt and to improve current fire scars mapping methods by enabling the discrimination of fires in primary forests and fires in previously burnt areas. The Change Vector Analysis method was applied to the Red and NIR bands of two MODIS/Terra images from key dates prior to the 2005 forest fire season, resulting in one change vector image with two components: direction and magnitude of changes. A decision tree was designed and evaluated through the C 4.5 algorithm to classify 2,400 sample pixels extracted from four selected classes inside the change vector images: (A) forest; (B) agricultural areas; (C) fire risk in primary forest; and (D) fire risk in already degraded areas. The decision tree achieved a global accuracy of 90.21%. Samples from classes B and D were the main contributors to the decision tree confusion, with omission errors of 9.5% and 24.5%, respectively. The method was tested in 14 municipalities for the year of 2005, 2006, and 2007 and compared with MODIS hotspots, resulting in a correlation coefficient of 0.84.

Qian, Yan, Duan, and Kong (2009) simulated HJ-1B satellite imagery, including Red, NIR, MIR, and TIR channels to detect fire. Based on the MODIS version 4 contextual algorithm and the characteristics of HJ-1B sensor, a contextual fire detection algorithm was proposed and tested using simulated HJ-1B data. It was evaluated by the probability of fire detection and false alarm as functions of fire temperature and fire area. Results indicate that when the simulated fire area is larger than 45 m^2 and the simulated fire temperature is larger than 800 K, the algorithm has a higher probability of detection. But if the simulated fire area is smaller than 10 m^2, only when the simulated fire temperature is larger than 900 K may the fire be detected. For fire areas about 100 m^2, the proposed algorithm has a higher detection probability than that of the MODIS product. Finally, the omission and commission error were evaluated which are important factors to affect the performance of this algorithm. It has been demonstrated that HJ-1B satellite data are much sensitive to smaller and cooler fires than MODIS or AVHRR data.

Ruthamnong (2010) analyzed MODIS hotspots acquired in 2008 over 17 provinces in the Northern region of Thailand and developed an algorithm for classifying the false hotspots. In the study, the hotspots were statistically analyzed using descriptive statistics. The spatial hotspot layer was assigned their attributes according by additional 3 GIS layers: water body, wetland, and urban. The attribute was assigned into 2 types, true and false (hotspot was located inside 3 GIS layers). The T-test analysis was thus performed to find significant difference of hotspot properties (REF2: reflectance of channel 2, BT21, BT31, FRP, and FC) between true and false hotspots. The upper and lower bounds resulting from the T-Test analysis were then used as a threshold value in the decision tree algorithms which used for false hotspot classification. The best of decision tree algorithm proposed in this study was selected from the highest accuracy assessment. The accuracy assessments were re-examined by applying the best algorithm on hotspots in 2007 and analyzing NDVI changes during before-on-after days of the acquired hotspots. The results showed that there were 11,783 hotspots in 2008 which occurred in Maehongson (14.33%), Tak (13.29%), Nan (11.81%), and Chiang Mai (11.08%), respectively. Hotspots of 79.54% were detected by Aqua, 82.36%of hotspots occurred in daytime, and 88.37% occurred in fire seasons. Most hotspots were temporally occurred in March (60.57%), April (15.79%), and February (12.01%). The EQ.5-BT31-REF2-FC-EQ.2 algorithm was the best algorithm with accuracy of 86.98%. The best of decision tree algorithm includes 5 parameters: EQ.5 [(BT21 - BT31) X (BT21 / 127) X (FRP / 400)], BT31, REF2, FC, and EQ.2 [(BT21 - BT31) X (BT21 / 127)] could identify 96.85% of false hotspot and 87.17% of true hotspot in 2007. Also, NDVI changing studies found that 96.58% has NDVI decreased from the day before hotspot.

Harris, Veraverbeke, and Hook (2011) used high spatial and high spectral resolution MODIS/ASTER (MASTER) airborne simulator data acquired over three 2007 southern California burns to evaluate the effectiveness of 19 different spectral indices, including the widely used NBR, for assessing fire severity in southern California chaparral. The ordinal logistic regression was used to assess the goodness of fit between the spectral index values and ordinal field data of severity. The NBR and three indices used surface temperature and emissivity band. They are found NSTv1, NSEv1, and NSEv2 revealed the best performance. The findings support the operational use of the NBR in chaparral ecosystems by Burned Area Emergency Rehabilitation (BAER) projects, and demonstrate the potential of combining optical and thermal data for assessing fire severity.

Veraverbeke et al. (2011) used high spatial and spectral resolution MASTER airborne simulator data acquired over three 2007 southern California burns to evaluate the sensitivity of different spectral indices for discriminating burned land shortly after a fire. The performance of the indices, which included both traditional and new band combinations, was assessed by means of a separability index that provides an assessment of the effectiveness of a given index for discriminating between burned and unburned land. In the context of burned land applications results demonstrated: (1) the highest sensitivity of the longer SWIR spectral region (1.9 to 2.5 μm) was found at the band interval from 2.31 to 2.36 μm, (2) the high discriminatory power of the mid infrared spectral domain (3 to 5.5 μm), and (3) the high potential of emissivity data. As a consequence, a newly proposed index which combined NIR, longer SWIR and emissivity outperformed all other indices when results were averaged over the three fires. In addition, the separability index values higher than one, these indices are the NSEv2, NSEv1, NSTv1, NBR, SAVI, VI3, NDVI and the best performance was obtained by the NSEv2.

Veraverbeke et al. (2012) developed an alternative index based on single date SWIR and MIR reflectance, namely the SWIR-MIR index (SMI), that is robust against scattering caused by smoke plumes over the fires allowing fire severity assessments to be generated when the area is still obscured by smoke. The SMI was generated using MASTER airborne simulator data acquired over 2011 Wallow fire in Arizona, USA. The simulation experiments showed SMI is more sensitive to char fractional cover than the NBR. Then performed a regression analysis in which 92 Geo

Composite Burn Index (GeoCBI) field plots of severity were randomly assigned to two equal. Currently although no spaceborne sensors with pixel sizes smaller than 100 m offer the possibility of a SWIR-MIR band combination, the airborne results illustrate the potential of this band combination for the remote sensing of post-fire effects.

Wang, Miao, and Peng (2012) developed algorithm to detect fire using HJ-infrared sensor (HJ-IRS) following the MODIS fire detection contextual algorithm. The improved algorithm was programmed in IDL7.1 and tested using HJ forest fire data from Heilongjiang Province in 2009. Results show that improving the forest fire detection contextual algorithm to adapt HJ-IRS is feasible and highly accurate. HJ data are much more sensitive to smaller and cooler fires than MODIS or the AVHRR data, and the improved capabilities offers a good potential for application in forest fire detection. The improved algorithm process is shown in Figure 2.7.

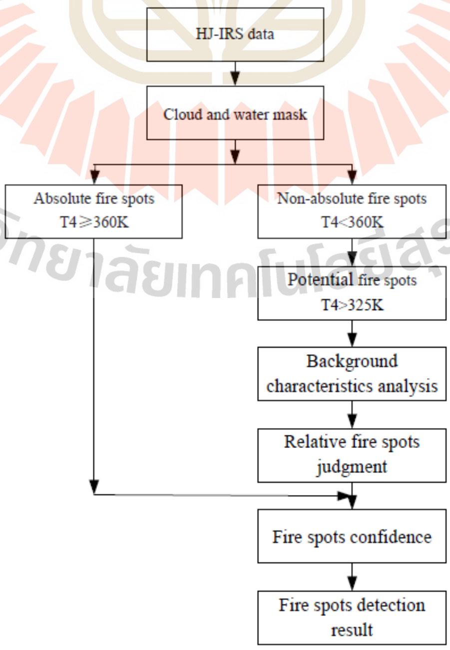

Source: Wang et al. (2012).

Figure 2.7 Fire detection process using HJ-IRS.

2.6.2 Validation of MODIS hotspot data

Hawbaker et al. (2008) carried out an accuracy assessment with reference fires mapped from independent Landsat data to assess the validity of active fire data or MODIS hotspot (MOD14/MYD14) across the United States. MODIS active fire detections were compared to 361 reference fires (larger fires, between 18 ha and 48,000 ha) that had been delineated using pre-fire and post-fire Landsat imagery. Reference fires were considered detected if at least oneMODIS active fire pixel occurred within 1 km of the edge of the fire. When active fire data from both Aqua and Terra were combined, 82% of all reference fireswere found, but detection rates were less for Aqua and Terra individually (73% and 66% respectively). Hence, their analysis is not apt to assess the detection rates for small fires, but they assume that many may go undetected. They further conclude that detection rates increased when fire records from both Aqua and Terra are used and also that detection rates increased with fire size.

Schroeder et al. (2008) implemented a comprehensive analysis to validate the MODIS and GOES satellite active fire detection products (MOD14 and WFABBA, respectively) on the Brazilian part of Amazonia and characterize their major sources of omission and commission errors which have important implications for a large community of fire data users. The analyses were primarily based on the use of 30 m resolution ASTER and ETM+ imagery as the validation data. Here in, the study found that at the 50% true positive detection probability mark, WFABBA requires four times more active fire area than is necessary for MOD14 to achieve the same probability of detection, despite the 16× factor separating the nominal spatial resolutions of the two products. Approximately 75% and 95% of all fires sampled were omitted by the MOD14 and WFABBA instantaneous products, respectively; whereas an omission error of 38%

was obtained for WFABBA when considering the 30-minute interval of the GOES data. Commission errors for MOD14 and WFABBAwere found to be similar and highly dependent on the vegetation conditions of the areas imaged, with the larger commission errors (approximately 35%) estimated over regions of active deforestation.

Tanpipat, Honda, and Nuchaiya (2009) validated the MODIS hotspot by using field survey data. A quantitative evaluation of hotspot products had been carried out during forest fire season in 2007, 2008, and 2009. The chosen hotspots were scattered throughout the country and within the protected areas of the National Parks and Wildlife Sanctuaries. Three areas were selected as test sites for validation guidelines. The results found high accuracy of 91.84%, 95.60% and 97.53% for the 2007, 2008, and 2009, respectively. In addition, fire seasons were increased confidence in the use of hotspots for forest fire control and management in Thailand.

CHAPTER III

RESEARCH METHODOLOGY

Equipment and details of research methodology include (1) data collection and preparation, (2) evaluation of the optimal top three burned area spectral indices, and (3) identification of an optimal burned area and fire detection algorithms are here explained in this chapter.

3.1 Equipment

Equipment includes hardware and software is summarized in Table 3.1.

Table 3.1 List of hardware and software.

Equipment		**Application**	**Source**
Hardware	Global Positioning System (GPS)	Ground surveying	Personnel
	Desktop computer	Data analysis and documentation	Personnel
	Notebook	Data analysis and documentation	Personnel
	Digital camera	Ground surveying	Personnel
	Laser printer	Documentation	Personnel

Table 3.1 (Continued) List of hardware and software.

Equipment		Application	Source
Software	Burned Area Mapping Software (BAMS)	Burned area extraction	www.bastarrika.wordpress.com
	ERDAS Imagine	Digital image processing	Remote sensing laboratory, SUT
	ENVI	Digital image processing	Remote sensing laboratory, SUT
	ESRI ArcMap	Geospatial analysis and mapping	Remote sensing laboratory, SUT
	SPSS Statistic software	Ordinal logistic regression analysis and decision tree construction	Remote sensing laboratory, SUT
	Microsoft Excel	Spectral indices calculation and reporting	Remote sensing laboratory, SUT

3.2 Research methodology

The framework of the research methodology, which aims to identify an optimal algorithm for burned area and fire detection using MODIS and Landsat data, is displayed in Figure 3.1. Under this framework, three main components include (1) data collection and preparation, (2) an optimal top three burned area spectral indices evaluation, and (3) an optimal burned and fire detection algorithm identification. Detail of each component is separately described below.

3.2.1 Data collection and preparation

The main collected input data for the study consists of remote sensing, GIS and field data about fires (both primary and secondary data) as shown in Table 3.2. Meanwhile, details of important collection and preparation data are separately summarized as follows.

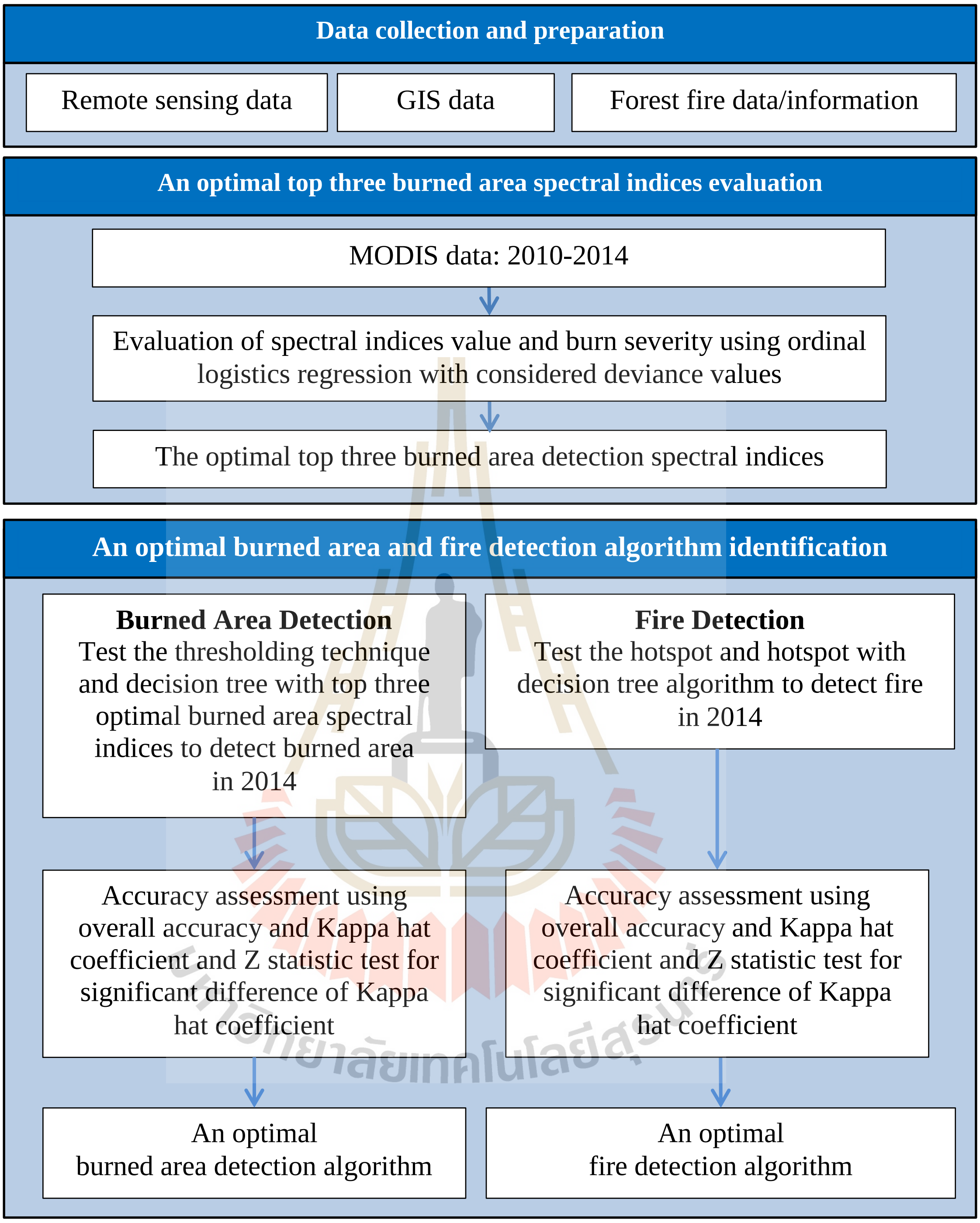

Figure 3.1 Workflow of research methodology framework.

Table 3.2 List of dataset used for the study.

NO.	Dataset	Data type	Source	Scale/ Resolution
1	Landsat data 2010-2014	Grid	GISTDA, USGS	30 m
2	MODIS Level 1B 2010-2014	Grid	LAADS	1 km
3	Hotspots data 2010-2014	Grid	LANCE-FIRMS	1 km
4	RFD fire record 2014	Point	Generate from RFD report	-
5	Spot height	Point	RTSD	1:50,000
6	Contour	Line	RTSD	1:50,000
7	Water body	Polygon	DWR	1:50,000
8	Stream/river	Line	DWR	1:50,000
9	Road	Line	RTSD	1:50,000
10	Village	Point	RTSD	1:50,000
11	Administrative boundary	Polygon	RTSD	1:50,000
12	Legal forest boundary	Polygon	RFD, DNP	1:50,000
13	Forest type	Polygon	RFD	1:50,000
14	Land use	Polygon	LDD	1:25,000
15	Elevation	Grid	Generate from DEM	1 km
16	Slope	Grid	Generate from DEM	1 km

Note:

LANCE	Land Atmosphere Near real-time Capability for EOS,
FIRMS	Fire Information for Resources Management System of NASA,
LAADS	Level 1 and Atmosphere Archive and Distribution System of NASA,
USGS	United States Geological Survey,
GISTDA	Geo-Informatics and Space Technology Development Agency,
RFD	Royal Forest Department,
RTSD	Royal Thai Survey Department,
DWR	Department of Water Resources,
DNP	Department of National Park Wildlife and Plant Conservation,
LDD	Land Development Department.

3.2.1.1 Landsat data

Landsat 5 TM data in 2010 and Landsat 8 OLI/TIRS data in 2013 and 2014 are downloaded from USGS website for burned area extraction using BAMS. The derived burned areas are further applied to classify burn severity data. Basic information of 16 scenes Landsat 5 TM and Landsat 8 OLI/TIRS in 2010, 2013, and 2014, which are firstly prepared and used for burned area extraction using BAMS for optimum burned area detection algorithm identification, is summarized in Table 3.3. It can be observed that during 2011 and 2012 there is unavailable Landsat data via USGS website. In addition, only one scene of Path 130 Row 47 and Path 131 Row 47 is available and they are extracted burned area by BAMS. Example of false color composite of Landsat 5 TM: Band 7, 4, and 2 (RGB), LT51300472010045 and Landsat 8 OLI/TIRS: Band 7, 5, and 3 (RGB), LC81300472014088 for burned area extraction is shown in Figure 3.2.

Table 3.3 List of used Landsat 5 TM and Landsat 8 OLI/TIRS data.

No	Path-Row	Year	Day	Date	Time	Satellite Data	Fire event for BAMS
1	130047	2010	029	29 January 2010	10:33	L5 TM	Pre-fire
2	130047	2010	045	14 February 2010	10:33	L5 TM	Post-fire
3	131047	2010	036	5 February 2010	10:39	L5 TM	Pre-fire
4	131047	2010	052	21 February 2010	10:39	L5 TM	Post-fire/Pre-fire
5	131047	2010	084	25 March 2010	10:39	L5 TM	Post-fire/Pre-fire
6	131047	2010	116	26 April 2010	10:39	L5 TM	Post-fire
7	130047	2013	101	11 April 2013	10:46	LS8 OLI/TIRS	Not applicable
8	131047	2013	108	18 April 2013	10:50	LS8 OLI/TIRS	Not applicable
9	130047	2014	040	9 February 2014	10:43	LS8 OLI/TIRS	Pre-fire
10	130047	2014	056	25 February 2014	10:43	LS8 OLI/TIRS	Post-fire/Pre-fire
11	130047	2014	072	13 March 2014	10:43	LS8 OLI/TIRS	Post-fire/Pre-fire
12	130047	2014	088	29 March 2014	10:42	LS8 OLI/TIRS	Post-fire
13	131047	2014	047	16 February 2014	10:49	LS8 OLI/TIRS	Pre-fire
14	131047	2014	063	4 March 2014	10:49	LS8 OLI/TIRS	Post-fire/Pre-fire
15	131047	2014	079	20 March 2014	10:49	LS8 OLI/TIRS	Post-fire/Pre-fire
16	131047	2014	095	5 April 2014	10:49	LS8 OLI/TIRS	Post-fire

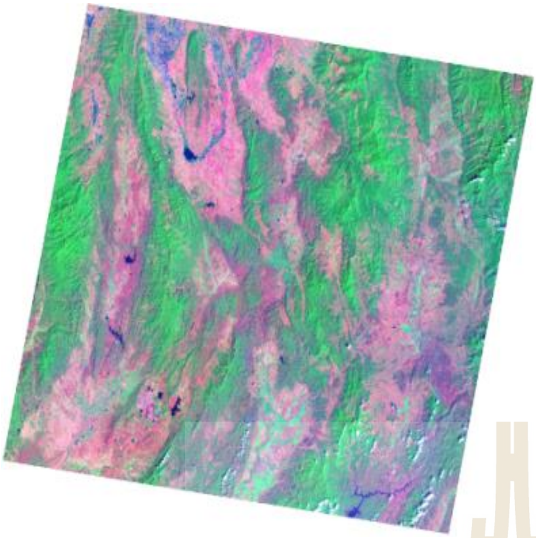 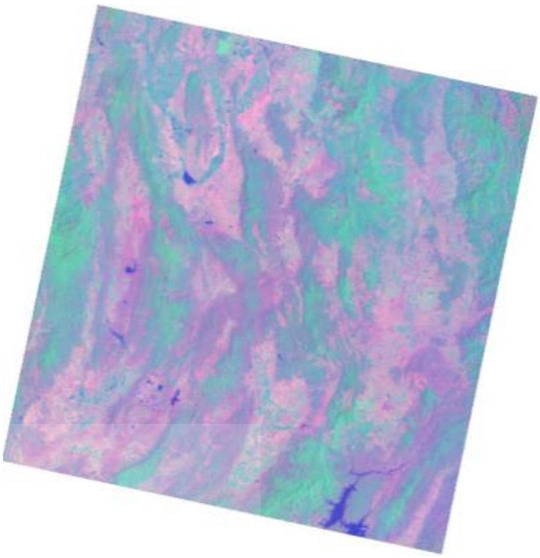

Landsat-5: LT51300472010045 Band 7, 4, and 2 (RGB)

Landsat-8: LC81300472014088 Band 7, 5, and 3 (RGB)

Figure 3.2 Example of false color composite of Landsat 5 and 8.

3.2.1.2 MODIS Level 1B

MODIS Terra/Aqua Level 1B calibrated radiances 1 km that covered the selected spectral band of spectral indices (MODIS/Terra called MOD021KM and MODIS/Aqua called MYD021KM) are obtained from LAADS, NASA. These data distributed through website http://www.ladsweb.nascom.nasa.gov/data/search.html. Basic information of 12 Scenes of MODIS Level 1B data, which are used to extract spectral index for identify an optimum top three burned area spectral indices, is summarized in Table 3.4. Herein, acquisition date of MODIS Level 1B data are related with acquisition date of Landsat for burned areas extraction using one day offset (date of burned area +1 day). Example of false color composite of MODIS Level 1B data: band 7, 2, 1 (RGB) of scene number 2010046.0350.005 and 2014089.0400.005 is shown in Figure 3.3.

Table 3.4 List of used MODIS Level 1B data.

No	MODIS Level 1B scene	Date	Time (Local Time)	Source
1	2010046.0350.005	15 February 2010	10.50 AM	LAADS
2	2010053.0400.005	22 February 2010	11.00 AM	LAADS
3	2010085.0350.005	26 March 2010	10.50 AM	LAADS
4	2010117.0400.005	27 April 2010	11.00 AM	LAADS
5	2013102.0350.005	12 April 2013	10.50 AM	LAADS
6	2013109.0400.005	19 April 2013	11.00 AM	LAADS
7	2014057.0350.005	26 February 2014	10.50 AM	LAADS
8	2014073.0350.005	14 March 2014	10.50 AM	LAADS
9	2014089.0400.005	30 March 2014	11.00 AM	LAADS
10	2014064.0400.005	5 March 2014	11.00 AM	LAADS
11	2014080.0400.005	21 March 2014	11.00 AM	LAADS
12	2014096.0400.005	6 April 2014	11.00 AM	LAADS

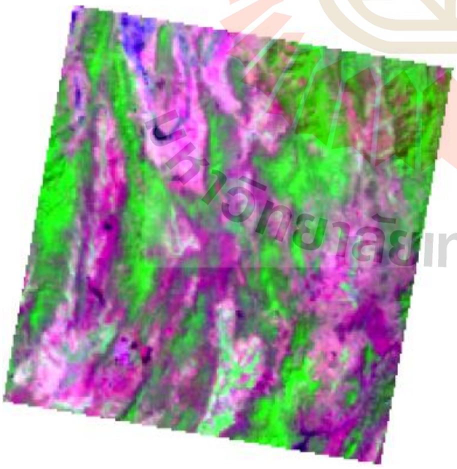

MODIS Level 1B: 2010046.0350.005

Band 7, 2, 1 (RGB)

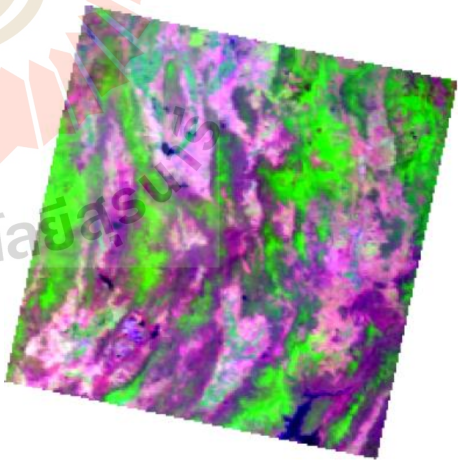

MODIS Level 1B: 2014089.0400.005

Band 7, 2, 1 (RGB)

Figure 3.3 Example of false color composite of MODIS data.

3.2.1.3 MODIS hotspot

MODIS hotspot calculated by the MODIS rapid response system and reported by LANCE-FIRMS with multiple reported fields are used in the study. The available fire data has distributed through website http://www.earth data.nasa.gov/data/near-real-time data/firms/active-fire-data (NASA FIRMS, 2015). The hotspots attribute fields include latitude and longitude at center point location, scan and track, acquisition date, time of the overpass of the satellite, satellite name, version of algorithm, brightness temperature of either channel 21 or 22 (BT21 or BT22), fire confidence percentage (FC), brightness temperature of channel 31 (BT31), and fire radiative power (FRP). In practice, after the downloaded hotspot data are imported to ArcGIS software, they are generated to be points and re-projected to be WGS 1984 coordinate system, UTM Zone 47 North. Available MODIS hotspot and its attribute data during fire season between 2010 and 2014 are pre-processing under ERSI ArcGIS software for an optimum algorithm for fire detection identification. Example of MODIS hotspot over study area, date 29 March 2014 is shown in Figure 3.4.

3.2.1.4 RFD fire record

Ground fire records in 2014 are obtained from RFD, the important field easting and northing coordinates are used to generate fire location as point of ArcGIS shape format. The important data include, date, time, place, burned area, and cause are attached as attribute data. The RFD fire records are applied as ancillary data for burn severity classification from Landsat data. Ground fire records of RFD in 2014 were extracted from daily fire report for accuracy assessment as shown Figure 3.5.

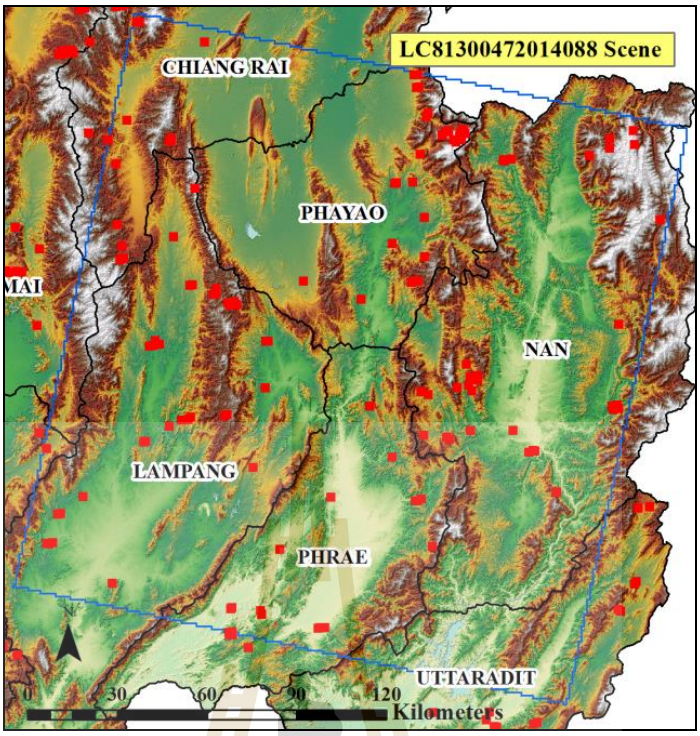

Figure 3.4 Example of MODIS hotspot distribution over study area: Date 29 March 2014.

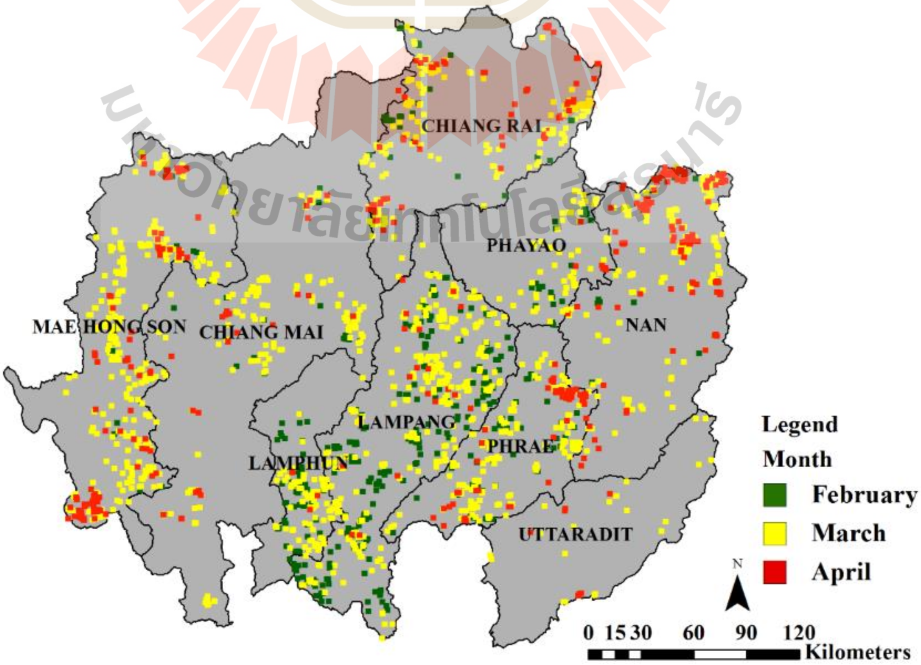

Figure 3.5 Distribution ground fire record by RFD during fire season in 2014.

3.2.1.5 GIS Data

The used GIS data in shape format includes the RFD fire record in 2014, spot height, contour, water body, stream/river, road, village, administrative boundary, legal forest boundary, forest type, land use and land cover, elevation, and slope, are used to construct hotspot detection algorithm by decision tree classification from MODIS hotspot data. These GIS dataset are collected and prepared in advanced for data analysis.

3.2.2 Evaluation of the optimal top three burned area spectral indices

Under this component, the extracted spectral indices values deriving from MODIS Level 1B and burn severity classes deriving from Landsat data using BAMS are used to calculate deviance under ordinal logistic regression analysis for an optimal top three burned spectral indices detection evaluation (Figure 3.6).

For burned area extraction, Landsat data of pre-and post-fire events are used as input data for burned area classification using BAMS. In practice, BAMS is firstly extract decision tree structure for burned area from pre- and post- fire images with "AND" logical operation based on spectral indices (NDVI, GEMI, NBR, BAIM, and MIRBI) from training area. Herein, the reflectance values are multiplied with a scale factor of 10,000, truncating the result into 16 bit integer data type. The derived decision trees are then combined to map burned area using two-phase burned area strategy for reducing commission and omission errors. (See detail in Section 2.5.3). Then burned areas are overlaid with 1x1 km grid that conforms to MODIS Level 1B pixel to calculate the percentage of burned area and reclassify burn severity into 5 classes (none, low, moderate, high, and very high). In addition, the extracted burned areas in 2014 is validated with ground fire survey data of RFD.

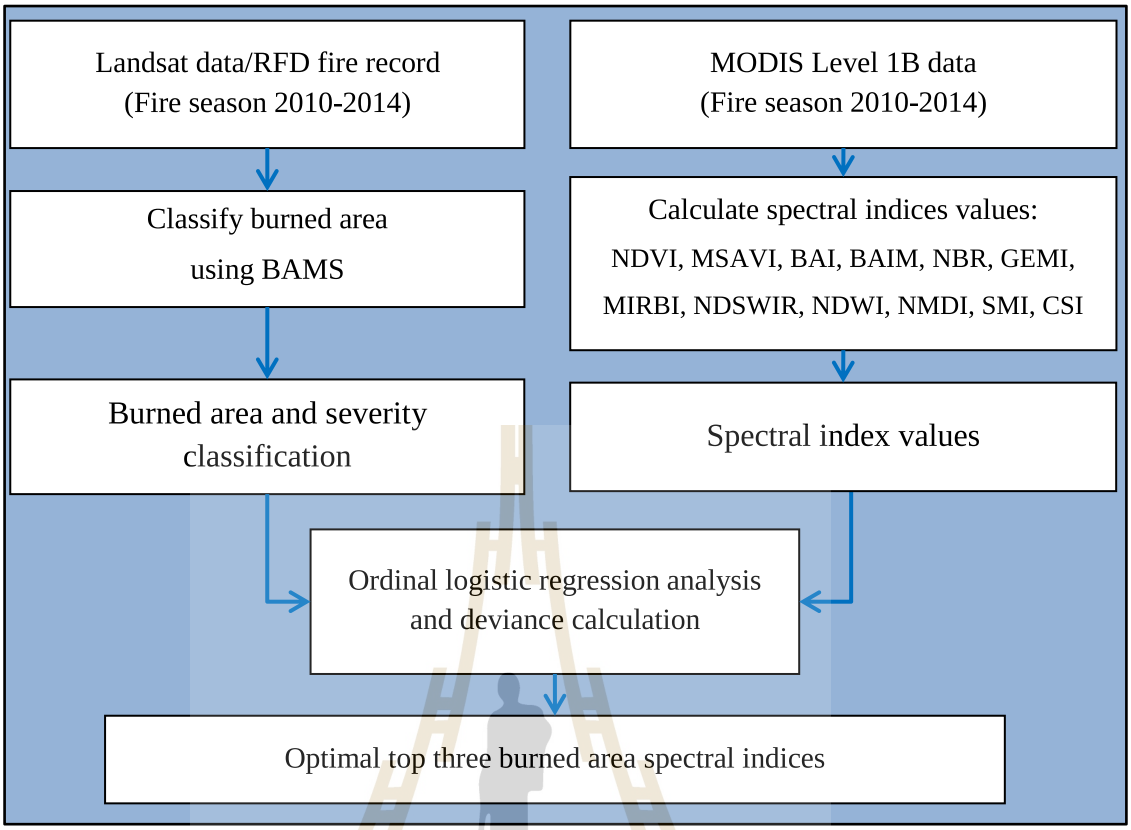

Figure 3.6 Schematic workflow of an optimal top three burned area spectral indices evaluation component.

For spectral indices values extractions, MODIS Level 1B are used to calculate the selected 12 spectral indices values (see formulae in Table 3.5). After that, ordinal logistic regression analysis is performed to compare spectral index values with burn severity by consideration of deviance values. The top three spectral indices which provide minimal deviance values are identified as optimal top three burned area spectral indices.

In practice, all deviance values of each spectral index from 12 different dates are then scoring and ranking from the best to worst fit for an optimal top three burned area spectral indices identification. The derived optimum top three spectral indices are further used to extract burned area in the next component.

For ordinal logistic regression analysis, dependent variable is an ordinal burn severity classes while spectral index values are independent variables. Hosmer and Lemeshow (2000) stated that the ordinal logistic regression model for a single independent variable can be written in equation form as:

$$ln\left[\frac{\pi_i(x)}{1-\pi_i(x)}\right] = \alpha_i + \beta_i X, \tag{3.1}$$

where $\pi_i(x)$ represents the probability of occurrence of the ordinal class i given the independent variable x. Separate intercept α_i and slope β_i coefficients are calculated for each ordinal class i. An ordinal logistic regression model uses the maximum likelihood approach to estimate regression coefficients.

The goodness of fit of the ordinal logistic regression model can be estimated using the deviance (D) (Hosmer and Lemeshow, 2000) as:

$$D = -2\sum_i^m \sum_j^n \left[y_{i,j} \times ln\left(\frac{\hat{\pi}_{i,j}}{y_{i,j}}\right) + (1-y_{i,j}) \times ln\left(\frac{1-\hat{\pi}_{i,j}}{1-y_{i,j}}\right)\right], \tag{3.2}$$

where $y_{i,j}$ denotes a dichotomous outcome variable for class i,

$\hat{\pi}_{i,j}$ is the maximum likelihood estimate of $\pi_i(x_j)$,

m is the number of ordinal classes, and

n is the sample size.

In a similar way, deviance can be thought as the residual sum of squares in ordinary linear regression models. A lower D values thus represent a better goodness of fit. In this study D is used to compare the performance of the different spectral indices as predictor of burn severity.

Table 3.5 List of 12 selected spectral indices for ordinal logistic regression analysis.

Spectral Index	Abbreviation	Formula
Normalized Burn Ratio	NBR	NBR = (NIR - lSWIR)/(NIR + lSWIR)
Burned Area Index	BAI	BAI = $1/((\text{NIR} - 0.06)^2 + (\text{red} - 0.1)^2)$
Burned Area Index Modified	BAIM	BAIM = $1/((\text{NIR} - 0.05)^2 + (\text{lSWIR} - 0.2)^2)$
Char Soil Index	CSI	CSI = NIR/lSWIR
Normalized Difference Shortwave Infrared	NDSWIR	NDSWIR = (NIR - sSWIR)/(NIR + sSWIR)
Normalized Difference Vegetation Index	NDVI	NDVI = (NIR - red)/(NIR + red)
Modified Soil Adjusted Vegetation Index	MSAVI	MSAVI = $(2\text{NIR} + 1 - ((2\text{NIR} + 1)^2 - 8(\text{NIR} - \text{red}))^{1/2})/2$
Global Environment Monitoring Index	GEMI	GEMI = $\gamma(1 - 0.25\,\gamma) - ((\text{Red} - 0.125)/(1 - \text{Red}))$ with $\gamma = (2(\text{NIR}^2 - \text{Red}^2) + 1.5\text{NIR} + 0.5\text{Red})/(\text{NIR} + \text{Red} + 0.5)$
Mid InfraRed Burn Index	MIRBI	MIRBI = 10lSWIR - 9.8sSWIR + 2
Normalized Difference Water Index	NDWI	NDWI = (NIR - sSWIR)/(NIR + sSWIR)
Normalized Multi-band Drought Index	NMDI	NMDI = (NIR - (sSWIR - lSWIR))/(NIR + (sSWIR - lSWIR))
SWIR-MIR Index	SMI	SMI = (sSWIR - MIR)/(sSWIR + MIR)

Remark: The corresponding wavebands of MODIS were 0.620-0.670 µm (red), 0.841-0.876 µm (NIR), 1.628-1.652 µm (sSWIR), 2.105-2.155 µm (lSWIR), and 3.929-3.989 µm (MIR), that respectively in bands 1, 2, 6, 7, and 21.

3.2.3 An optimal burned area and fire detection algorithm identification

In this component, there are two main tasks include (1) the identification of an optimal burned area detection algorithm based on thresholding technique and decision tree method and (2) identification of an optimal fire detection algorithm based on MODIS hotspot and MODIS hotspot with Decision Tree (Figure 3.7).

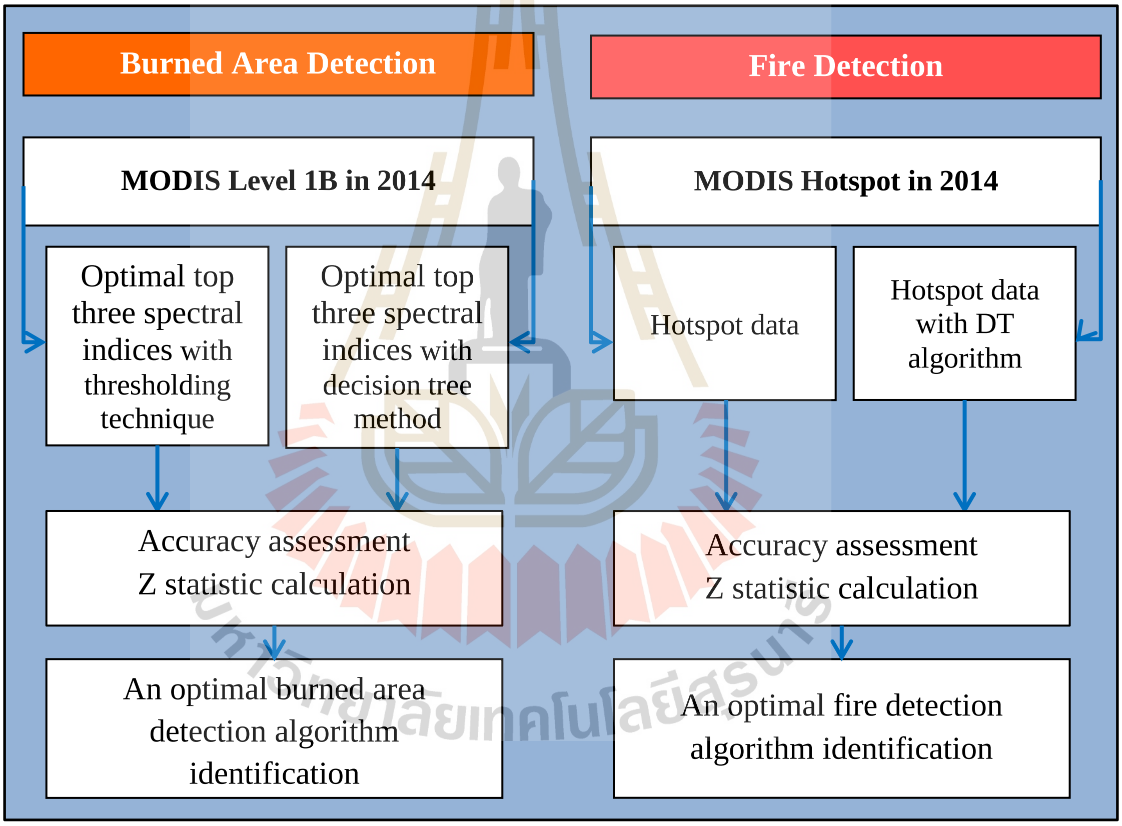

Figure 3.7 Schematic workflow of identification algorithm for burned area and fire detection using MODIS data component.

3.2.3.1 Identification of an optimal burned area detection algorithm

In this study, two approaches are applied to identify optimum burned area detection. The first approach, the derived spectral index data from MODIS Level 1B dataset in 2014 based on top three optimum spectral indices from the previous component are directly applied to classify burned and unburned data by Thresholding techniques (Yang, Skidmore, Melick, Zhou, and Xu, 2006). In the study, the whole range of the derived spectral indices (minimum and maximum values) are here examined for thresholding value setting. The minimum value as initial value is constantly added by an appropriate constant value for the sequential threshold values until they reach the maximum value.

In practice, an extracted burned and unburned areas are considered based on the percentage of burned area from Landsat 8 data that acquired in peak fire season in 2014 over 1 sq. km grid of MODIS data. If percent of burned area in grid equal or more than 25%, it will classifies as burned grid. Meanwhile, the derived top three spectral indices are also further analyzed under SPSS software to classify burned and unburned area using CRT algorithm in the second approach. Herein, dependent variable is burned and unburned areas derived from Landsat 8 and independent variables are top three spectral data and its combination.

After that the derived output from both approaches are then compared with Landsat data, RFD fire reports and field survey for accuracy assessment. An overall accuracy and Kappa hat coefficient are here calculated with references data according to confusion matrix (see Table 3.6).

Table 3.6 Confusion matrices for burned area/fire detection and its calculation.

Reference data	**Burned area/Fire detection data**	
	Burned/Fire	**Unburned/Non-fire**
Burned/Fire	a	b
Unburned/Non-fire	c	d

In practice, the overall accuracy of the burned area or fire detection rate, are evaluated as the proportion of the total number of correct hits as:

$$\text{Overall accuracy} = (a + d) / (a + b + c + d). \tag{3.3}$$

The burned area/fire detection rate is defined as the ratio of burned/fire cases that are detected correctly by test method to the total number of the events as:

$$\text{Burned area/Fire detection rate} = a / (a + b). \tag{3.4}$$

The false alarm rate (commission error) is the proportion of unburned/non-fire cases that are incorrectly classified as:

$$\text{False alarm rate} = c / (c + d). \tag{3.5}$$

In addition, calculating the value of K_{hat} as follows:

$$K_{hat} = \frac{N\sum_{i=1}^{r} x_{ii} - \sum_{i=1}^{r}(x_{i+} \times x_{+i})}{N^2 - \sum_{i=1}^{r}(x_{i+} \times x_{+i})}, \tag{3.6}$$

Where r is the number of column/row of the error matrix,

N is the total number of observations,

x_{ii} is the number of coincident observations (diagonal elements in the matrix)

x_{i+} and x_{+i} are the marginal totals for row i and column i respectively.

K_{hat} value represents the proportion of agreement between two categorical maps after chance agreement is removed. A value of $K_{hat} = 0$, represent the level of agreement expected for two random maps, and $K_{hat} = 1$, represent perfect agreement.

Furthermore, significant different of accuracy based on Kappa hat coefficients among top three spectral indices under the first approach and between the first and second approaches are tested using standard normal distribution or Z statistics as suggestion by Congalton and Green (2008) as:

$$Z = \frac{|\widehat{K_1} - \widehat{K_2}|}{\sqrt{\widehat{var}(\widehat{K_1}) + \widehat{var}(\widehat{K_2})}}, \tag{3.7}$$

where Z is normalized and standard normal distribution,

$\widehat{K_1}$ is K_{hat} for dataset I,

$\widehat{K_2}$ is K_{hat} for dataset II,

$\widehat{var}(\widehat{K_1})$ is variance of K_{hat} for dataset I, and

$\widehat{var}(\widehat{K_2})$ is variance of K_{hat} for dataset II.

At the same time, variance of K_{hat} is calculated by

$$\widehat{var}(\widehat{K}) = \frac{1}{n}\left\{\frac{\theta_1(1-\theta_1)}{(1-\theta_2)^2} + \frac{2(1-\theta_1)(2\theta_1\theta_2-\theta_3)}{(1-\theta_2)^3} + \frac{(1-\theta_1)^2(\theta_4-4\theta_2{}^2)}{(1-\theta_2)^4}\right\}, \tag{3.8}$$

where $\theta_1 = \frac{1}{n}\sum_{i=1}^{k} n_{ii}$,

$\theta_2 = \frac{1}{n^2}\sum_{i=1}^{k} n_{i+}n_{+i}$,

$\theta_3 = \frac{1}{n^2}\sum_{i=1}^{k} n_{ii}(n_{i+} + n_{+i})$, and

$\theta_4 = \frac{1}{n^3}\sum_{i=1}^{k}\sum_{j=1}^{k} n_{ij}(n_{j+} + n_{+i})^2$.

Herewith, given the null hypothesis H_0: $(\widehat{K_1} - \widehat{K_2}) = 0$, and the alternative H_1: $(\widehat{K_1} - \widehat{K_2}) \neq 0$, H_0 is rejected if $Z \geq Z_{\alpha/2}$, where $\alpha/2$ is the confidence level of the two-tailed Z test and the degrees of freedom are assumed to be ∞ (infinity).

Finally, an optimal burned area detection algorithm is then identified according to overall accuracy, Kappa hat coefficient with pair-wise Z-test. Herein, Z-test statistics that only use in case of the compared method has overall accuracy are very similar.

3.2.3.2 Identification of an optimal fire detection algorithm

MODIS hotspot data with MOD14/MYD14 algorithm and MODIS hotspot data with Decision Tree algorithm are here used to identify an optimal fire detection algorithm. In practice, MODIS hotspot dataset (MOD14/MYD14 algorithm) in 2014 are directly assessed thematic accuracy using overall accuracy and Kappa hat coefficient. Meanwhile the MODIS hotspot with Decision Tree classifications are examined based on the combination of the selected 13 biophysical factors including elevation, slope, NDVI, distance from stream, distance from water body, distance from road, distance from village, distance from fire ground survey, distance from agricultural area, distance from shifting cultivation, distance from evergreen forest, distance from deciduous forest, and distance from degraded forest. Finally, an optimal fire detection algorithm is then identified according to overall accuracy.

For decision tree construction, hotspots from 2014 are firstly imported to ArcGIS software and then separated hotspot into two groups: “false” and “true” with new attribute of 1 and 2, respectively. In this study, all hotspots are compared with Landsat data and RFD fire information for false and true identification. At the same time, the biophysical factors for all identified hotspots are extracted. After that attribute data of false and true hotspots as dependent variable and biophysical data as independent variables are exported as spreadsheet format to SPSS software for decision tree construction. Herein, decision tree structure is created based on the relationship between attribute values of dependent (false and true hotspots) and independent variables (biophysical attributes) with CRT algorithm. The extracted decision tree structure is then used to classify hotspots in 2014.

CHAPTER IV

RESULTS AND DISCUSSION

The main results for identification of an optimal burned area and fire detection algorithm using MODIS and Landsat data which included (1) optimum top three burned area spectral indices evaluation (2) optimum burned area detection algorithm identification and (3) optimum algorithms for fire detection identification were here separately explained and discussions.

4.1 Optimal top three burned area spectral indices evaluation

Results and findings under this section were separately explained and discussed according to major tasks of the optimal top three burned area spectral indices evaluation in the following sections.

4.1.1 Burned area extraction

Figure 4.1 shows the appearance of burned area and major land cover in various locations for visual interpretation of training area identification using BAMS. Herewith, Landsat 8 OLI/TIRS with color combination of band 7, 5, and 3 (RGB), active fire appears as orange to red, vegetation is green, cloud is white, and bare land is light pink and orange. In addition, heavily burned area appears as dark magenta while partially burned area appears as light magenta.

The development of fire can be sequentially identified in three stages: pre-fire, active fire and post-fire based on the continuity of Landsat acquisition date as shown in Figure 4.2. In addition, MODIS hotspot data as ancillary data for visual interpretation had overlaid on Landsat data to verify burned area as shown in Figure 4.3.

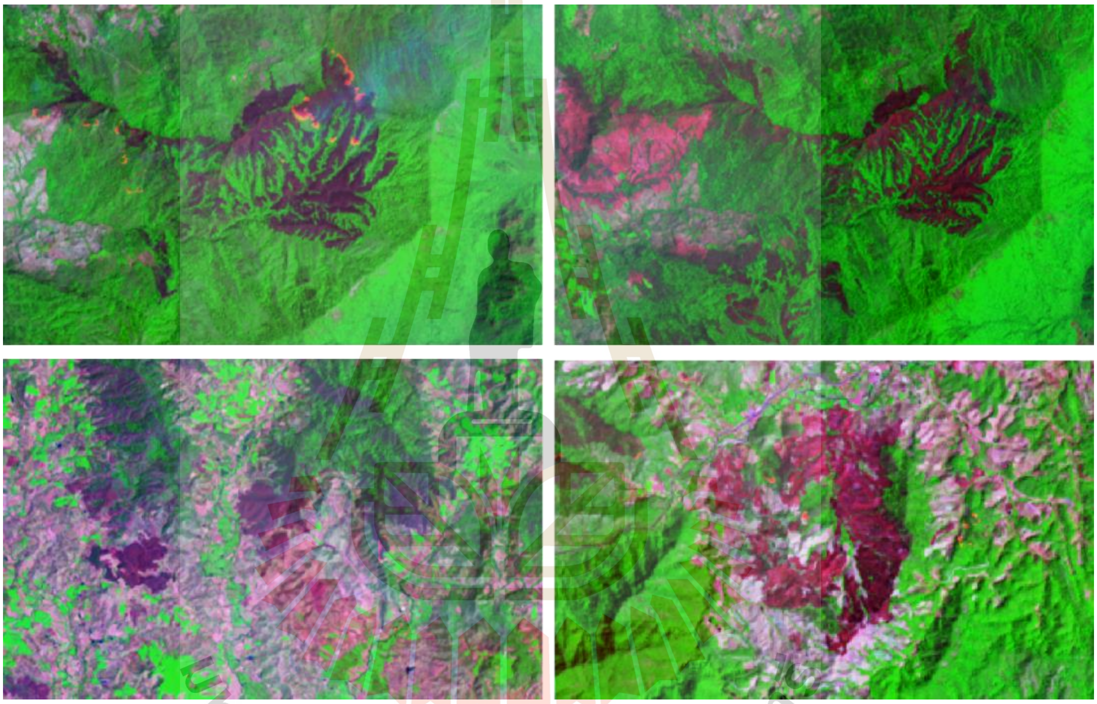

Figure 4.1 Appearance of burned area with major land cover in various locations on color composite image of Landsat-8: Band 7, 5, and 3 (RGB).

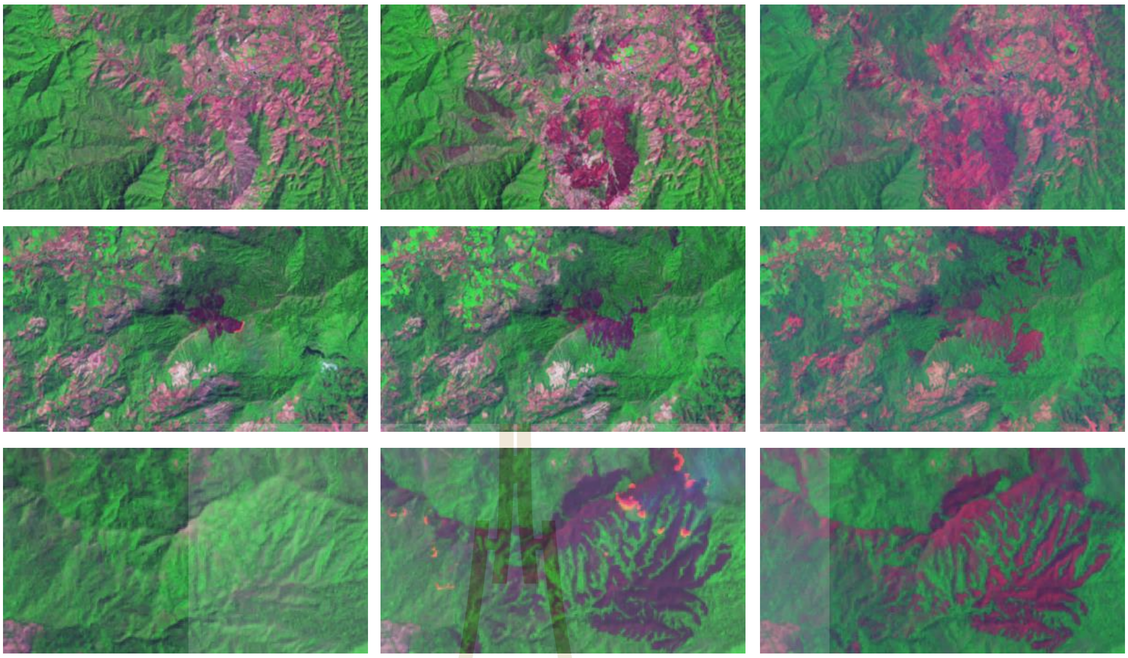

(a) (b) (c)

Figure 4.2 Development of fire: (a) pre-fire: (25 February 2014), (b) active fire: (13 March 2014), and post-fire: (29 March 2014).

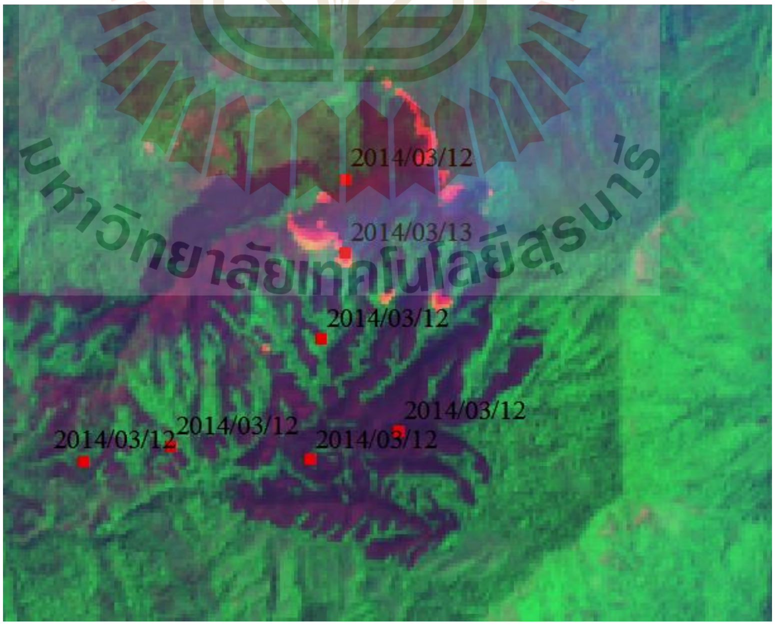

Figure 4.3 MODIS hotspot data as ancillary data overlaid on Landsat data (13 March 2014) for visual interpretation.

The result of burned area extraction for a pair of Landsat scene using BAMS based on threshold values, which were derived from training areas from multi-temporal difference (pre- and-post fire scenes) of spectral indices, that reflectance values are multiplied with a scale factor of 10,000, is summarized as raster map algebra in Table 4.1. Two raster maps algebra of first and second phases were here used two-phase burned area strategy to generate burned area map. Figure 4.4 shows an example of small and large patch of burned area extraction using BAMS and multi-temporal change of burned area is displayed in Figure 4.5.

Meanwhile, the result of burned area extraction for no pair of Landsat scene (pre- and-post fire scenes) in 2013 (Scene 130047 and 131047) which were extracted using Expert System under ERDAS Imagine is summarized in Table 4.2. Herein, BAMS was firstly applied to create TOA reflectance and spectral indices (NDVI, BAIM, GEMI, NBR, and MIRBI) and then identified minimum and maximum value of burned training areas for burned area mapping under Expert System.

Area and percentage of burned area for 12 Landsat scenes is summarized in Table 4.3 and distribution of burned area of each Landsat scene in 2010, 2013 and 2014 is displayed in Figure 4.6.

As results, it can be observed that the highest burned area during fire season (February to April) in 2014 occurs in March, and it covers area about 1,187.62 sq. km or 1.87%. (See detail in Table 4.3).

Table 4.1 Threshold values extraction using supervised training area of two-phase algorithm.

Scene	First phase	Second phase	Remark
1300472010	BAIM ≥ 62 and Diff_BAIM ≥ -139 and NBR ≤ 537 and Diff_NBR ≤ 1,121 and NDVI ≤ 2,753 and Diff_NDVI ≤ 576 and GEMI ≤ 4,647 and Diff_GEMI ≤ 593 and MIRBI ≥ 13,548 and Diff_MIRBI ≥ -1,831	BAIM ≥ 53 and Diff_BAIM ≥ -1 and NBR ≤ 1,924 and Diff_NBR ≤ -64 and NDVI ≤ 2,027 and Diff_NDVI ≤ -818 and GEMI ≤ 4,352 and Diff_GEMI ≤ -408 and MIRBI ≥ 15,796 and Diff_MIRBI ≥ 1,832	Pre-fire image: 29 January 2010 Post-fire image: 14 February 2010 Apply for burned area date: 14 February 2010
1310472010	BAIM ≥ 48 and Diff_BAIM ≥ -123 and NBR ≤ 1,047 and Diff_NBR ≤ 1,186 and NDVI ≤ 2,331 and Diff_NDVI ≤ 139 and GEMI ≤ 4,861 and Diff_GEMI ≤ 854 and MIRBI ≥ 13,749 and Diff_MIRBI ≥ -2,172	BAIM ≥ 37 and Diff_BAIM ≥ -16 and NBR ≤ 2,182 and Diff_NBR ≤ -1,736 and NDVI ≤ 2,354 and Diff_NDVI ≤ -1,424 and GEMI ≤ 4,455 and Diff_GEMI ≤ -398 and MIRBI ≥ 16,478 and Diff_MIRBI ≥ 1,084	Pre-fire image: 21 February 2010 Post-fire image: 25 March 2010 Apply for burned area date: 21 February 2010 25 March 2010 26 April 2010
1300472014	BAIM ≥ 42 and Diff_BAIM ≥ -32 and NBR ≤ 2,736 and Diff_NBR ≤ 722 and NDVI ≤ 3,347 and Diff_NDVI ≤ 699 and GEMI ≤ 729 and Diff_GEMI ≤ 161 and MIRBI ≥ 15,321 and Diff_MIRBI ≥ -1,725	BAIM ≥ 47 and Diff_BAIM ≥ -17 and NBR ≤ 2,463 and Diff_NBR ≤ 708 and NDVI ≤ 2,779 and Diff_NDVI ≤ 595 and GEMI ≤ 687 and Diff_GEMI ≤ 644 and MIRBI ≥ 15,717 and Diff_MIRBI ≥ -1,672	Pre-fire image: 13 March 2014 Post-fire image: 29 March 2014 Apply for burned area date: 25 February 2014 13 March 2014 29 March 2014
1310472014	BAIM ≥ 35 and Diff_BAIM ≥ -45 and NBR ≤ 3,102 and Diff_NBR ≤ 1,198 and NDVI ≤ 3,714 and Diff_NDVI ≤ 1,655 and GEMI ≤ 533 and Diff_GEMI ≤ 49 and MIRBI ≥ 14,342 and Diff_MIRBI ≥ -3,534	BAIM ≥ 42 and Diff_BAIM ≥ -37 and NBR ≤ 2,839 and Diff_NBR ≤ 1,394 and NDVI ≤ 3,387 and Diff_NDVI ≤ 1,655 and GEMI ≤ 554 and Diff_GEMI ≤ 768 and MIRBI ≥ 15,537 and Diff_MIRBI ≥ -3,739	Pre-fire image: 20 March 2014 Post-fire image: 5 April 2014 Apply for burned area date: 4 March 2014 20 March 2014 5 April 2014

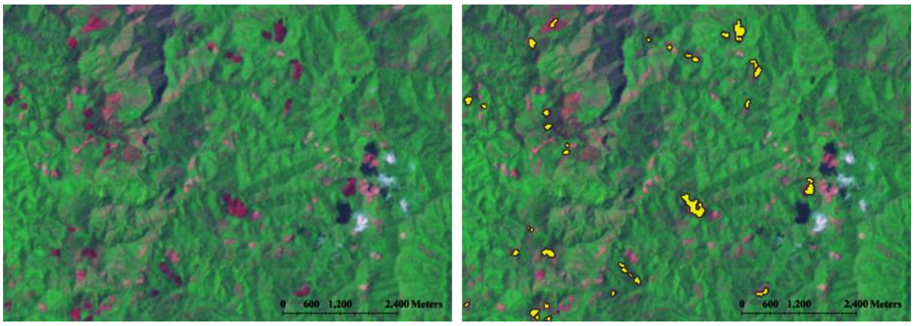

(a)

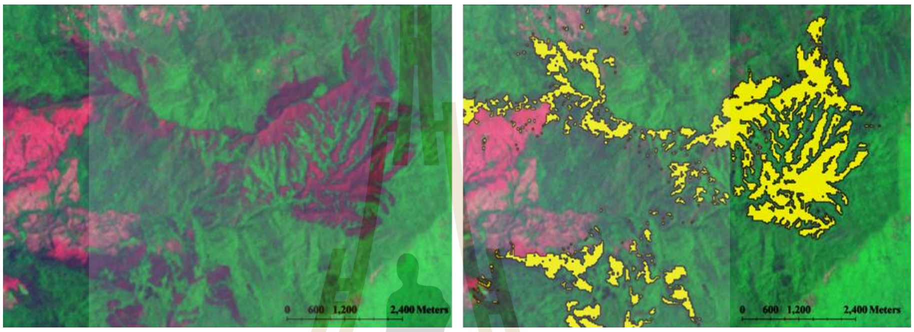

(b)

Figure 4.4 Example of burned area extraction using BAMS: (a) small patch and (b) large patch.

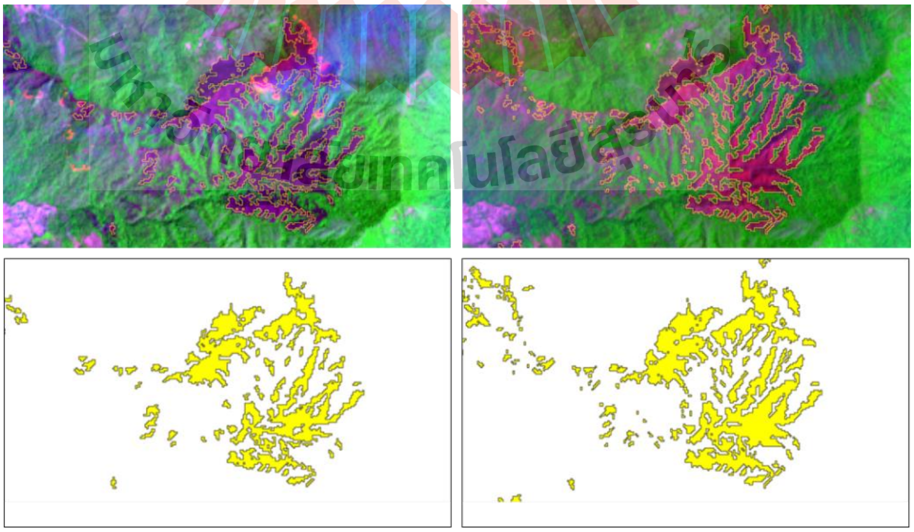

13 March 2014 29 March 2014

Figure 4.5 Multi-temporal burned area comparison between 13 March 2014 and 29 March 2014.

Table 4.2 Decision tree structure for burned area extraction of no-pair Landsat data.

Scene	Second iteration	Remark
1300472013	Min_BAIM > 40 and Max_BAIM ≤ 74 and Min_GEMI > 1 and Max_GEMI ≤ 203 and Min_MIRBI > 11,723 and Max_MIRBI ≤ 19,638 and Min_NBR > 2 and Max_NBR ≤ 1,796 and Min_NDVI > 799 and Max_NDVI ≤ 2,893	Apply for burned area date: 11 April 2013
1310472013	Min_BAIM > 62 and Max_BAIM ≤ 251 and Min_GEMI > 123 and Max_GEMI ≤ 627and Min_MIRBI > 16,563 and Max_MIRBI ≤ 21,199 and Min_NDVI > 1,589 and Max_NDVI ≤ 2,873	Apply for burned area date: 18 April 2013

Table 4.3 Area and percentage of burned area for 12 Landsat scenes.

No.	Scene ID	Date	Total area (sq.km)	Burned area (sq.km)	Burned area (%)
1	LT51300472010045	14 February 2010	31,729.62	276.17	0.87
2	LT51310472010052	21 February 2010	31,718.22	148.11	0.47
3	LT51310472010084	25 March 2010	31,718.22	382.98	1.21
4	LT51310472010116	26 April 2010	31,718.22	104.33	0.33
5	LC81300472013101	11 April 2013	31,729.62	73.68	0.23
6	LC81310472013108	18 April 2013	31,718.22	92.24	0.29
7	LC81300472014056	25 February 2014	31,729.62	175.83	0.55
8	LC81300472014072	13 March 2014	31,729.62	626.11	1.97
9	LC81300472014088	29 March 2014	31,729.62	234.66	0.74
10	LC81310472014063	4 March 2014	31,718.22	504.91	1.59
11	LC81310472014079	20 March 2014	31,718.22	561.52	1.77
12	LC81310472014095	5 April 2014	31,718.22	389.51	1.23

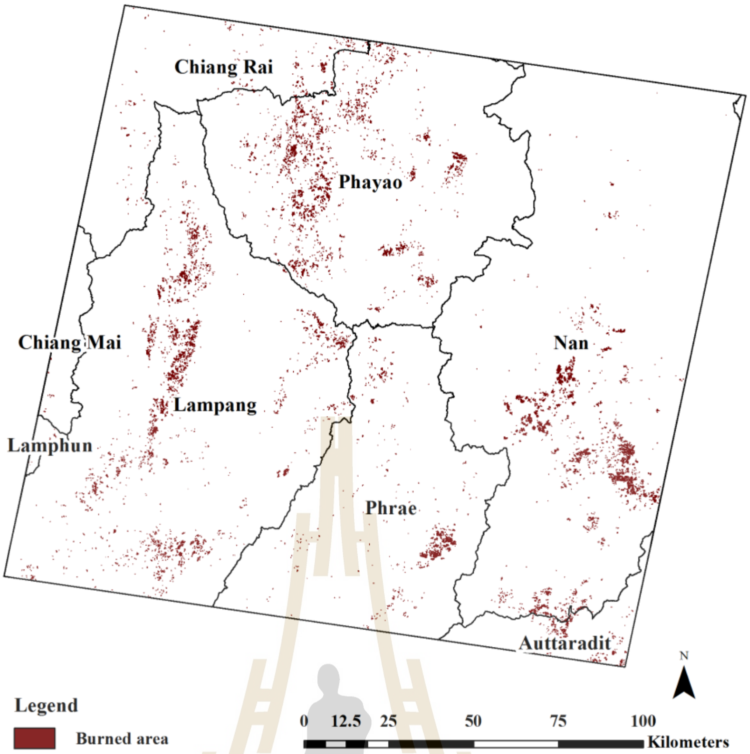

LT51300472010045; 14 February 2010

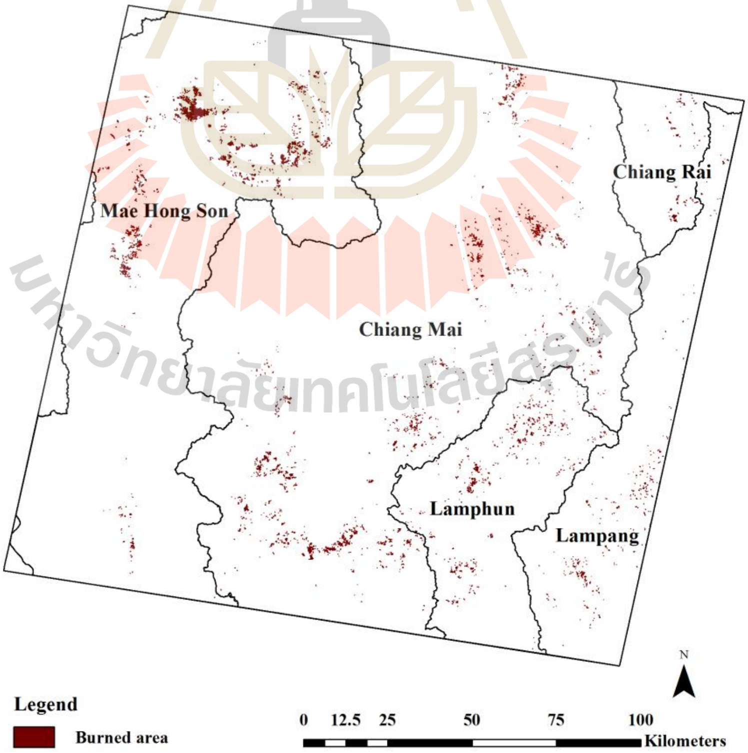

LT51310472010052; 21 February 2010

Figure 4.6 Distribution of burned area for 12 Landsat scenes.

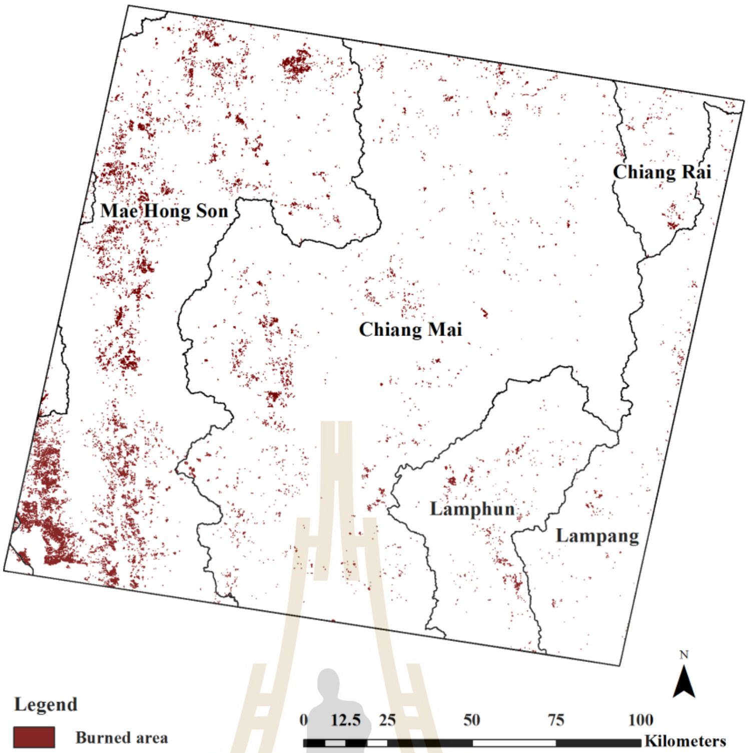

LT51310472010084; 25 March 2010

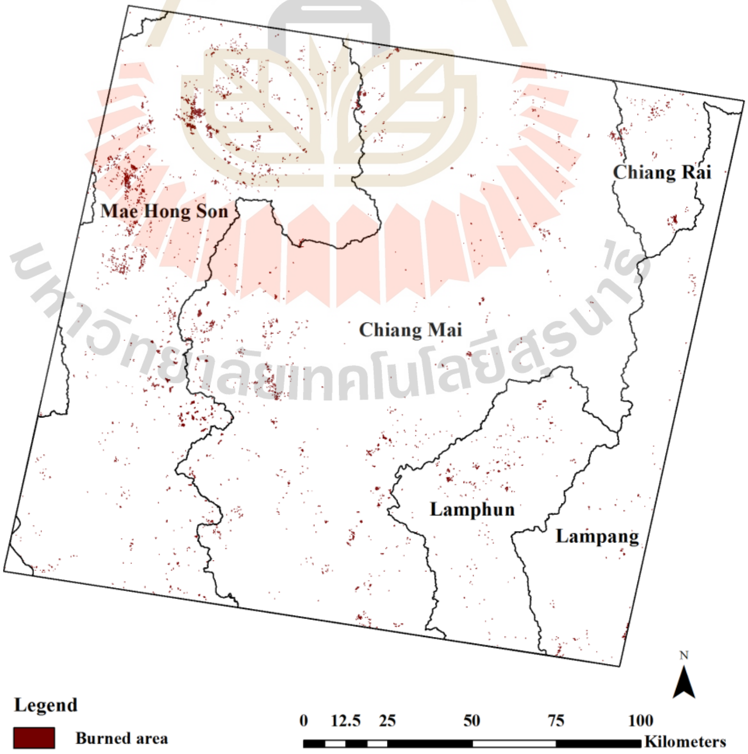

LT51310472010116; 26 April 2010

Figure 4.6 (Continued) Distribution of burned area for 12 Landsat scenes.

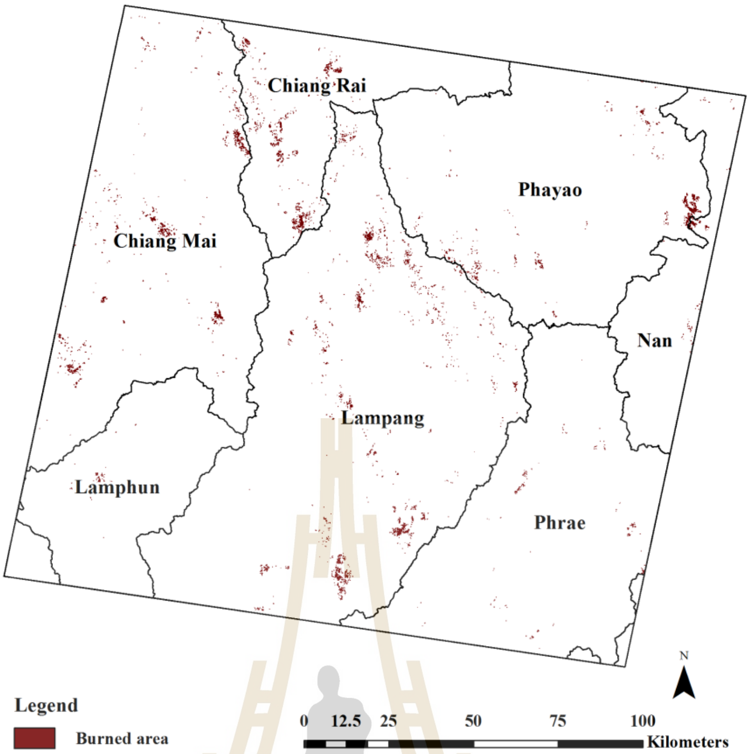

LC81300472013101; 11 April 2013

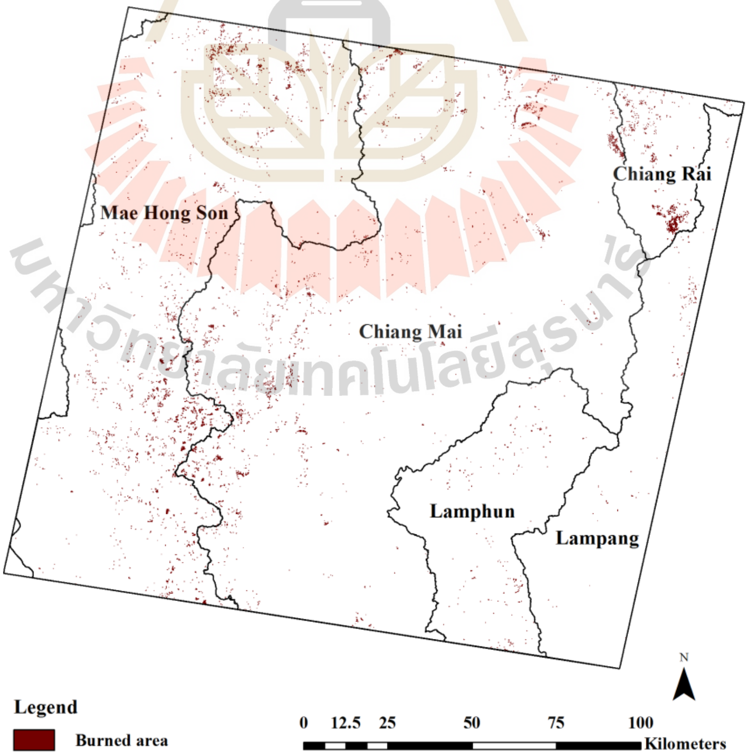

LC81310472013108; 18 April 2013

Figure 4.6 (Continued) Distribution of burned area for 12 Landsat scenes.

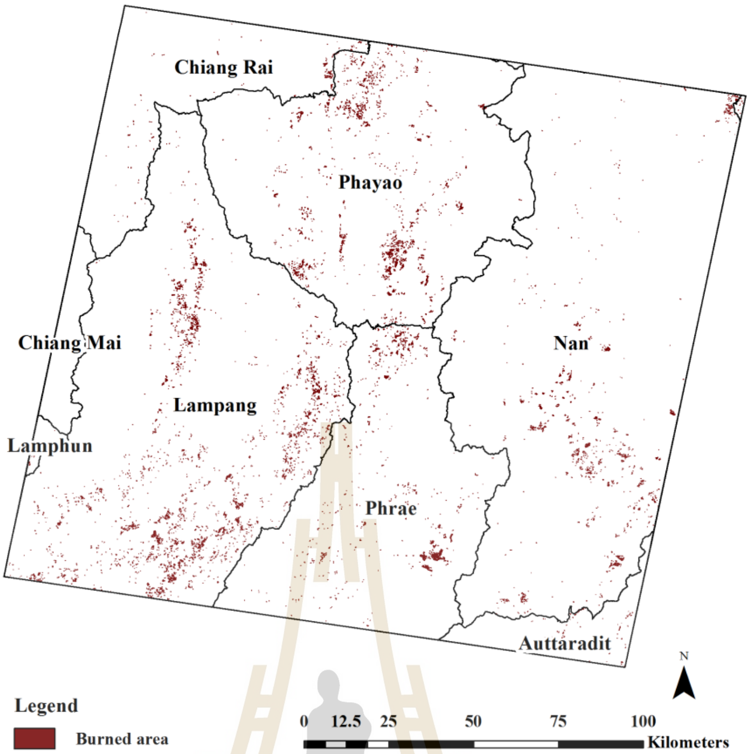

LC81300472014056; 25 February 2014

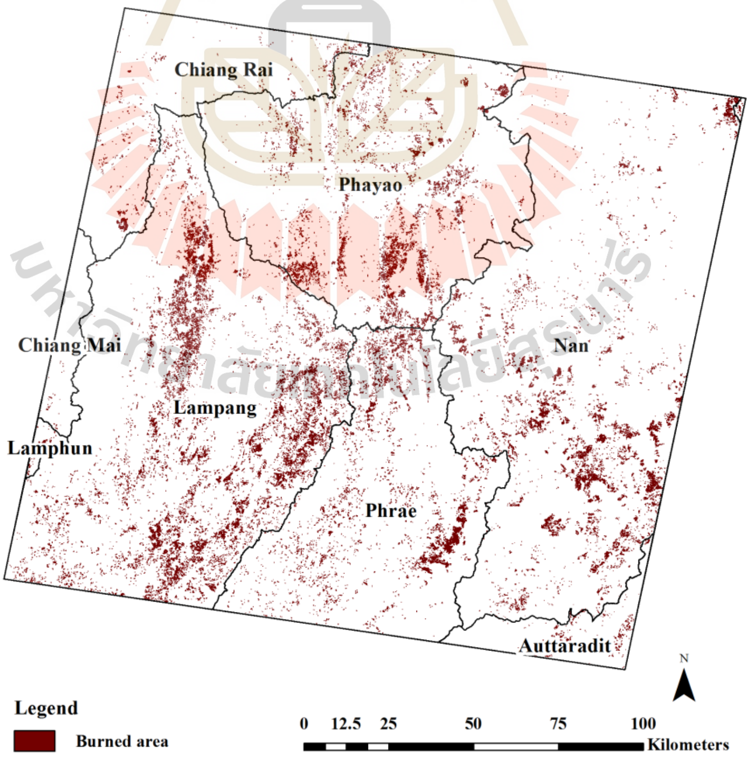

LC81300472014072; 13 March 2014

Figure 4.6 (Continued) Distribution of burned area for 12 Landsat scenes.

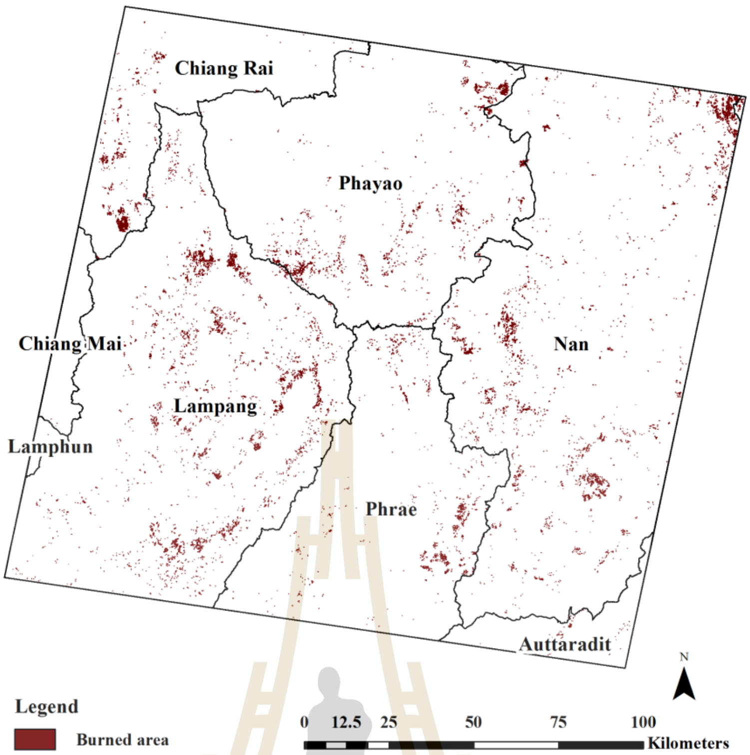

LC81300472014088; 29 March 2014

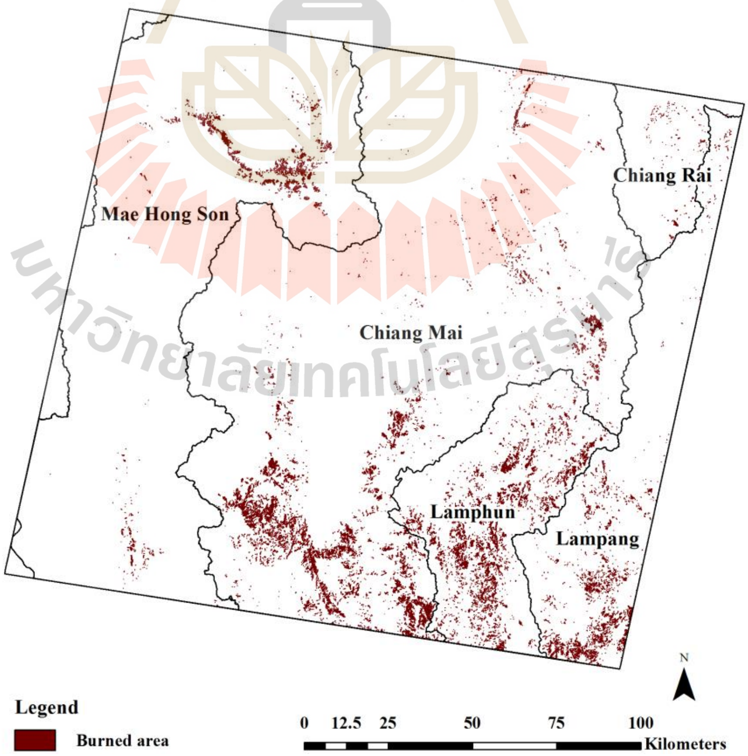

LC81310472014063; 4 March 2014

Figure 4.6 (Continued) Distribution of burned area for 12 Landsat scenes.

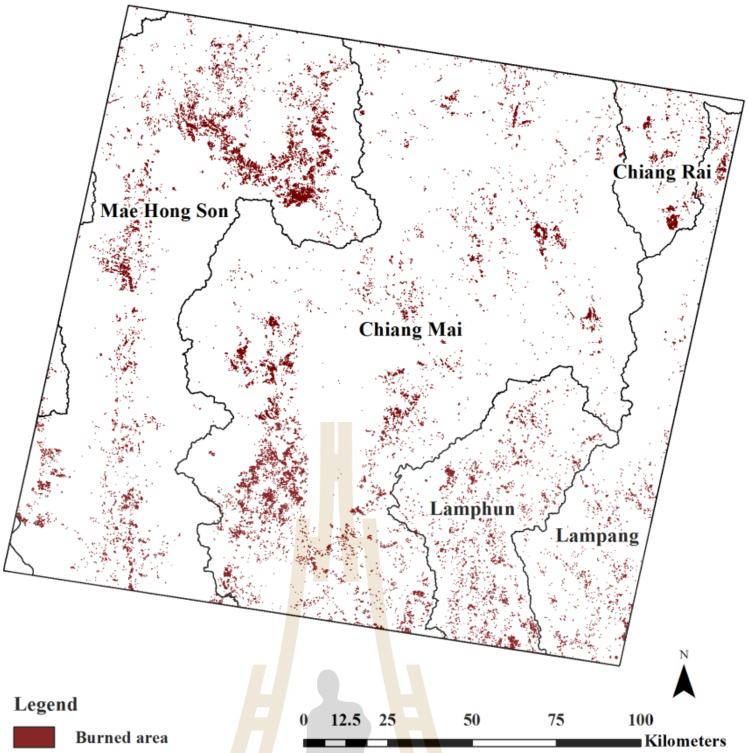

LC81310472014079; 20 March 2014

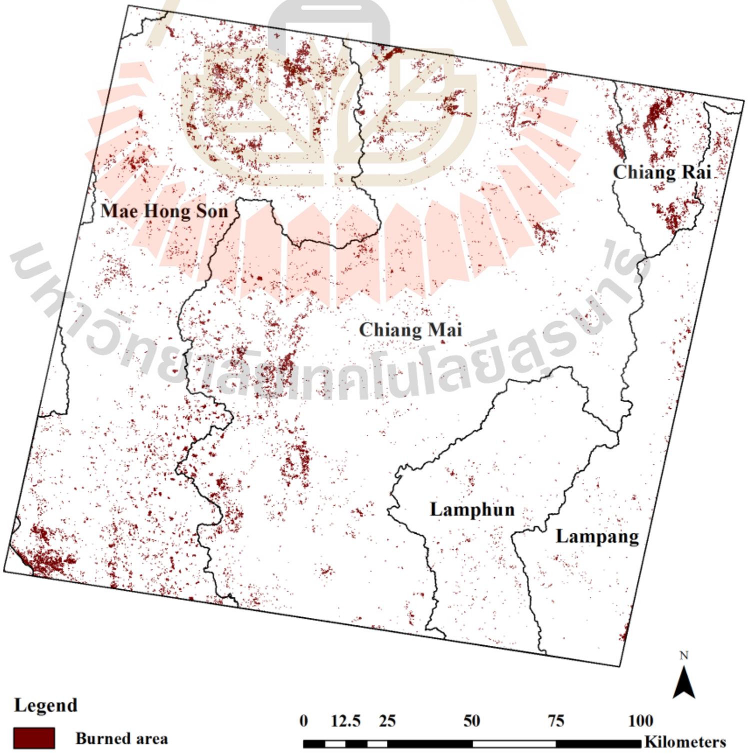

LC81310472014095; 5 April 2014

Figure 4.6 (Continued) Distribution of burned area for 12 Landsat scenes.

For validation of burned area extraction in 2014 by BAMS according RFD ground fire records during fire season between February and April 2014 it was found that corrected points of all scenes varied between 79.58% and 94.06%. As result, it can be concluded that accuracy of burned areas extraction using BAMS is acceptable. Detail of accuracy assessment of each Landsat scene is summarized in Table 4.4.

Table 4.4 Accuracy assessment of burned area extraction in 2014 by BAMS.

Landsat		Date of data	Number of RFD's point	Number of point		Percent	
Path/Row	**Date**			**Correct**	**Incorrect**	**Correct**	**Incorrect**
130047	25 February 2014	10-25 February 2014	101	96	5	94.06	5.94
130047	13 March 2014	26 February to 13 March 2014	251	234	17	93.23	6.77
130047	29 March 2014	14-29 March 2014	123	100	23	82.11	17.89
131047	4 March 2014	17 February to 4 March 2014	68	63	5	92.65	7.35
131047	20 March 2014	5-20 March 2014	194	176	18	90.72	9.28
131047	5 April 2014	21 March to 5 April 2014	142	113	29	79.58	20.42

4.1.2 Burn severity classification

For burn severity classification, the derived burned area from Landsat image is firstly overlaid over 1 sq. km grid of MODIS data for percentage calculation and then classified burn severity classes into 5 classes: none, low, moderate, high, and very high as defining in Section 1.5. The example burned area extraction and burn severity class with 1 sq. km grid size is shown in Figure 4.7. Area and percentage of burn severity classes is summarized in Table 4.5 and distribution of burn severity classification of 12 Landsat scenes is displayed in Figure 4.8. Theses burned severity classes of 12 scenes as dependent variable is further used in ordinal logistic regression analysis with 12 spectral indices as independent variables for optimal top three burned area spectral indices identification.

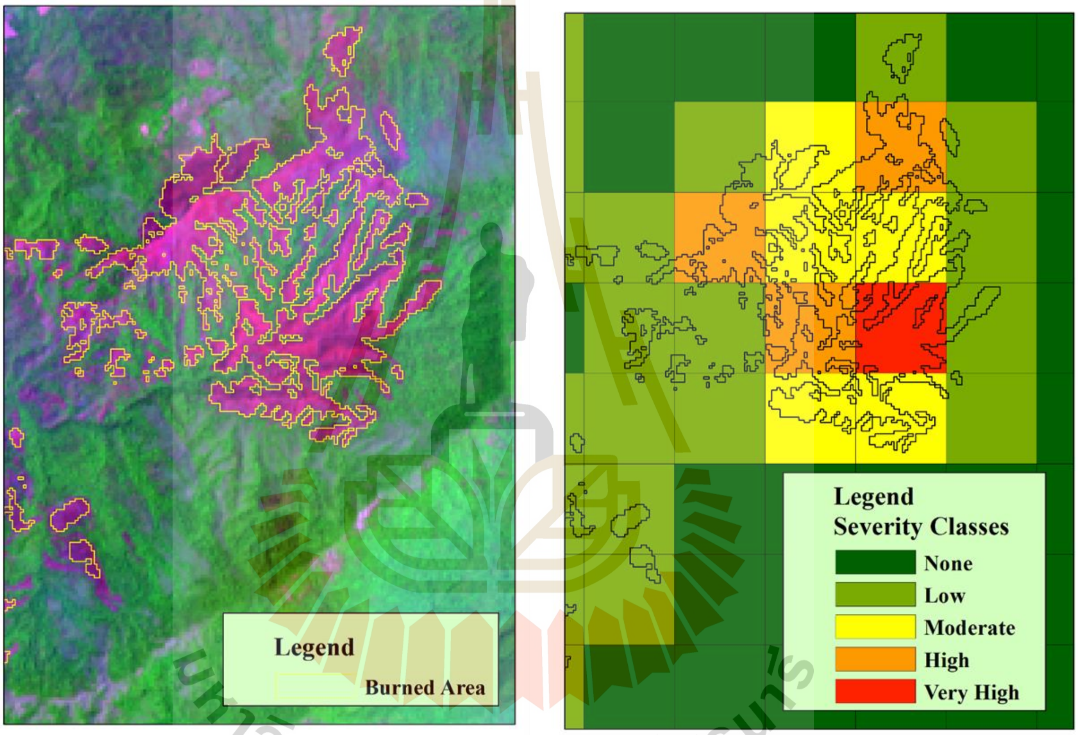

Figure 4.7 Burned area extraction and burn severity with 1 sq.km grid size.

Table 4.5 Area and percentage of burn severity classification.

Landsat scene	Date	Area of burn severity classification (sq. km)					Percentage of burn severity				
		None	Low	Moderate	High	Very high	None	Low	Moderate	High	Very high
LT51300472010045	14 February 2010	27,438	3,676	186	15	2	87.61	11.74	0.59	0.05	0.01
LT51310472010052	21 February 2010	29,047	2,155	86	12	6	92.78	6.88	0.28	0.04	0.02
LT51310472010084	25 March 2010	26,270	4,715	272	44	3	83.92	15.06	0.87	0.14	0.01
LT51310472010116	26 April 2010	28,989	2,287	29	3	-	92.59	7.31	0.09	0.01	-
LC81300472013101	11 April 2013	29,669	1,614	32	2	-	94.74	5.15	0.10	0.01	-
LC81310472013108	18 April 2013	28,246	3,044	15	-	-	90.23	9.72	0.05	-	-
LC81300472014056	25 February 2014	27,951	3,295	72	3	-	89.24	10.52	0.23	0.01	-
LC81300472014072	13 March 2014	21,556	9,294	416	47	5	68.82	29.68	1.33	0.15	0.02
LC81300472014088	29 March 2014	27,516	3,670	118	13	-	87.86	11.72	0.38	0.04	-
LC81310472014063	4 March 2014	26,298	4,415	519	72	3	84.00	14.10	1.66	0.23	0.01
LC81310472014079	20 March 2014	23,413	7,492	353	44	5	74.79	23.93	1.13	0.14	0.02
LC81310472014095	5 April 2014	22,623	8,484	179	16	4	72.26	27.10	0.58	0.05	0.01

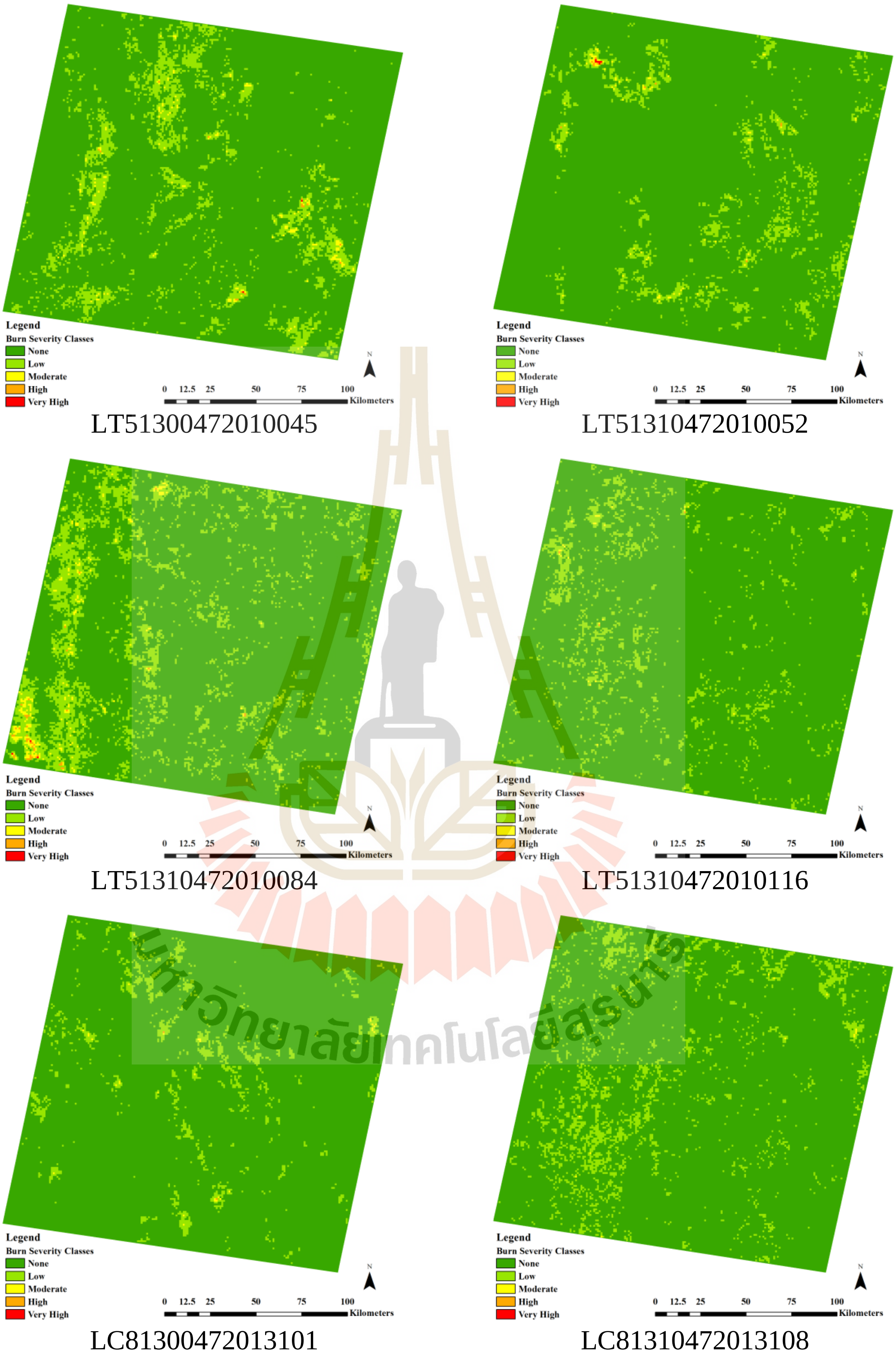

Figure 4.8 Distribution of burn severity for 12 Landsat scenes.

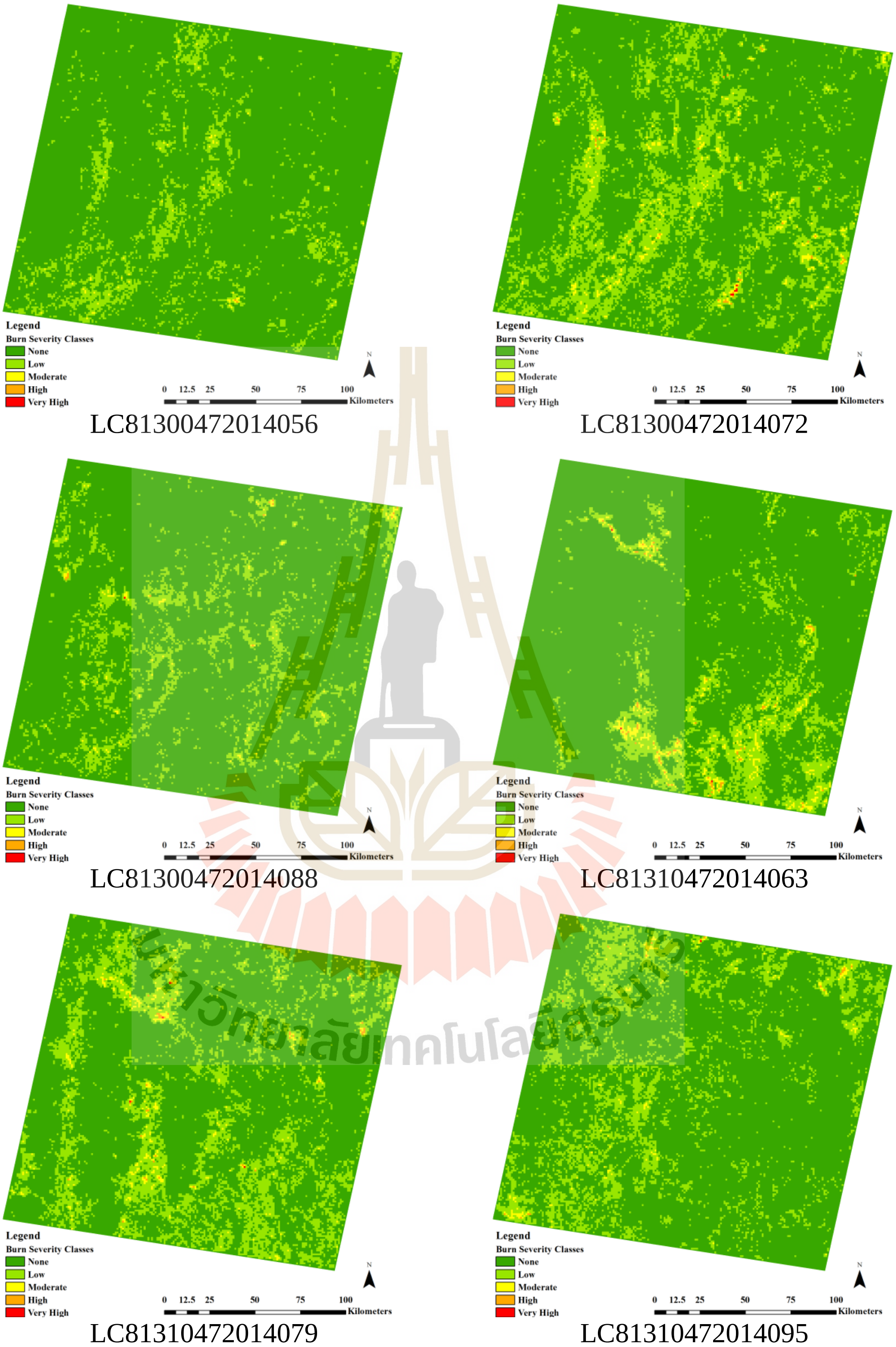

Figure 4.8 (Continued) Distribution of burn severity for 12 Landsat scenes.

4.1.3 Spectral indices calculation

Under this stage spectral indices data of the 12 selected spectral indices: NDVI, MSAVI, BAI, BAIM, NBR, GEMI, MIRBI, NDSWIR, NDWI, NMDI, SMI and CSI were constructed from selected MODIS data as summary in Table 4.6. Figure 4.9 and 4.10 comparatively displayed the normalized calculated spectral indices data of MODIS scene: 2014057.0350.005 and 2014064.0400.005 respectively. Table 4.7 summarized original basic descriptive statistical data of 12 spectral indices from 12 MODIS scenes while Table 4.8 summarized normalize data of 12 spectral indices.

Table 4.6 Selected MODIS data according to Landsat data used for burn severity classification.

MODIS data		**Landsat data**	
MODIS scene	**Date**	**Landsat scene**	**Date**
2010046.0350.005	15 February 2010	LT51300472010045	14 February 2010
2010053.0400.005	22 February 2010	LT51310472010052	21 February 2010
2010085.0350.005	26 March 2010	LT51310472010084	25 March 2010
2010117.0400.005	27 April 2010	LT51310472010116	26 April 2010
2013102.0350.005	12 April 2013	LC81300472013101	11 April 2013
2013109.0400.005	19 April 2013	LC81310472013108	18 April 2013
2014057.0350.005	26 February 2014	LC81300472014056	25 February 2014
2014073.0350.005	14 March 2014	LC81300472014072	13 March 2014
2014089.0400.005	30 March 2014	LC81300472014088	29 March 2014
2014064.0400.005	5 March 2014	LC81310472014063	4 March 2014
2014080.0400.005	21 March 2014	LC81310472014079	20 March 2014
2014096.0400.005	6 April 2014	LC81310472014095	5 April 2014

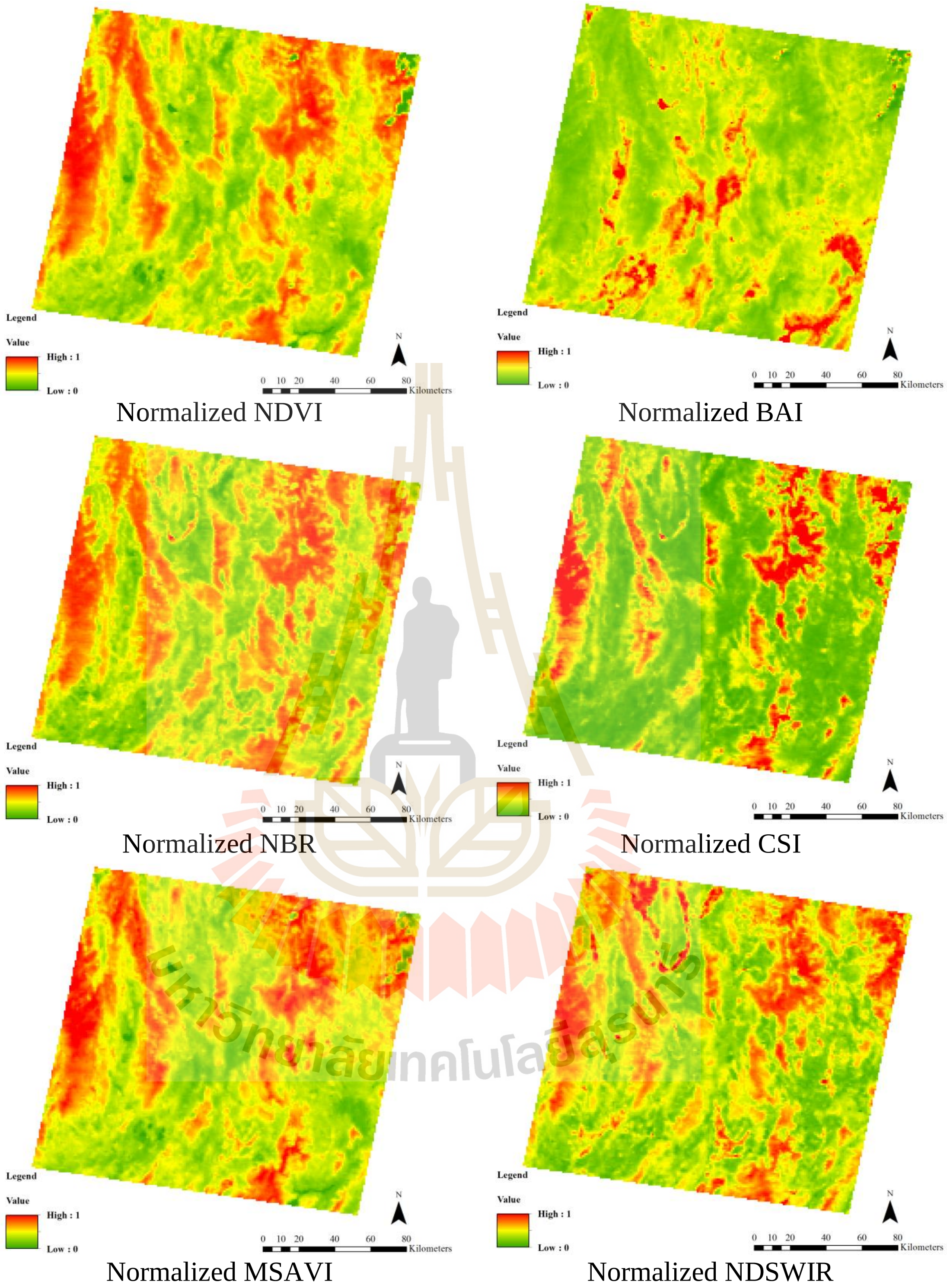

Figure 4.9 Spectral indices from MODIS scene 2014057.0350.005: 26 February 2014.

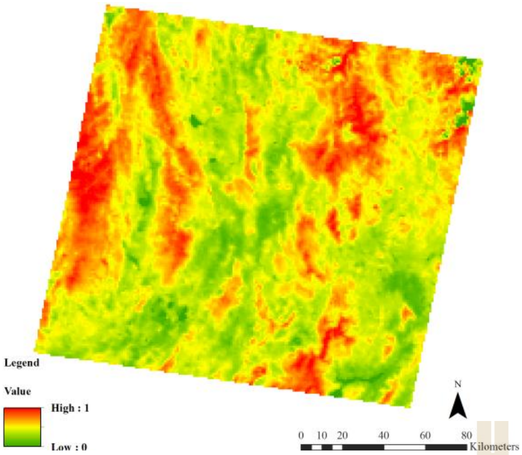

Normalized GEMI

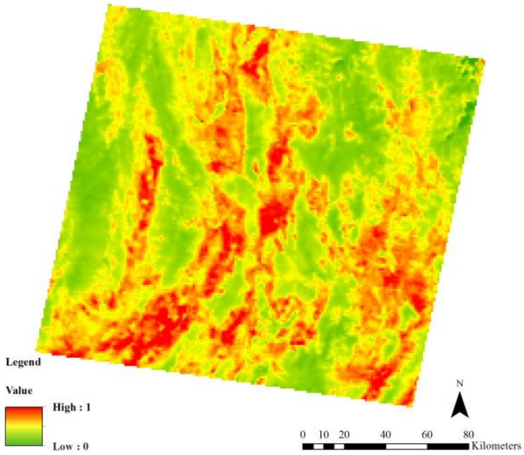

Normalized BAIM

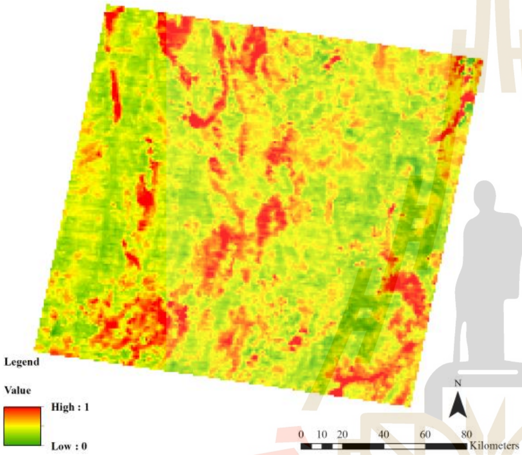

Normalized MIRBI

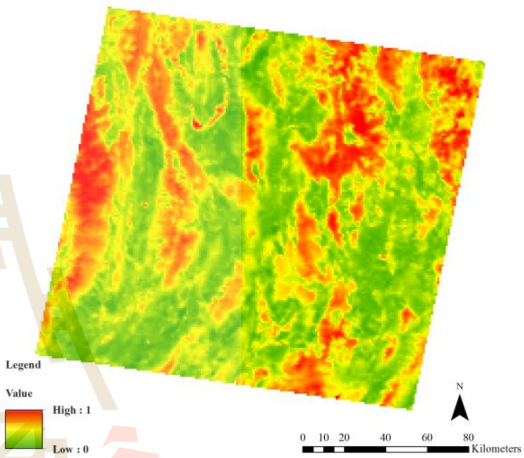

Normalized NDWI

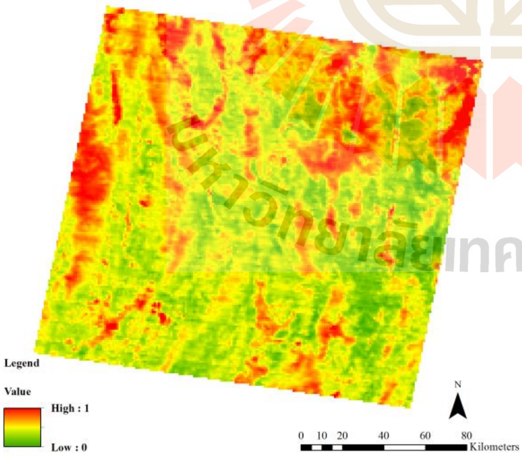

Normalized NMDI

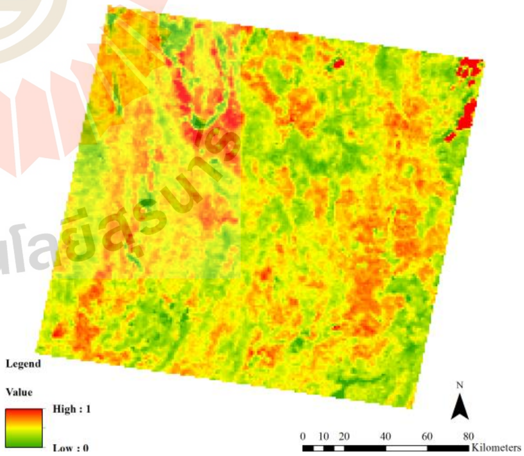

Normalized SMI

Figure 4.9 (Continued) Spectral indices from MODIS scene 2014057.0350.005: 26 February 2014.

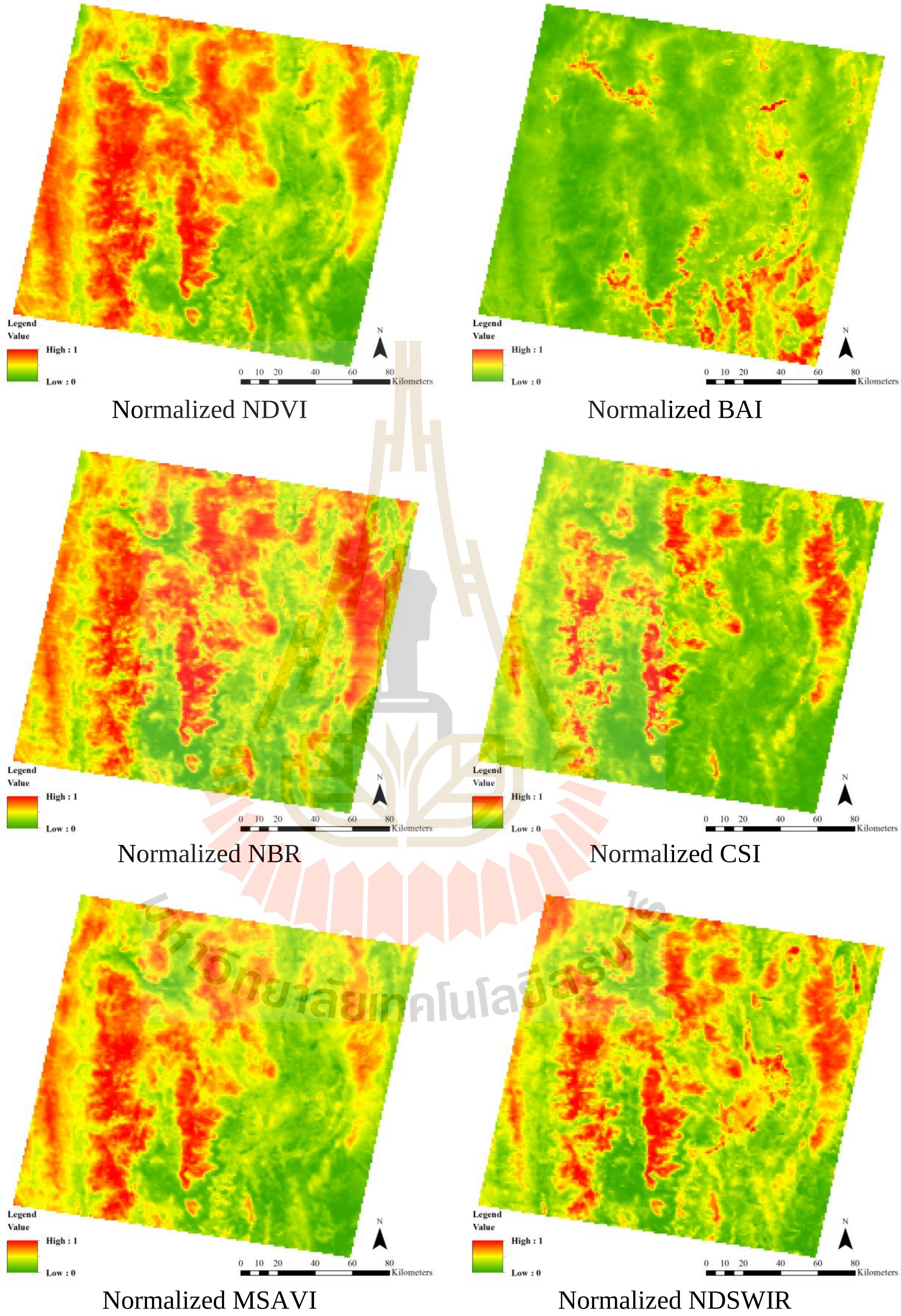

Figure 4.10 Spectral indices from MODIS scene 2014064.0400.005: 5 March 2014.

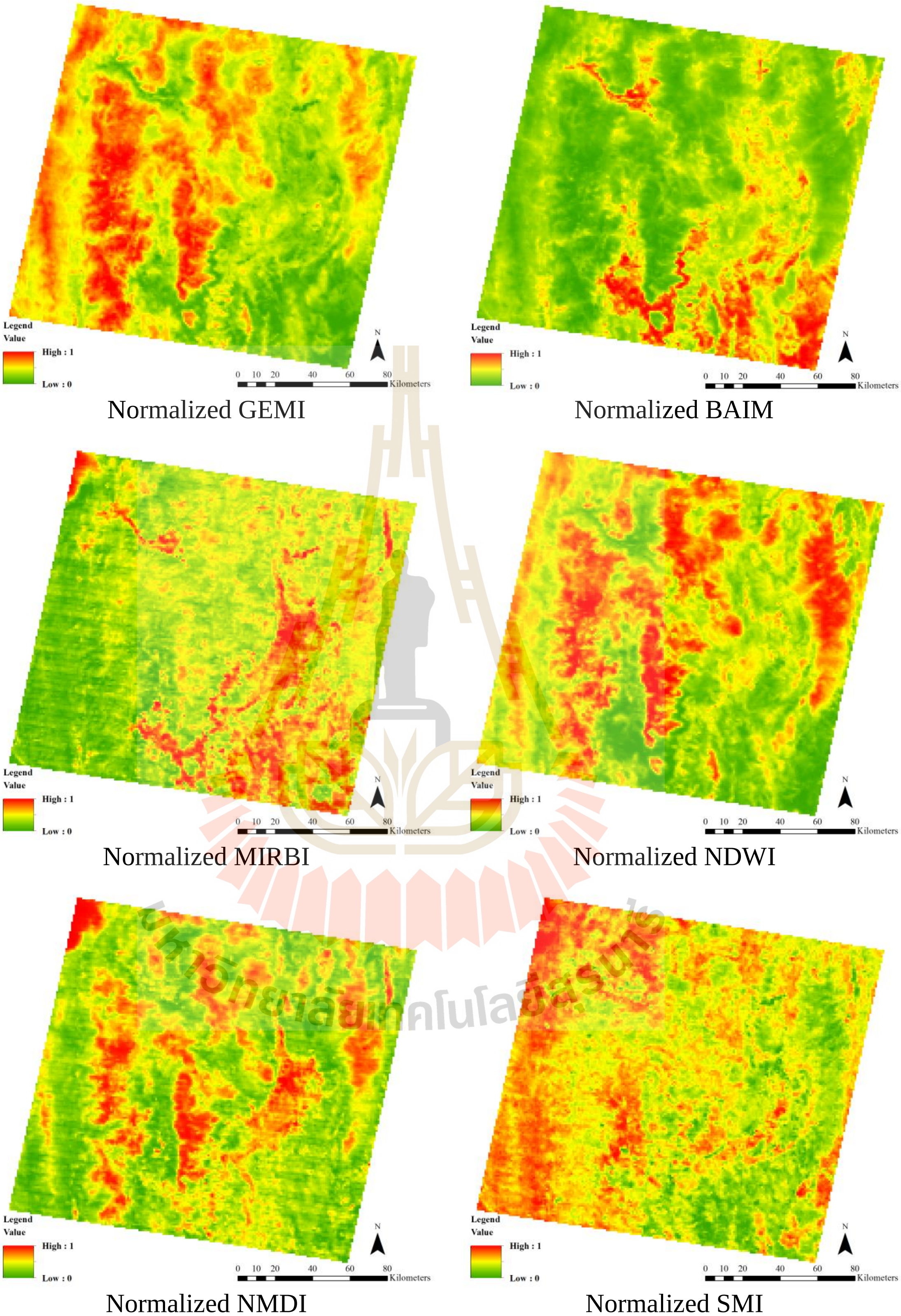

Figure 4.10 (Continued) Spectral indices from MODIS scene 2014064.0400.005: 5 March 2014.

Table 4.7 Basic descriptive statistical data of original spectral indices data of 12 MODIS scenes.

Spectral index	Descriptive Statistics			
	Avg. Minimum	**Avg. Maximum**	**Avg. Mean**	**Avg. S.D.**
NDVI	- 0.0590	0.6876	0.3707	0.1126
MSAVI	- 0.0598	0.4532	0.1929	0.0425
BAI	10.0022	436.9930	45.1309	17.7744
BAIM	8.7443	94.1042	31.6245	9.5527
NBR	- 0.0217	0.7787	0.3816	0.1617
GEMI	- 0.1962	0.7114	0.5113	0.0404
MIRBI	0.6297	1.7496	1.1257	0.1282
NDSWIR	- 0.2035	0.1779	- 0.0664	0.1013
NDWI	- 0.1695	0.4387	0.0841	0.1613
NMDI	0.2873	0.6685	0.4224	0.0805
SMI	- 0.7387	- 0.1928	- 0.5115	0.4233
CSI	1.4456	12.7275	3.8383	5.2917

Table 4.8 Basic descriptive statistical data of normalized spectral indices of 12 MODIS scenes.

Spectral index	Descriptive Statistics			
	Avg. Minimum	**Avg. Maximum**	**Avg. Mean**	**Avg. S.D.**
NDVI	0.0000	1.0000	0.5583	0.0889
MSAVI	0.0000	1.0000	0.4702	0.0725
BAI	0.0000	1.0000	0.1457	0.1711
BAIM	0.0000	1.0000	0.2910	0.0657
NBR	0.0000	1.0000	0.5094	0.0476
GEMI	0.0000	1.0000	0.6866	0.1822
MIRBI	0.0000	1.0000	0.4684	0.1302
NDSWIR	0.0000	1.0000	0.3698	0.1037
NDWI	0.0000	1.0000	0.4207	0.0556
NMDI	0.0000	1.0000	0.3618	0.0593
SMI	0.0000	1.0000	0.4963	0.2057
CSI	0.0000	1.0000	0.2121	0.0384

4.1.4 Ordinal logistic regression analysis

For ordinal logistic regression analysis, the 1 km grid of burn severity classes from each Landsat scene is firstly prepared and simultaneously linked with 12 extracted spectral indices using MS-Excel spreadsheet and then is exported to SPSS statistical software for deviance calculation.

The calculated deviance value of 12 Landsat scenes with its ranking is summarized in Table 4.9. Theoretically, the lower deviance value represents a better goodness of fit as the residual sum of squares in ordinary linear regression models (Hosmer and Lemeshow, 2000). As results, CSI and BAI provides the lowest deviance value in 4 of 12 scenes, NDSWIR provides the lowest deviance value in2 scenes, while SMI and GEMI can provide the lowest deviance value in one scene. On the other hand, BAIM, NMDI, and MIRBI provide high deviance value. In addition, it can be observed that deviance values are highly related with burn severity class, therefore, assignment of burned severity classes is very important because it directly effect on deviance value calculation.

Table 4.9 Deviance values of each spectral index and its rank.

Scene name/Date	Statistics/Value	Spectral indices											
		NDVI	**MSAVI**	**BAI**	**BAIM**	**NBR**	**GEMI**	**MIRBI**	**NDSWIR**	**NDWI**	**NMDI**	**SMI**	**CSI**
LT51300472010045	Deviance	110.22	110.89	104.39	163.71	128.05	121.09	141.68	93.44	103.86	121.36	154.33	65.37
	Rank	5	6	4	12	9	7	10	2	3	8	11	1
LT51310472010052	Deviance	70.23	55.50	10.63	100.38	74.92	121.09	80.21	52.64	75.54	121.25	45.29	55.35
	Rank	6	5	1	10	7	11	9	3	8	12	2	4
LT51310472010084	Deviance	195.96	213.71	182.42	282.71	200.51	59.70	215.34	173.77	177.99	173.05	96.62	143.85
	Rank	8	10	7	12	9	1	11	5	6	4	2	3
LT51310472010116	Deviance	75.45	61.29	63.21	85.77	85.95	62.72	64.69	57.14	71.12	67.37	63.16	51.08
	Rank	10	3	6	11	12	4	7	2	9	8	5	1
LC81300472013101	Deviance	70.23	55.50	10.63	100.38	74.92	121.09	80.21	92.64	75.54	121.25	45.29	55.35
	Rank	5	4	1	10	6	11	8	9	7	12	2	3
LC81310472013108	Deviance	37.39	54.813	33.792	33.376	34.504	50.352	36.54	34.726	52.115	35.26	30.435	31.139
	Rank	9	12	4	3	5	10	8	6	11	7	1	2
LC81300472014056	Deviance	77.28	92.86	55.43	91.55	73.73	69.41	138.57	52.59	64.32	127.81	146.53	31.72
	Rank	7	9	3	8	6	5	11	2	4	10	12	1
LC81300472014072	Deviance	171.43	159.12	17.26	233.79	210.28	181.04	276.52	85.57	198.54	707.70	334.02	120.73
	Rank	5	4	1	9	8	6	10	2	7	12	11	3
LC81300472014088	Deviance	88.70	106.24	42.66	164.30	135.19	113.09	241.06	72.96	112.11	413.59	177.32	86.14
	Rank	4	5	1	9	8	7	11	2	6	12	10	3
LC81310472014063	Deviance	289.42	291.97	157.95	194.07	258.77	236.59	624.96	139.35	235.36	427.78	229.23	170.30
	Rank	9	10	2	4	8	7	12	1	6	11	5	3
LC81310472014079	Deviance	222.76	154.32	144.71	203.88	181.02	160.76	226.74	134.71	135.08	320.05	165.09	93.35
	Rank	10	5	4	9	8	6	11	2	3	12	7	1
LC81310472014095	Deviance	204.31	205.25	165.71	233.05	201.24	183.02	223.49	123.98	179.81	203.20	308.79	136.29
	Rank	8	9	3	11	6	5	10	1	4	7	12	2

4.1.5 Optimal top three burned area spectral indices identification

According to deviance values from 12 Landsat scenes and its rank (Table 4.9), total score was derived by addition of score (rank) and ranked it again for optimal top three burned area spectral indices identification as shown in Table 4.10. As result, it was found that an optimal top three spectral indices were CSI, BAI, and NDSWIR. These indices provide a better goodness of fit with burn severity classes and they were further applied for burned area detection using threshold technique and decision tree classification.

Table 4.10 Total score value and ranking of spectral indices for optimal top three burned area spectral indices identification.

No.	Spectral index	12 Scenes of Landsat	
		Total score	Rank
1	CSI	27	1
2	BAI	37	2
3	NDSWIR	37	2
4	NDWI	74	4
5	GEMI	80	5
6	SMI	80	5
7	MSAVI	82	7
8	NDVI	86	8
9	NBR	92	9
10	BAIM	108	10
11	NMDI	115	11
12	MIRBI	118	12

This finding was agreed with the previous study of Schepers et al. (2014) who examined 9 spectral indices (NDVI, GEMI, EVI, SAVI, MSAVI, BAI, NBR, CSI, and MIRBI) to assess the burn severity of fire in the Kalmthoutse Heide, Belgium using Airborne Imaging Spectroscopy (APEX). They found that CSI was the best index to assess burn severity in dry heath vegetation and the NBR performed rather poorly. On contrary, Harris et al. (2011) who evaluated 19 spectral indices to assess the burn severity in Chaparral Ecosystems (Southern California) using MODIS/ASTER (MASTER). They found that NBR was the best non thermal index to assess burn severity with best goodness-of-fit of the ordinal logistic regression model. However, the second best index of their study was CSI.

4.2 An optimum burned area detection algorithm identification

The main results of two approached are applied to identify optimum burned area detection using the derived spectral indices: (1) thresholding technique and (2) decision tree classification with CRT growing method.

4.2.1 Burned area detection algorithm testing using thresholding technique

An extracted burned and unburned areas are here considered based on the percentage of burned area from Landsat 8 data, scene number LC8131047 2014063, date 4 March 2014 in peak fire season in 2014 over 1 sq. km grid of MODIS data. If percent of burned area in grid equal or more than 25%, it classified burned grid. The results showed that 30,747 grids were unburned areas and 560 grids were burned areas. This result was also used as a reference data for accuracy assessment of burned area detection from top three spectral indices from MODIS Level 1B data

(Scene 2014064), date 5 March 2014. For calculated 560 burned grids, it was found that mean and standard deviation of CSI, BAI and NDSWIR were 1.2439 and 0.2228, 103.7142 and 18.7191, and -0.1513 and 0.0213, respectively (Table 4.11).

Table 4.11 Descriptive statistics of top three spectral indices over 560 burned grids.

Spectral index	Minimum	Maximum	Mean	S.D.
CSI	0.8624	2.4669	1.2439	0.2228
BAI	54.7674	165.0381	103.7142	18.7191
NDSWIR	-0.2032	-0.0894	-0.1513	0.0213

By using thresholding technique, it was found that BAI with threshold value between 104.7674 and 124.7674 (If 104.7674 ≤BAI value ≤124.7674, then, it is burned area), provided overall accuracy between 97.8855% and 98.1059%, false alarm rate between 0.6667% and 0.3740%, burned area detection rate between 18.3929% and 14.6429%, and Kappa hat coefficient between 22.7512% and 20.9283% (Table 4.12 and Figure 4.11. At the same time, CSI with threshold value between 0.9624 and 1.0624 provided overall accuracy at 97.3712%, false alarm rate at 1.1286%, burned area detection rate at 15.0000%, and Kappa hat coefficient at 15.6400% (Table 4.13 and Figure 4.12). Similarly, NDSWIR with threshold value between -0.1832 and -0.1782 provided overall accuracy at 97.5660%, false alarm rate at 0.7773%, burned area detection rate at 6.6071%, and Kappa hat coefficient at 7.7623% (Table 4.14 and Figure 4.13).

Distribution of burned and unburned areas detection by top three spectral indices (BAI, CSI, and NDSWIR) using thresholding technique that was compared with reference burned area is displayed in Figure 4.14.

Table 4.12 Accuracy assessment of burned area detection using thresholding technique with BAI.

ID	Threshold		Correct burned hit (pixel)	Burn Missing (pixel)	False Alarm (pixel)	Correct unburned hit (pixel)	Overall Accuracy (%)	False alarm rate (%)	Burn detection rate (%)	Kappa hat (%)
	Minimum	Maximum								
1	54.7674	64.7674	8	552	3,119	27,628	88.2742	10.1441	1.4286	-2.6815
2	64.7674	74.7674	28	532	1,642	29,105	93.0559	5.3404	5.0000	-0.1725
3	74.7674	84.7674	51	509	1,028	29,719	95.0906	3.3434	9.1071	3.9615
4	84.7674	94.7674	101	459	683	30,064	96.3523	2.2214	18.0357	13.2188
5	94.7674	104.7674	109	451	351	30,396	97.4383	1.1416	19.4643	20.0832
6	104.7674	114.7674	103	457	205	30,542	97.8855	0.6667	18.3929	22.7521
7	114.7674	124.7674	82	478	115	30,632	98.1059	0.3740	14.6429	20.9283
8	124.7674	134.7674	48	512	36	30,711	98.2496	0.1171	8.5714	14.5079
9	134.7674	144.7674	23	537	11	30,736	98.2496	0.0358	4.1071	7.5548
10	144.7674	154.7674	6	554	7	30,740	98.2081	0.0228	1.0714	2.0147
11	154.7674	164.7674	0	560	3	30,744	98.2017	0.0098	-	-0.0191
12	164.7674	165.0381	1	559	0	30,747	98.2145	-	0.1786	0.3502

Table 4.13 Accuracy assessment of burned area detection using thresholding technique with CSI.

ID	Threshold		Correct burned hit (pixel)	Burn Missing (pixel)	False Alarm (pixel)	Correct unburned hit (pixel)	Overall Accuracy (%)	False alarm rate (%)	Burn detection rate (%)	Kappa hat (%)
	Minimum	Maximum								
1	0.8624	0.9624	39	521	131	30,616	97.9174	0.4261	6.9643	9.9346
2	0.9624	1.0624	84	476	347	30,400	97.3712	1.1286	15.0000	15.6400
3	1.0624	1.1624	94	466	573	30,174	96.6813	1.8636	16.7857	13.6425
4	1.1624	1.2624	95	465	757	29,990	96.0967	2.4620	16.9643	11.5467
5	1.2624	1.3624	102	458	985	29,762	95.3908	3.2036	18.2143	10.2675
6	1.3624	1.4624	71	489	1,164	29,583	94.7200	3.7857	12.6786	5.5870
7	1.4624	1.5624	31	529	1,308	29,439	94.1323	4.2541	5.5357	0.7616
8	1.5624	1.6624	21	539	1,321	29,426	94.0588	4.2964	3.7500	-0.3242
9	1.6624	1.7624	8	552	1,383	29,364	93.8193	4.4980	1.4286	-1.7758
10	1.7624	1.8624	5	555	1,333	29,414	93.9694	4.3354	0.8929	-2.0467
11	1.8624	1.9624	3	557	1,313	29,434	94.0269	4.2703	0.5357	-2.2461
12	1.9624	2.0624	4	556	1,240	29,507	94.2633	4.0329	0.7143	-2.0747
13	2.0624	2.1624	-	560	1,261	29,486	94.1834	4.1012	-	-2.5402
14	2.1624	2.2624	1	559	1,222	29,525	94.3112	3.9744	0.1786	-2.4006
15	2.2624	2.3624	-	560	1,144	29,603	94.5571	3.7207	-	-2.4609
16	2.3624	2.4624	-	560	1,087	29,660	94.7392	3.5353	-	-2.4182
17	2.4624	2.4669	1	559	47	30,700	98.0643	0.1529	0.1786	0.0466

Table 4.14 Accuracy assessment of burned area detection using thresholding technique with NDSWIR.

ID	Threshold		Correct burned hit (pixel)	Burn Missing (pixel)	False Alarm (pixel)	Correct unburned hit (pixel)	Overall Accuracy (%)	False alarm rate (%)	Burn detection rate (%)	Kappa hat (%)
	Minimum	Maximum								
1	-0.2032	-0.1982	3	557	20	30,727	98.1570	0.0650	0.5357	0.8893
2	-0.1982	-0.1932	3	557	43	30,704	98.0835	0.1399	0.5357	0.7205
3	-0.1932	-0.1882	7	553	93	30,654	97.9366	0.3025	1.2500	1.5878
4	-0.1882	-0.1832	19	541	183	30,564	97.6874	0.5952	3.3929	4.0772
5	-0.1832	-0.1782	37	523	239	30,508	97.5660	0.7773	6.6071	7.7623
6	-0.1782	-0.1732	34	526	337	30,410	97.2434	1.0960	6.0714	5.9634
7	-0.1732	-0.1682	30	530	328	30,419	97.2594	1.0668	5.3571	5.2135
8	-0.1682	-0.1632	39	521	412	30,335	97.0198	1.3400	6.9643	6.2185
9	-0.1632	-0.1582	43	517	500	30,247	96.7515	1.6262	7.6786	6.1440
10	-0.1582	-0.1532	38	522	609	30,138	96.3874	1.9807	6.7857	4.4645
11	-0.1532	-0.1482	55	505	730	30,017	96.0552	2.3742	9.8214	6.2203
12	-0.1482	-0.1432	48	512	945	29,802	95.3461	3.0735	8.5714	3.9853
13	-0.1432	-0.1382	56	504	1,078	29,669	94.9468	3.5060	10.0000	4.3202
14	-0.1382	-0.1332	40	520	1,168	29,579	94.6082	3.7987	7.1429	2.1327
15	-0.1332	-0.1282	24	536	1,226	29,521	94.3719	3.9874	4.2857	0.1859
16	-0.1282	-0.1232	29	531	1,375	29,372	93.9119	4.4720	5.1786	0.4061
17	-0.1232	-0.1182	21	539	1,372	29,375	93.8959	4.4622	3.7500	- 0.4116
18	-0.1182	-0.1132	14	546	1,395	29,352	93.8001	4.5370	2.5000	- 1.1679
19	-0.1132	-0.1082	6	554	1,349	29,398	93.9215	4.3874	1.0714	- 1.9542
20	-0.1082	-0.1032	5	555	1,343	29,404	93.9375	4.3679	0.8929	- 2.0553
21	-0.1032	-0.0982	4	556	1,259	29,488	94.2026	4.0947	0.7143	- 2.0915
22	-0.0982	-0.0932	2	558	1,225	29,522	94.3048	3.9841	0.3571	- 2.2888
23	-0.0932	-0.0894	2	558	903	29,844	95.3333	2.9369	0.3571	- 1.9807

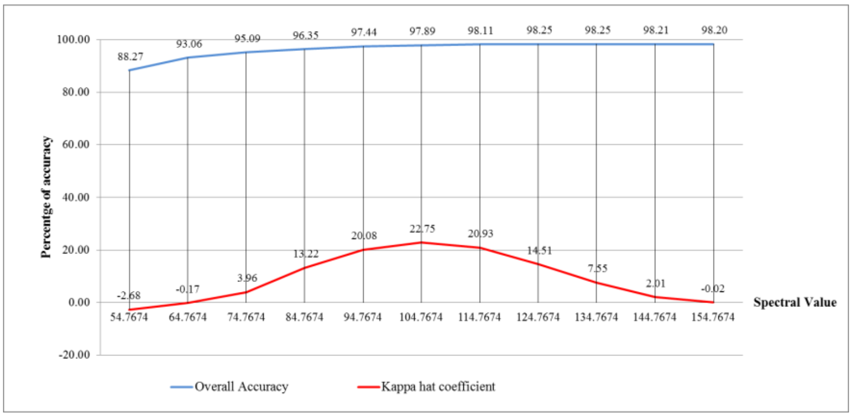

Figure 4.11 Accuracy assessment and Kappa hat coefficient of burned area detection using thresholding technique with BAI.

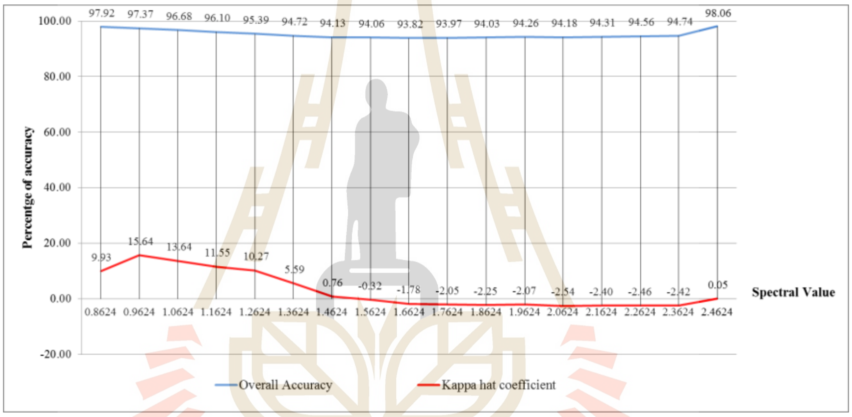

Figure 4.12 Accuracy assessment and Kappa hat coefficient of burned area detection using thresholding technique with CSI.

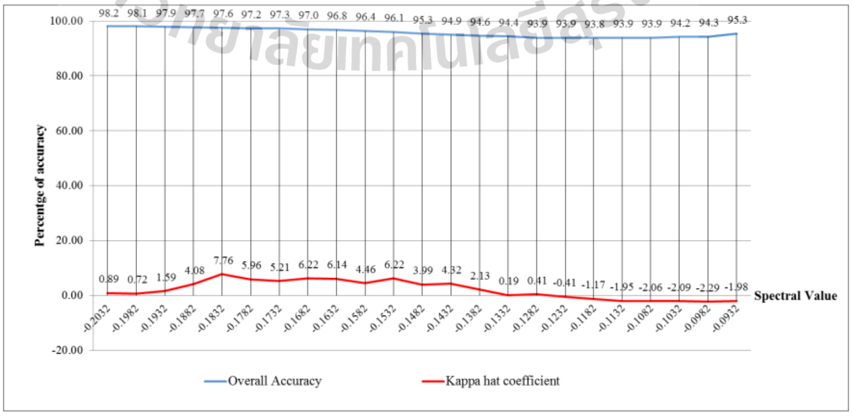

Figure 4.13 Accuracy assessment and Kappa hat coefficient of burned area detection using thresholding technique with NDSWIR.

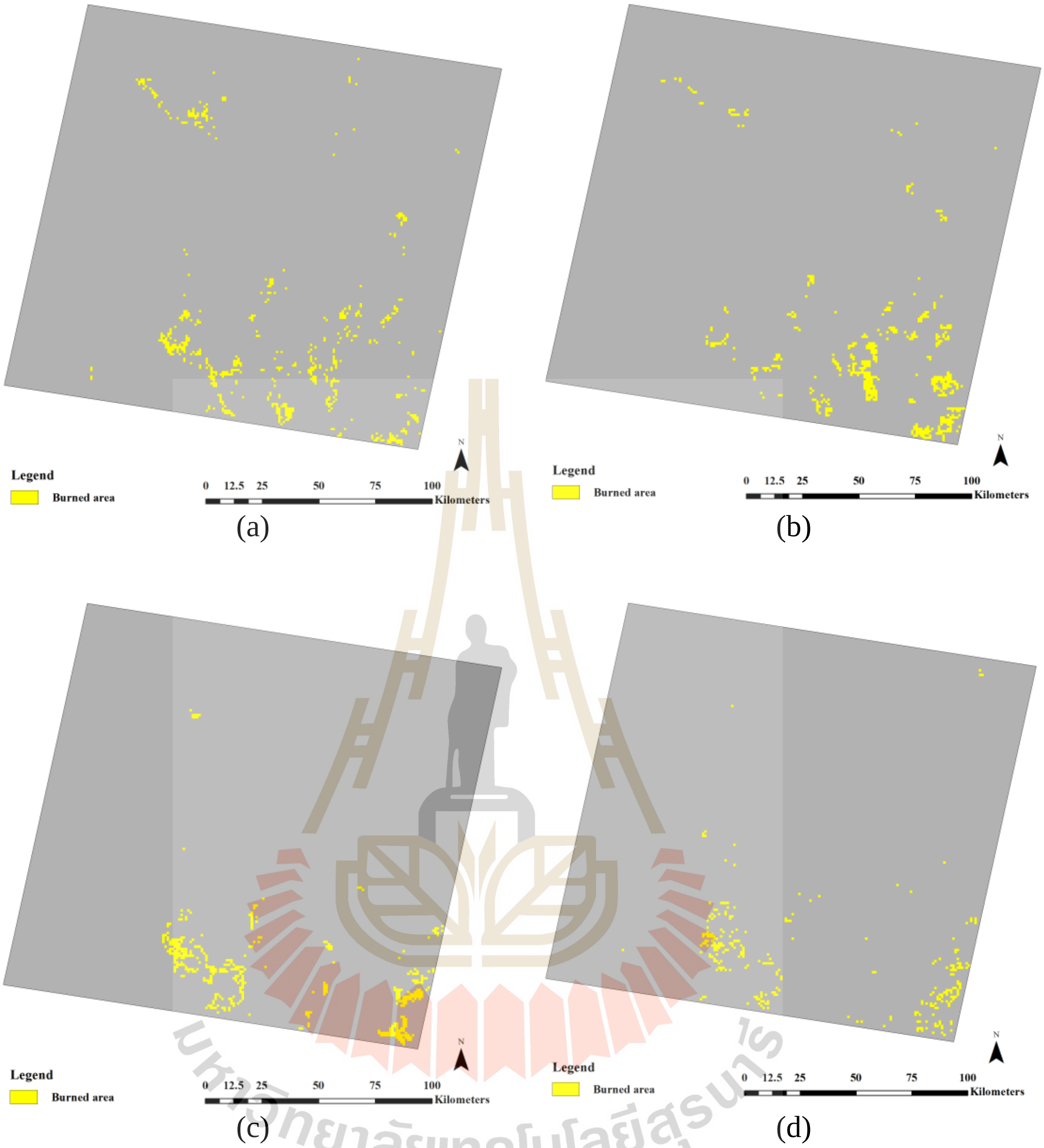

Figure 4.14 Distribution of burned and unburned area detection (a) reference burned area, (b) BAI, (c) CSI and (d) NDSWIR.

4.2.2 Burned area detection algorithm testing by decision tree classification

The derived MODIS Level 1B spectral data of top three spectral indices as independent variables and burned and unburned area derived from Landsat 8, scene number LC81310472014063, date 4 March, 2014 as dependent variable were here used to classify burned and unburned area using decision tree classification with CRT growing method under SPSS statistical software. The decision tree structure for burned and unburned area classification is displayed in Figure 4.15. The final criteria, which only include BAI and CSI of burned and unburned areas extraction, are as follows:

IF BAI value > 124.1677 AND CSI value ≤ 1.4650 (Node 12),

THEN, it is burned areas.

OTHERWISE,

IF BAI value > 96.1778 AND CSI value > 1.4650 (Node 6), OR

IF BAI value ≤ 96.1778 (Node 7), OR

IF BAI value > 71.6416 AND BAI value ≤ 96.1778 (Node 8), OR

IF BAI value > 83.9237 AND BAI value ≤ 96.1778 AND CSI value ≤ 1.4455 (Node 9), OR

IF BAI value > 83.9237 AND BAI value ≤ 96.1778 AND CSI value > 1.4455 (Node 10), OR

IF BAI value > 96.1778 AND BAI value ≤ 124.1677 AND CSI value ≤ 1.4650 (Node 11)

THEN, they are unburned areas.

This method provided overall accuracy at 98.3390%, false alarm rate at 0.1399%, burned area detection rate at 14.8214%, and Kappa hat coefficient at 23.6969%.

Distribution of burned and unburned areas detection by decision tree classification that was compared with reference burned area is displayed in Figure 4.16.

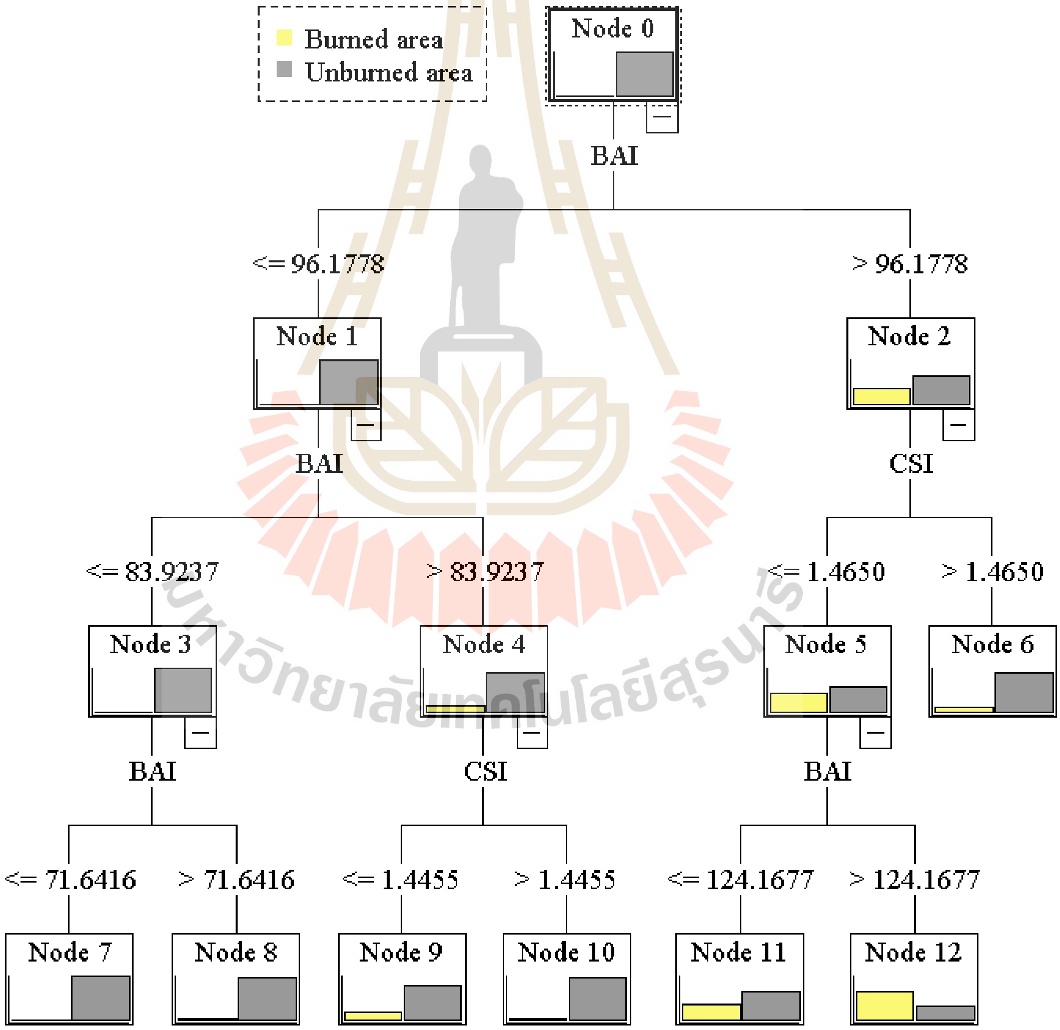

Figure 4.15 Decision tree structure for burned and unburned areas detection based on spectral indices.

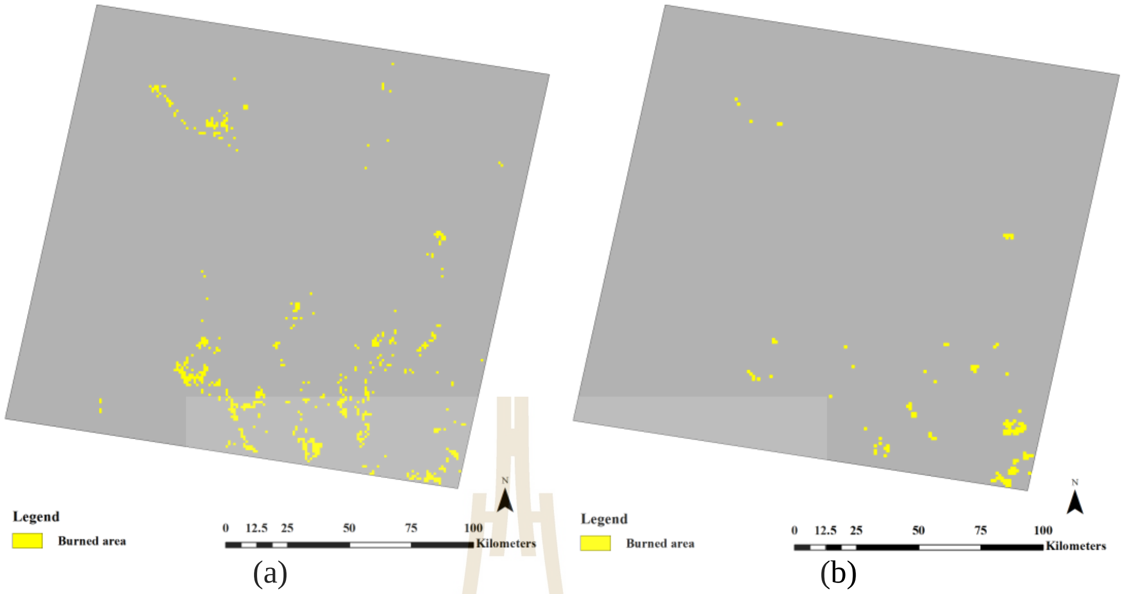

Figure 4.16 Distribution of burned and unburned area detection (a) reference burned area and (b) decision tree classification.

4.2.3 Optimal burned area detection algorithm identification

Based on accuracy assessment (overall accuracy and Kappa hat coefficient) of two approaches for burned area detection algorithm testing in the previous sections (4.3.1 and 4.3.2), it revealed that decision tree classification using CRT growing method provide the overall accuracy with value of 98.3390% higher than thresholding technique with BAI spectral index with value of 97.7800%. However, thresholding technique with BAI spectral index provide Kappa hat coefficient with value of 33.6157 higher than decision tree classification using CRT growing method with value of 23.6969%. In addition, burn detection rate of thresholding technique with value of 33.0357% was also higher than decision tree classification using CRT growing method with value of 14.8214% while false alarm rate of decision tree classification using CRT growing method with value of 0.1399%

was lower than thresholding technique with value of 1.0408% (Table 4.15). In addition result of pairwise Z-test between thresholding technique with BAI spectral index and decision tree classification using CRT growing method as summary in Table 4.16, it was found that Kappa hat accuracies from both techniques for burned and unburned extraction was significantly different at 90, 95, and 100% of confidence level.

Table 4.15 Accuracy comparison of two burned area detection algorithms.

Accuracy Statistics	**Thresholding technique**	**Decision tree classification**
Correct burn hit (pixel)	185	83
Burn missing (pixel)	375	477
False alarm (pixel)	320	43
Correct unburn hit (pixel)	30,427	30,704
Burn detection rate (%)	33.0357	14.8214
False alarm rate (%)	1.0408	0.1399
Overall accuracy (%)	97.7800	98.3390
Kappa hat coefficient (%)	33.6157	23.6969

Table 4.16 Pairwise Z test of Kappa hat coefficient value for burned area extraction between thresholding technique and decision tree classification.

<table>
<tr><th rowspan="2">Pairwise Z test</th><th rowspan="2">Kappa hat coefficient</th><th rowspan="2">Variance</th><th rowspan="2">Z-Statistic</th><th colspan="3">Two-side confidential level of critical value</th></tr>
<tr><th>90%</th><th>95%</th><th>100%</th></tr>
<tr><td>Thresholding technique</td><td>33.6157</td><td>0.00035934</td><td rowspan="2">3.3925</td><td rowspan="2">1.65</td><td rowspan="2">1.96</td><td rowspan="2">2.58</td></tr>
<tr><td>Decision tree classification</td><td>23.6969</td><td>0.00049550</td></tr>
</table>

Furthermore, the derived threshold value of thresholding technique and criteria of decision tree classification for burned area detection as reported above in Section 4.31 and 4.3.2 were here reexamined with other MODIS Level 1B datasets (Scene 2014080) over 20 March 2014 (LC81310472014079) for algorithm validation.

It was found that thresholding technique provided overall accuracy at 97.2945%, burned area detection rate at 30.8458%, false alarm rate at 1.8411%, and Kappa hat coefficient at 21.3704%. At the same time, decision tree classification provided overall accuracy at 98.7479%, burned area detection rate at 11.9403%, false alarm rate at 0.1230%, and Kappa hat coefficient at 19.3069% (Table 4.17). In addition, distribution of burned and unburned areas detection by thresholding technique with BAI spectral index and decision tree classification that was compared with reference burned area is displayed in Figures 4.17 and 4.18, respectively.

Table 4.17 Accuracy comparison of two burned area detection algorithms for algorithm validation.

Accuracy Statistics	Thresholding Technique	Decision tree classification
Correct burn hit (pixel)	124	48
Burn missing (pixel)	278	354
False alarm (pixel)	569	38
Correct unburn hit (pixel)	30,336	30,867
Burn detection rate (%)	30.8458	11.9403
False alarm rate (%)	1.8411	0.1230
Overall accuracy (%)	97.2945	98.7479
Kappa hat coefficient (%)	21.3704	19.3069

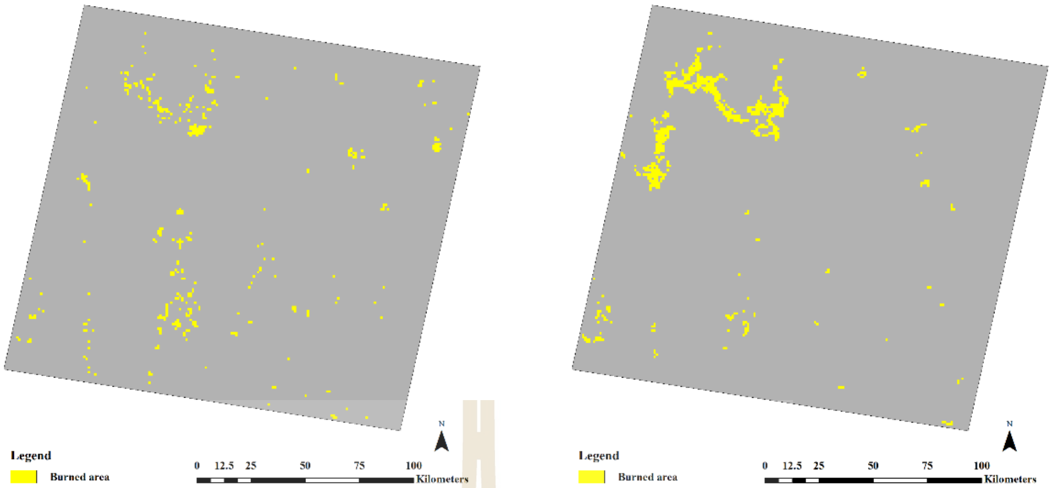

Reference area Thresholding technique

Figure 4.17 Distribution of burned and unburned area detection by thresholding technique with BAI spectral index.

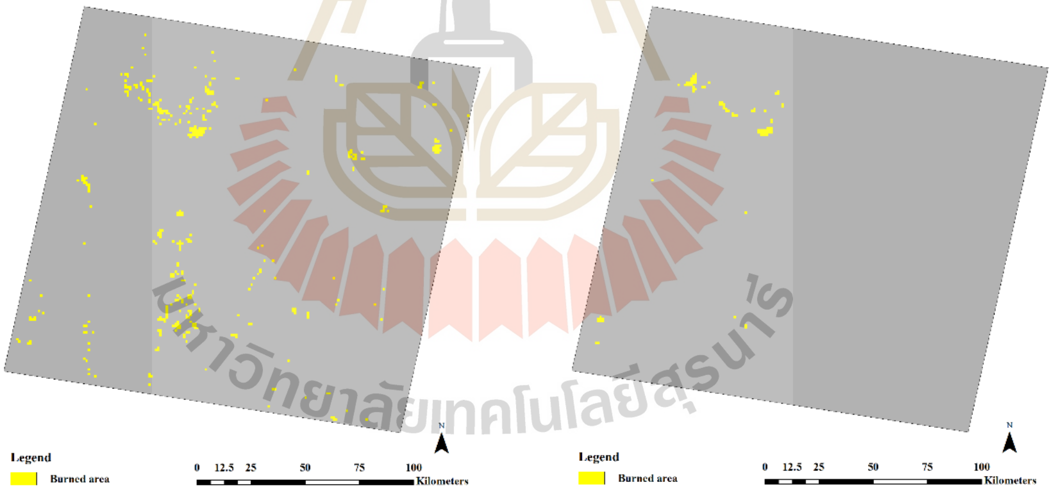

Reference area Decision tree classification

Figure 4.18 Distribution of burned and unburned area detection by decision tree classification with BAI and CSI spectral indices.

Furthermore, when detected burn areas from both approached based on two MODIS Level 1B scenes with 1 km spatial resolution were compared with extracted burn areas using BAMS based on two Landsat 8 data with 30 m spatial resolution, it was found that thresholding technique detected burned area better than decision tree classification (Table 4.18). Detected burn area by decision tree classification was too low when it was compared with thresholding technique or BAMS.

As results of accuracy assessment and validation mentioned above, it can be here concluded that thresholding technique with BAI spectral index was an optimum algorithm for burned area detection from MODIS Level 1B in this study.

Table 4.18 Comparison of detected/extracted burn area based on MODIS Level 1B and Landsat-8 data with three different approaches.

MODIS Level 1B	**Detected/extracted burn area in sq. km**		
	Thresholding technique	**Decision tree classification**	**BAMS**
Scene 2014064	505	126	504.91
Scene 2014080	693	86	561.52

4.3 An optimal algorithms for fire detection identification

The main results of an optimal algorithms for fire detection identification for MODIS hotspot using MODIS hotspot algorithm and MODIS hotspot data with decision tree classification are here separately described and discussed.

4.3.1 Fire detection based on MODIS hotspot algorithm

MODIS hotspot data with MOD14/MYD14 algorithm during fire season between 2010 and 2014 of Upper Northern of Thailand were directly retrieved and applied for accuracy assessment. The results revealed that totally 51,373 points were identified as hotspot and most of them were detected by Aqua satellite (83.04%).

Herewith, 13,755, 4,220, 12,220, 10,817, and 10,361 points were reported as hotspot in year 2010, 2011, 2012, 2013, and 2014, respectively. Most hotspots frequently occurred in March (57.00%) and followed by April (19.63%), February (17.92%), and January (2.60%). In addition, the most frequently time of fire occurrence was after 12.00 midday to 4.00 PM (82.03%). The summary statistics of MODIS hotspot record of Upper Northern of Thailand between 2010 and 2014 is summarized in Tables 4.19 and 4.21. Meanwhile distribution of MODIS hotspot is presented in Figure 4.19.

Furthermore, attribute data which were attached with MODIS hotspot included BT21/22, BT31, Difference of BT, FC, and FRP is summarized in Table 4.22. It was found that average brightness temperature of band 21/22 was 326.62° K, average brightness temperature of band 31 was 303.28° K, average difference brightness temperature of BT was 23.34° K, average FC was 68.22%, and average FRP was 44.62 MW. Herewith, range of FC and FRP was very wide. This infers about the existing of false hotspot. The distribution of MODIS hotspot attribute data which were systematic classified is shown in Figures 4.20 to 4.24.

Table 4.19 Basic statistical data of MODIS hotspot data by year between 2010 and 2014 of Upper Northern of Thailand.

Year	**Number of hotspot**	**Percent**
2010	13,755	26.77
2011	4,220	8.21
2012	12,220	23.79
2013	10,817	21.06
2014	10,361	20.17

Table 4.20 Basic statistical data of MODIS hotspot data by month between 2010 and 2014 of Upper Northern of Thailand.

Month	Number of hotspot	Percent
January	1,335	2.60
February	9,208	17.92
March	29,281	57.00
April	10,084	19.63
May	363	0.71
June	34	0.07
July	7	0.01
August	5	0.01
September	21	0.04
October	24	0.05
November	165	0.32
December	846	1.65

Table 4.21 Basic statistical data of MODIS hotspot data by period of time between 2010 and 2014 of Upper Northern of Thailand.

Time period	Number of hotspot	Percent
10.00 AM - 12.00 Midday	6,829	13.29
00.01 PM - 02.00 PM	31,986	62.26
02.01 PM - 04.00 PM	10,155	19.77
08.01 PM - 10.00 PM	12	0.02
10.01 PM - 12.00 Midnight	1,872	3.64
00.01 AM - 02.00 AM	519	1.02

Table 4.22 Basic Statistic data of MODIS hotspot attribute data.

MODIS hotspot data descriptive statistics						
MODIS hotspot Value	**Range**	**Minimum**	**Maximum**	**Mean**	**S.D.**	**Skewness**
BT21 or BT 22	196.00	305.00	501.00	326.62	15.04	2.62
BT31	131.40	268.70	400.10	303.28	5.34	- 0.34
Difference of BT	156.00	10.00	166.00	23.34	13.81	2.63
FC	100.00	0.00	100.00	68.22	18.90	- 0.46
FRP	1,712.80	4.30	1,717.10	44.62	73.48	6.92

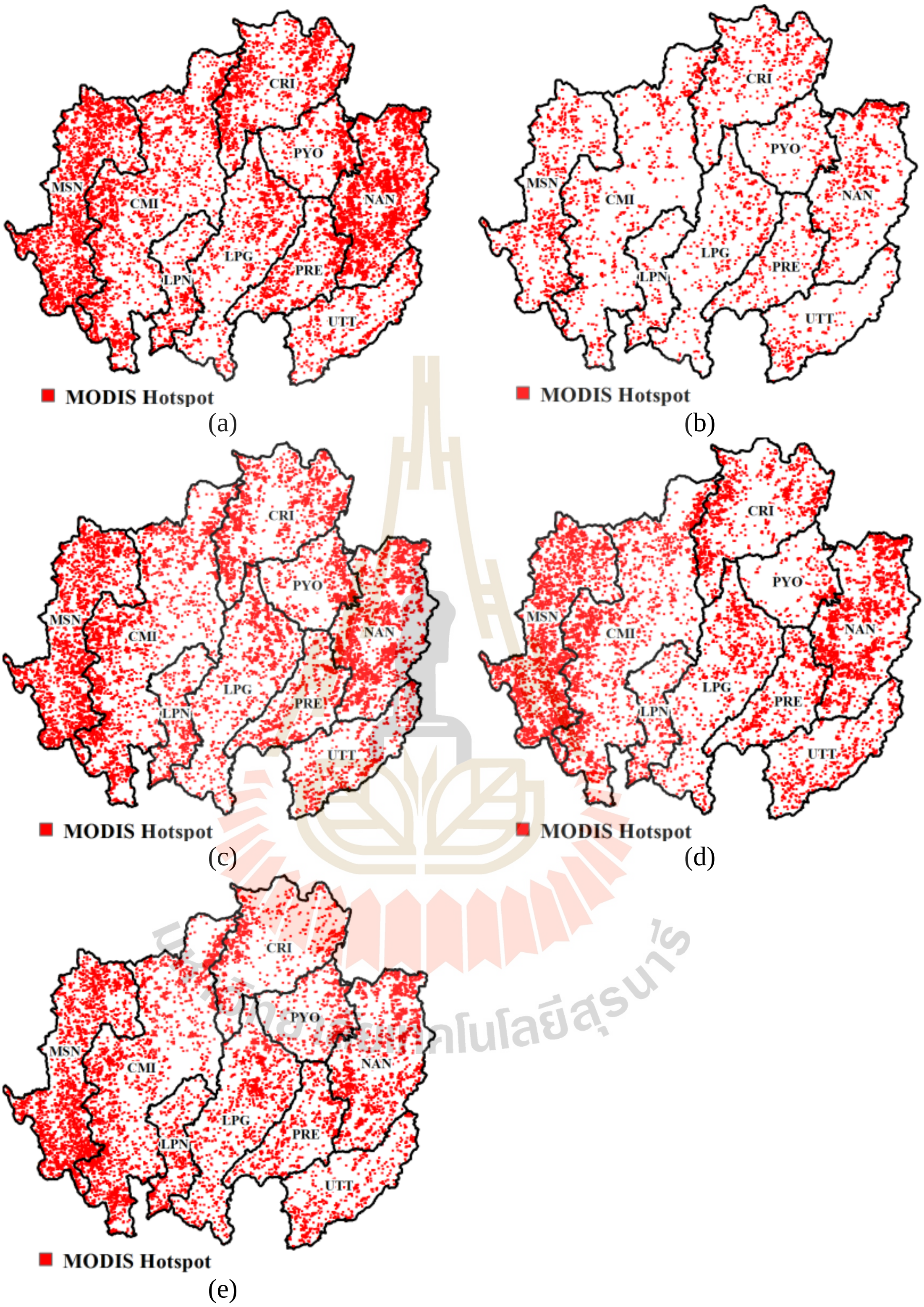

Figure 4.19 MODIS hotspot distributions, Upper Northern of Thailand: (a) 2010 (b) 2011 (c) 2012 (d) 2013 and (e) 2014.

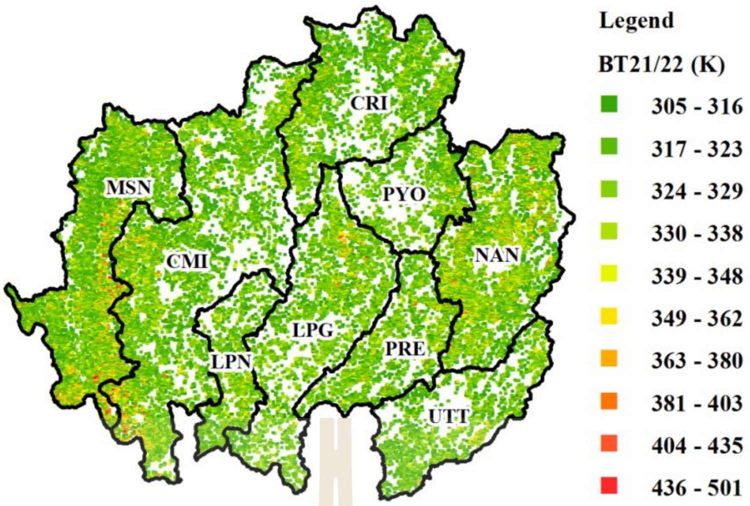

Figure 4.20 Distribution of brightness temperature of Band 21/22 from MODIS hotspot Upper Northern of Thailand between 2010 and 2014.

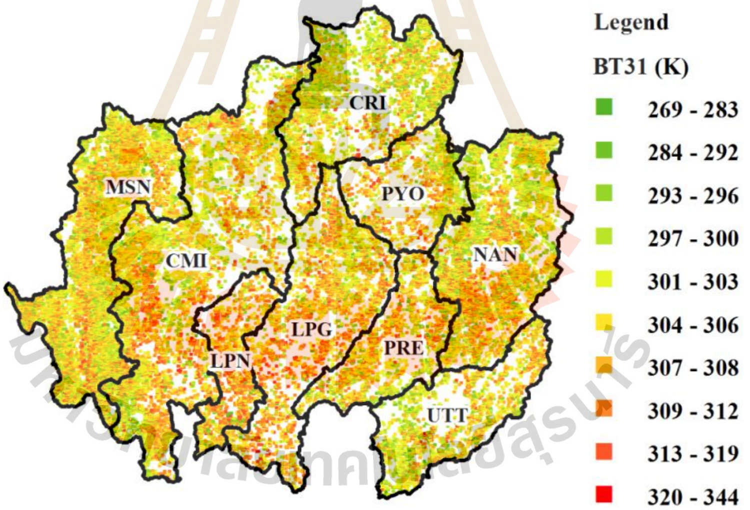

Figure 4.21 Distribution of brightness temperature of Band 31 from MODIS hotspot Upper Northern of Thailand between 2010 and 2014.

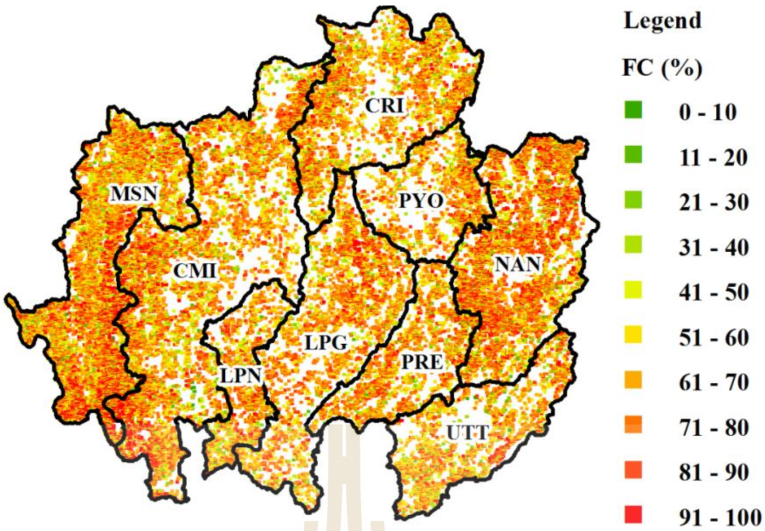

Figure 4.22 Distribution of fire confidence from MODIS hotspot Upper Northern of Thailand between 2010 and 2014.

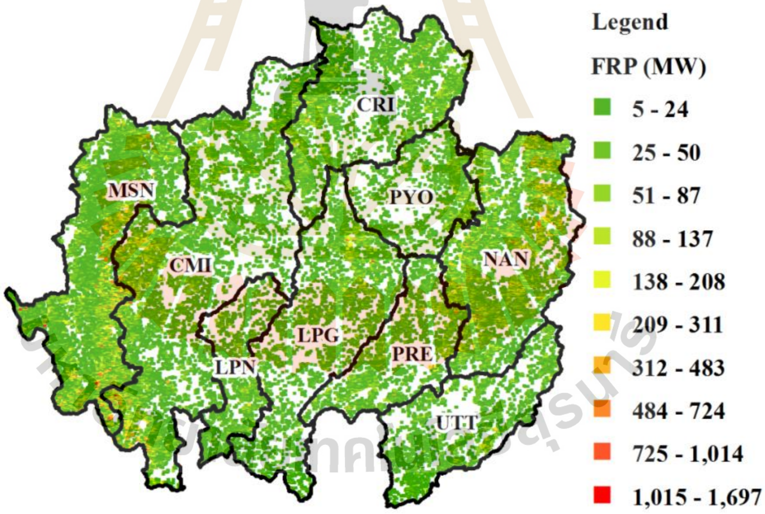

Figure 4.23 Distribution of fire radiative power from MODIS hotspot Upper Northern of Thailand between 2010 and 2014.

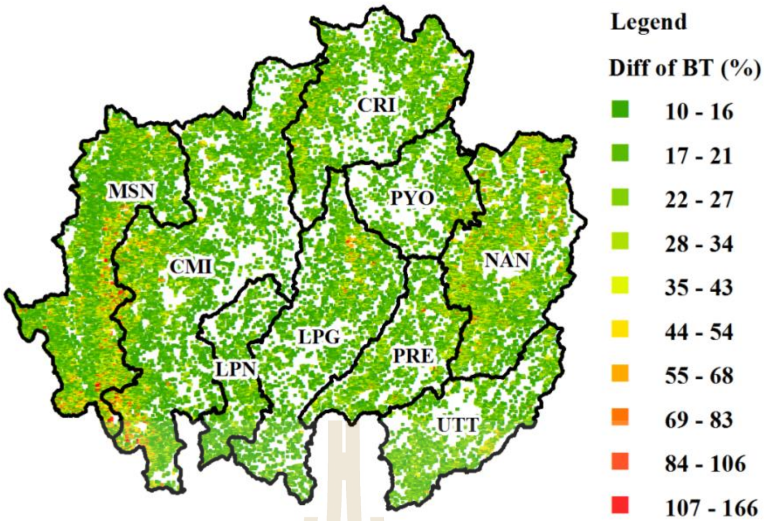

Figure 4.24 Distribution of difference of brightness temperature from MODIS hotspot Upper Northern of Thailand between 2010 and 2014.

For hotspot MODIS accuracy assessment, four selected Landsat 8 data: two scenes LC81300472014088, Path 130 and Row 47 dated on 13 and 29 March 2014 and two scenes LC81310472014079, Path 131 and Row 047 acquired on 4 and 20 March 2014, which represented fire occurrence, were here used to assess accuracy using visual interpretation with ancillary data and fire record by ground survey of RFD. Herewith, there were 882 MODIS hotspot points located over two scenes LC81300472014088 of Landsat 8 data and fire record by ground survey of RFD was 123 points. Likewise there were 1,554 MODIS hotspot points situated over two scenes LC81310472014079 of Landsat 8 data and ground fire record of RFD was 194 points. Distribution of hotspots over Landsat data is presented in Figure 4.25 while distribution of fire record by ground survey of RFD over two Landsat scenes is shown in Figure 4.26. An example of ground fire record and its attribute is shown in Figure 4.27.

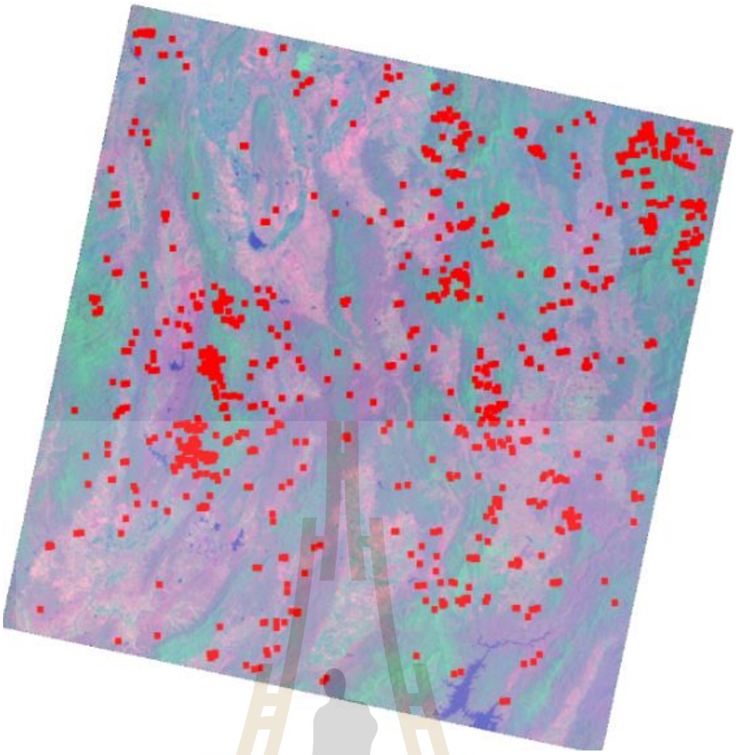

(a)

(b)

Figure 4.25 Distribution of hotspot over Landsat 8 image (a) Scene LC81300472014 088 and (b) scene LC81310472014079.

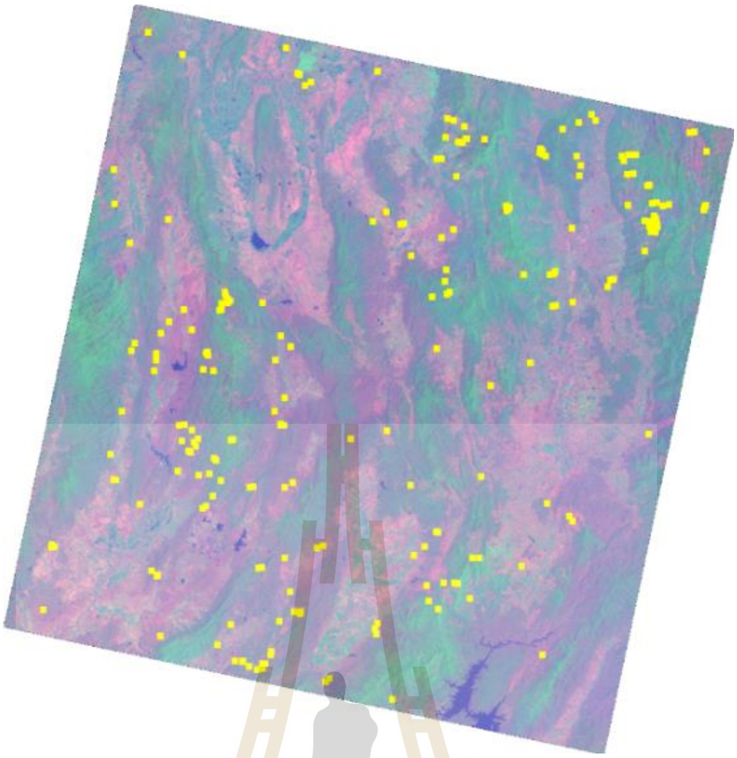

(a)

(b)

Figure 4.26 Distribution of fire record by ground survey of RFD over Landsat 8 image (a) Scene LC81300472014088 and (b) scene LC81310472014079.

l survey point 2014

Shape	DATE	X	Y	BAN	MOO	TAMBON	AMPHOE	PROVINCE	DAM_RAI
Point	5 กุมภาพันธ์ 2557	496399	1978459	แม่ตืน	3	แม่ตืน	ลี้	ลำพูน	2
Point	6 มีนาคม 2557	590802	2225311	ปงอ้อ	11	แม่จัน	แม่จัน	เชียงราย	10
Point	3 กุมภาพันธ์ 2557	632399	2103293	ดอนชัย	11	ปง	ปง	พะเยา	5
Point	22 มกราคม 2557	555127	2037286	นิคมพัฒนาตนเอง	6	นิคมพัฒนา	เมืองลำปาง	ลำปาง	8
Point	3 มีนาคม 2557	699960	1964084	ห้วยโป่ง	1	ห้วยมุ่น	น้ำปาด	อุตรดิตถ์	8
Point	25 กุมภาพันธ์ 2557	384756	2026599	ท่าผาปุ้ม	8	ท่าผาปุ้ม	แม่ลาน้อย	แม่ฮ่องสอน	2
Point	2 กุมภาพันธ์ 2557	596333	1969631	บ่อแก้ว	10	ไทรย้อย	เด่นชัย	แพร่	1
Point	26 กุมภาพันธ์ 2557	660552	2048616	ห้วยน้ำอุ่น	11	อ่ายนาไลย	เวียงสา	น่าน	10
Point	6 มีนาคม 2557	416640	1973700	อูตูม	6	นาเกียน	อมก๋อย	เชียงใหม่	2
Point	5 กุมภาพันธ์ 2557	497458	1978569	แม่ตืน	3	แม่ตืน	ลี้	ลำพูน	1
Point	16 มีนาคม 2557	632501	2244968	ไร่	7	แม่เงิน	เชียงแสน	เชียงราย	5
Point	3 กุมภาพันธ์ 2557	659967	2140813	น้ำต้ม	5	ผาช้างน้อย	ผาช้างน้อย	พะเยา	8
Point	20 มกราคม 2557	556076	2037732	นิคมพัฒนาตนเอง	6	นิคมพัฒนา	เมืองลำปาง	ลำปาง	5
Point	3 มีนาคม 2557	680446	1975630	ปากห้วยแค	5	เด่นเหล็ก	น้ำปาด	อุตรดิตถ์	20

Figure 4.27 An example of fire record and its attribute by ground survey of RFD.

For accuracy assessment of MODIS hotspots which were separated into 2 groups (true hotspot and false hotspot) based on visual interpretation with ancillary data, i.e. land use data of LDD and fire record of RFD revealed that in scene LC81300472014088 true hotspot was 865 points, false hotspot was 17 points and the percentage of true hotspot was 98.07% (Figure 4.28). Meanwhile true hotspot was 1,515 points, false hotspot was 39 points and the percentage of true hotspot was 97.49% in the scene LC81310472014079 as shown in Figure 4.29. An example of visual interpretation for accuracy assessment is presented in Figure 4.30. Validation of true and false MODIS hotspot by visual interpretation and fire record by ground survey of RFD is again summarized in Table 4.23.

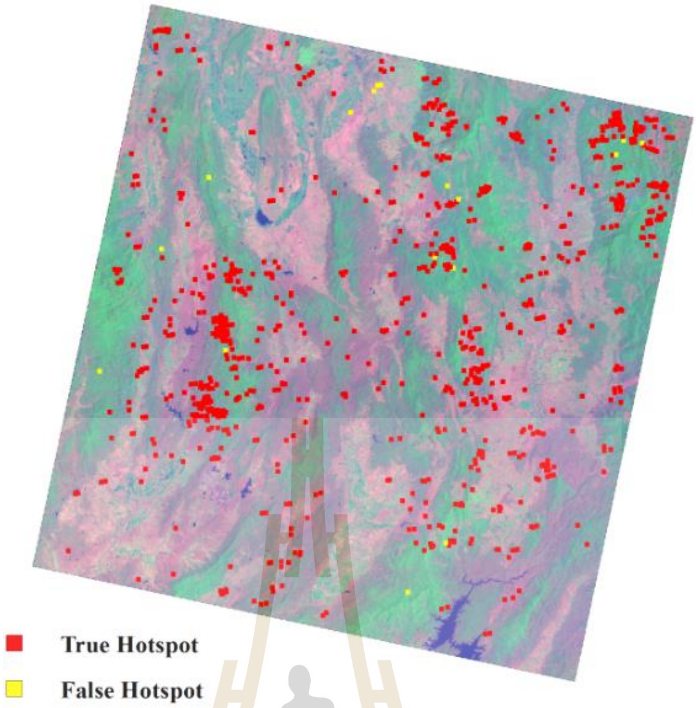

Figure 4.28 Distribution true and False MODIS hotspot over Landsat image scene, LC81300472014088.

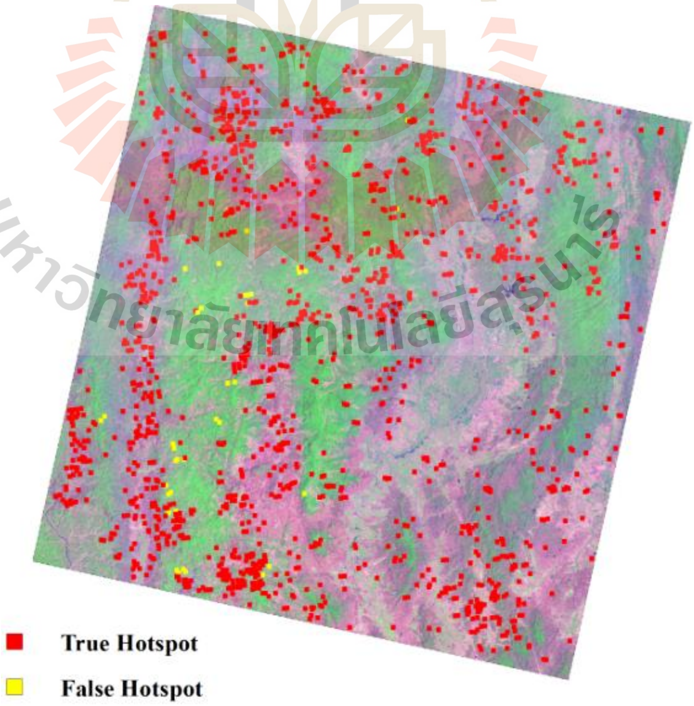

Figure 4.29 Distribution true and False MODIS hotspot over Landsat image scene, LC8 1310472014079.

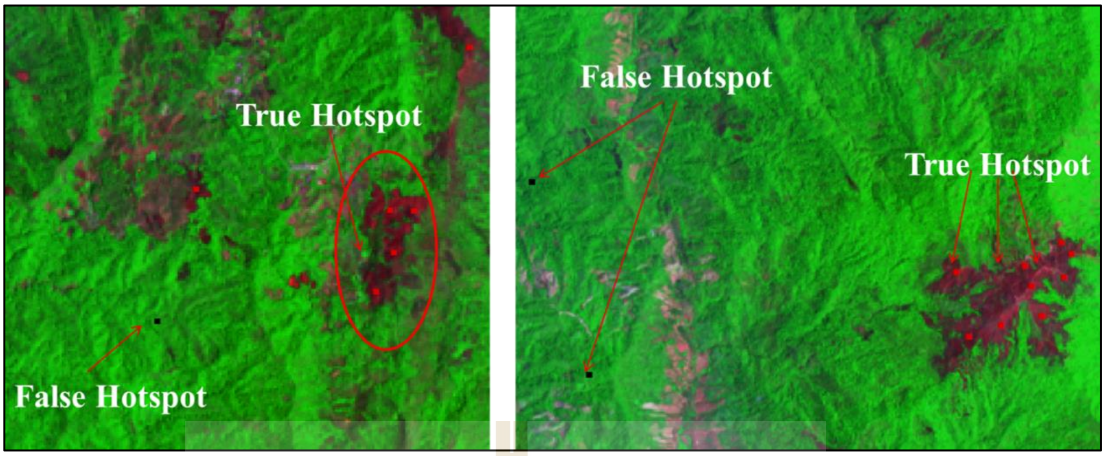

Figure 4.30 An example of MODIS hotspot validation by visual interpretation over Landsat data as true hotspot (red colored point) and false hotspot (yellow colored point) in various locations.

Table 4.23 Summary of accuracy assessment of MODIS hotspot.

Landsat scene	True Hotspot	False Hotspot	True Hotspot percentage
LC81300472014088	865	17	98.07
LC81310472014079	1,515	39	97.49

As results, it shows that the finding corresponds with the study of Tanpipat, Honda, and Nuchaiya (2009) who validated the MODIS hotspot data from year 2007, 2008 and 2009 in protected forest areas of national parks and wildlife sanctuaries in three represented region (North, Upper South and East) of Thailand by using both ground and aerial field surveys. The study found high accuracy of 91.84%, 95.60%, and 97.53% for the 2007, 2008, and 2009 in fire seasons, respectively.

4.3.2 Fire detection based on MODIS hotspot with decision tree classification

To construct of MODIS hotspot data with decision tree classification, 800 sampling points (previous 16 days) over Landsat 8 scene LC81300472014088 were here randomly selected and joined with 6 types of factor combination from 13 factors (elevation, slope, NDVI, distance from stream, distance from water body, distance from road, distance from village, distance from fire ground survey, distance from agricultural area, distance from shifting cultivation, distance from evergreen forest, distance from deciduous forest, and distance from degraded forest) as shown in Figure 4.31 and then created decision tree with CRT algorithm under SPSS statistic software.

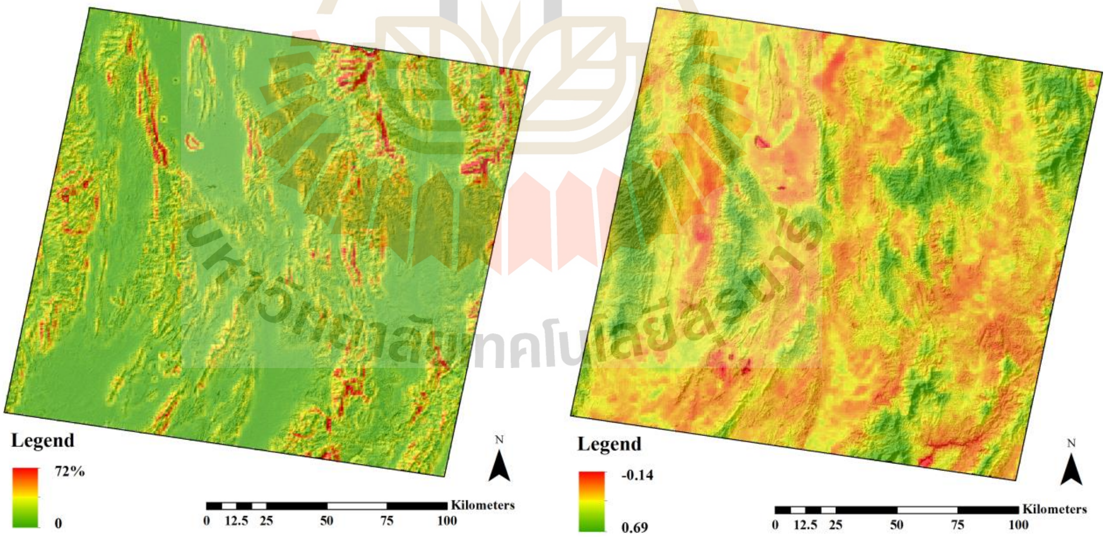

Slope NDVI

Figure 4.31 Biophysical factor maps.

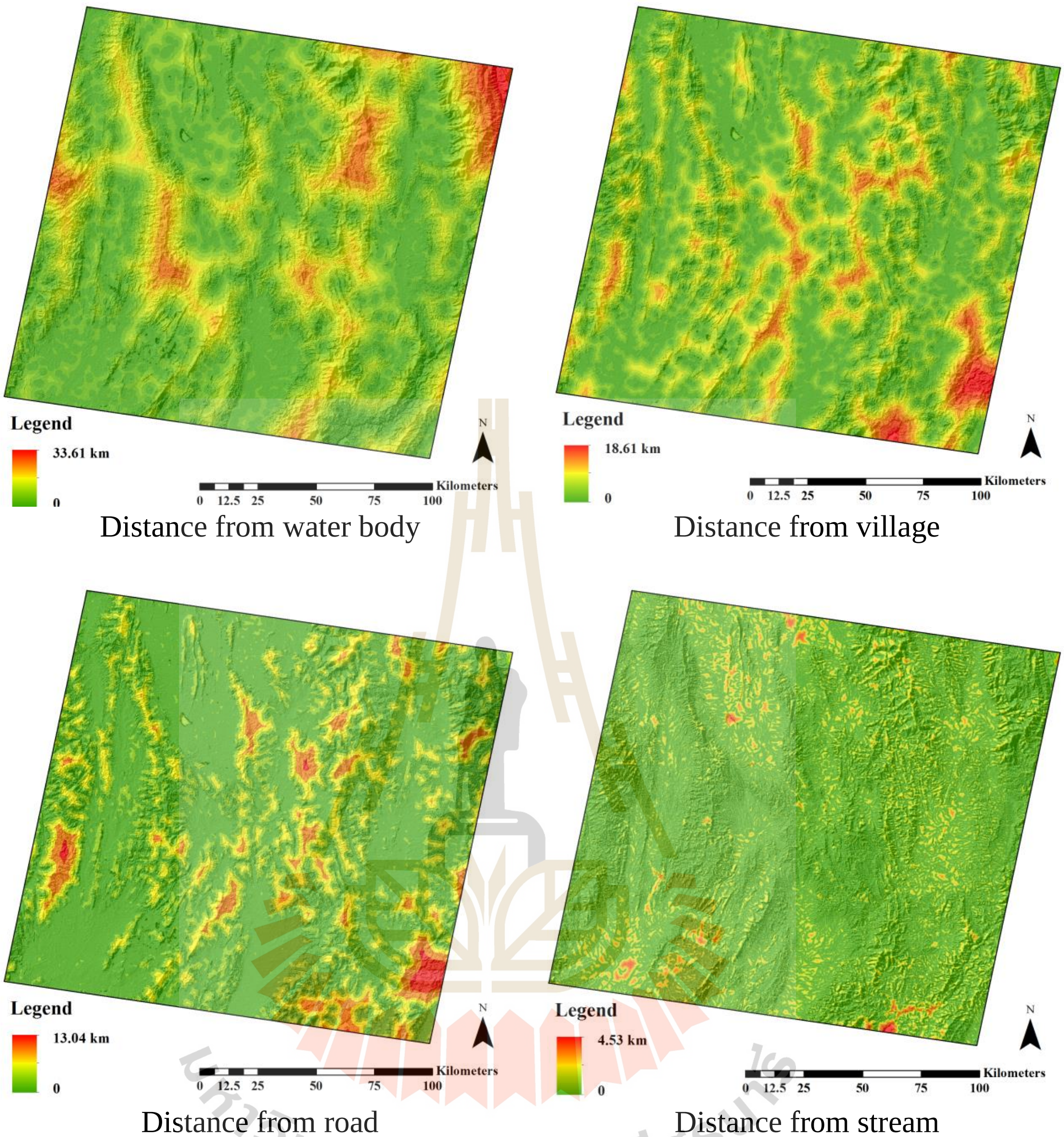

Figure 4.31 (Continued) Biophysical factor maps.

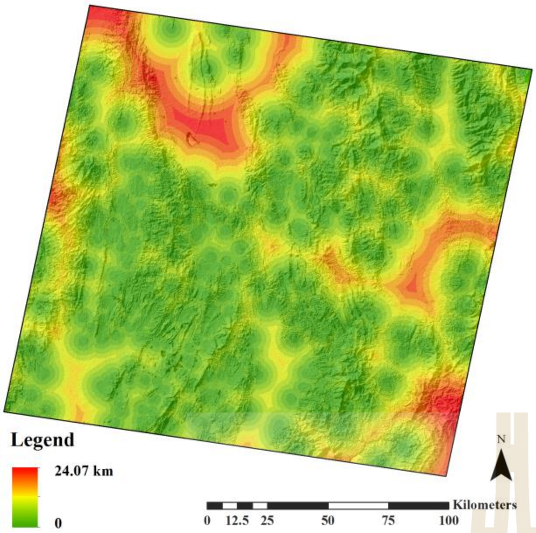

Distance from fire ground survey

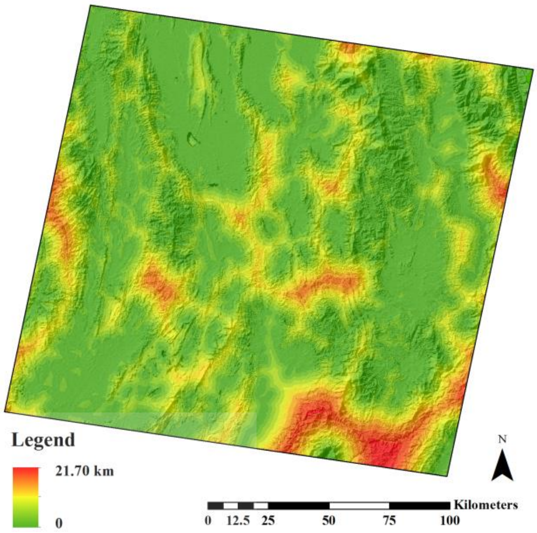

Distance from agricultural area

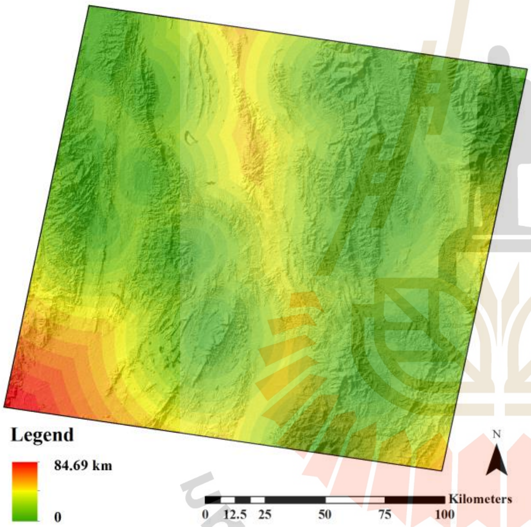

Distance from shifting cultivation

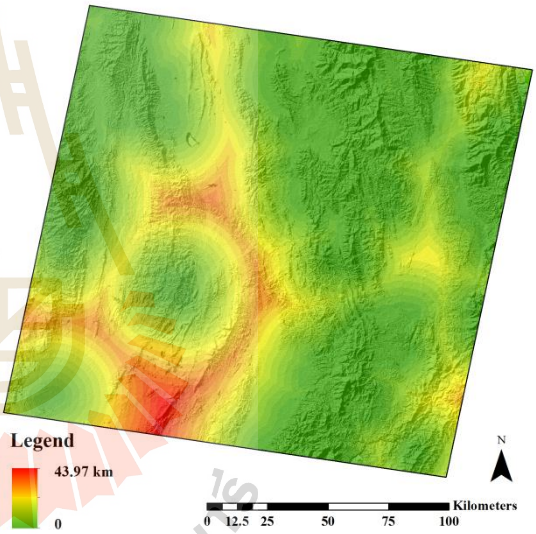

Distance from evergreen forest

Figure 4.31 (Continued) Biophysical factor maps.

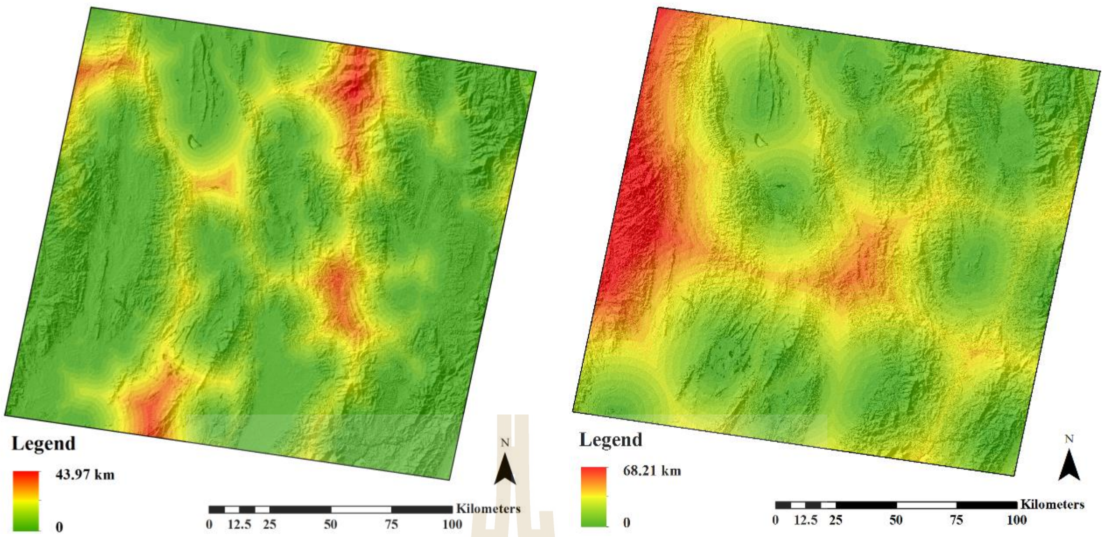

Distance from deciduous forest   Distance from degrade forest

Figure 4.31 (Continued) Biophysical factor maps.

The result based on 800 sampling hotspot points shows that decision tree with three biophysical factors include (1) distance from fire ground survey, (2) elevation and (3) slope can provide the highest overall accuracy at 71.00%. The derived decision tree structure for true and false MODIS hotspot of this combination is presented in Figure 4.32. The final criteria for true and false MODIS hotspot detection are as follows:

IF Distance from fire ground survey ≤ 1,053.42 (Node 3), OR

IF Distance from fire ground survey ≤ 2,538.24 AND Distance from fire ground survey > 1,053.42 (Node 4), OR

IF Distance from fire ground survey > 2,538.24 AND Elevation > 729.50 (Node 6),

THEN, they are True MODIS hotspot.

OTHERWISE,

IF Distance from fire ground survey > 9,527.83 AND Elevation ≤ 729.50 (Node 8), OR

IF Distance from fire ground survey > 2,538.24 AND Distance from fire ground survey ≤ 9,527.83 AND Elevation ≤ 729.50 AND Slope ≤ 1.78 (Node 9), OR

IF Distance from fire ground survey > 2,538.24 AND Distance from fire ground survey ≤ 9,527.83 AND Elevation ≤ 729.50 AND Slope > 1.78 (Node 10),

THEN, they are false MODIS hotspot.

Furthermore, simple decision tree with any biophysical factor (Type I) provided overall accuracy varied between 50% and 67.88%. Meanwhile decision tree with proximity factors and all 13 factors (Type V and VI) provides overall accuracy at 66.38% and 70.63%, respectively (Table 4.24).

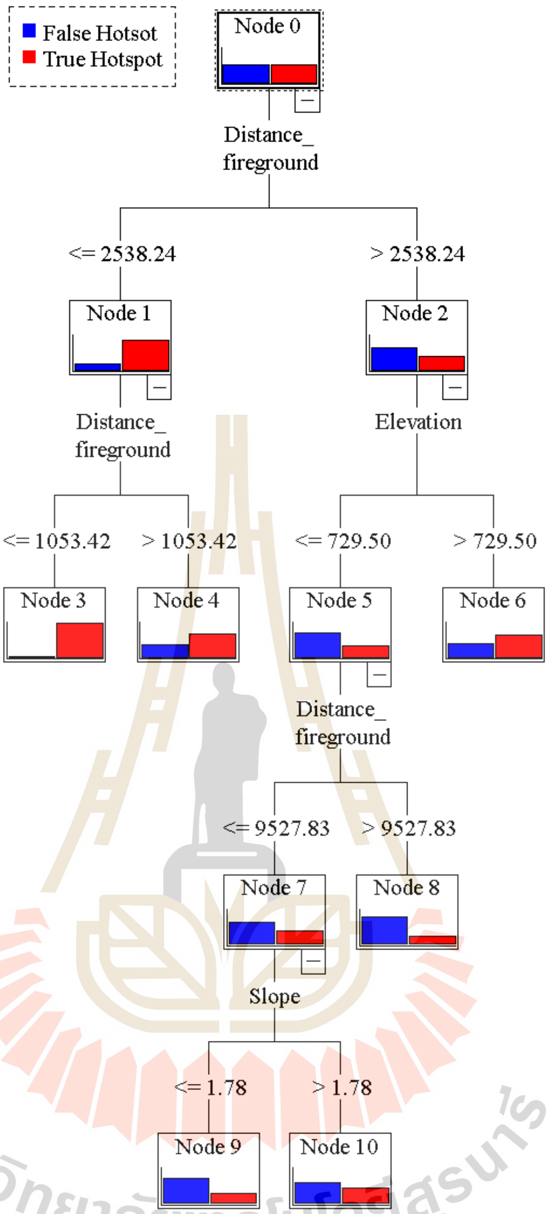

Figure 4.32 Optimum decision tree to classify true and false MODIS hotspot using distance from fire ground survey, elevation and slope.

Table 4.24 Overall accuracy comparison by various combination biophysical factors of decision tree classification.

Type	Biophysical factor and its combination	Total pixel	Correct fire hit	Fire missing	False alarm	Correct non-fire hit	False alarm rate	fire detection rate	Overall Accuracy	Kappa
	Elevation	800	232	168	142	258	35.50	58.00	61.25	22.50
	Slope	800	324	76	272	128	68.00	81.00	56.50	13.00
	NDVI	800	141	259	108	292	27.00	35.25	54.13	8.25
	Distance from water body	800	231	169	133	267	33.25	57.75	62.25	24.50
	Distance from village	800	270	130	215	185	53.75	67.50	56.88	13.75
	Distance from road	800	263	137	209	191	52.25	65.75	56.75	13.50
I	Distance from stream	800	-	400	-	400	-	-	50.00	-
	Distance from fire ground survey	800	214	186	71	329	17.75	53.50	67.88	35.75
	Distance from agricultural area	800	101	299	77	323	19.25	25.25	53.00	6.00
	Distance from shifting cultivation	800	289	111	205	195	51.25	72.25	60.50	21.00
	Distance from evergreen forest	800	-	400	-	400	-	-	50.00	-
	Distance from deciduous forest	800	-	400	-	400	-	-	50.00	-
	Distance from degrade forest	800	81	319	54	346	13.50	20.25	53.38	6.75
II	Elevation and slope	800	232	168	142	258	35.50	58.00	61.25	22.50
III	Elevation, slope, and NDVI	800	164	236	68	332	17.00	41.00	62.00	24.00
IV	Elevation, slope, and distance from fire ground survey	800	257	143	89	311	22.25	64.25	71.00	42.00
V	Proximity factors	800	224	176	93	307	23.25	56.00	66.38	32.75
VI	All 13 factors	800	285	115	120	280	30.00	71.25	70.63	41.25

By applying the criteria of the best decision tree of three factors (Type IV) with MODIS hotspot over Landsat 8 scene LC81300472014088 and LC81310472014079, it was found that overall accuracy based on visual interpretation with ancillary data, i.e. land use data of LDD and fire record of RFD was 62.47% and 63.84%, respectively as results shown in Figure 4.33 and Figure 4.34, respectively.

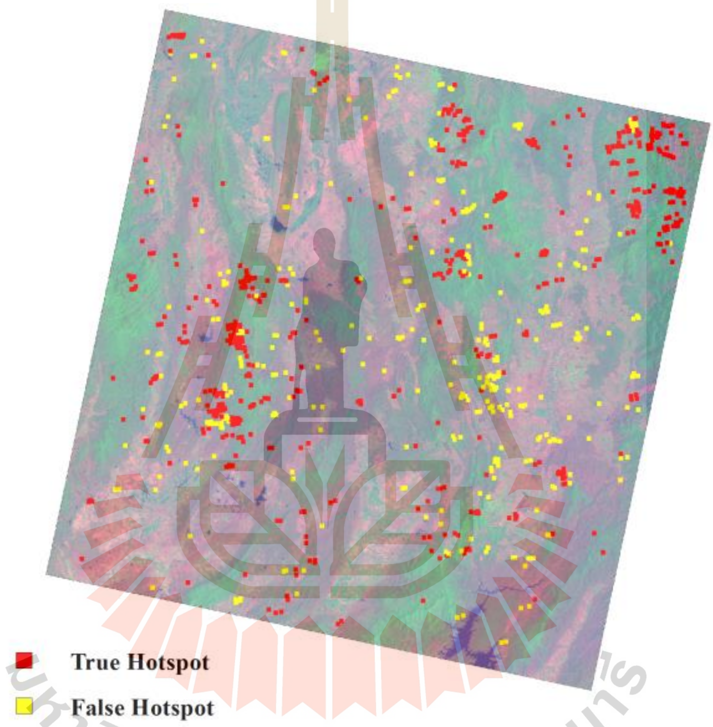

Figure 4.33 True and false hotspot classification using decision tree with three biophysical factors of MODIS hotspot over Landsat scene LC8130047 2014088.

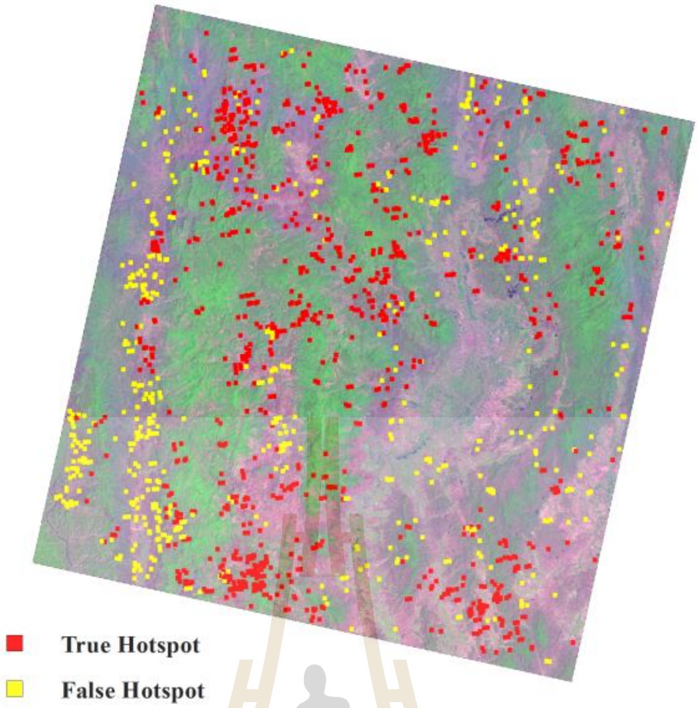

Figure 4.34 True and false hotspot classification using decision tree with three biophysical factors of MODIS hotspot over Landsat scene LC8 1310472014079.

4.3.3 Optimal fire detection algorithm

Based on accuracy assessment (overall accuracy) of two approaches for fire detection algorithm identification in the previous sections (4.4.1 and 4.4.2), it can be here concluded that hotspot (MOD14/MYD14 algorithm) of MODIS was an optimal fire detection algorithm for Upper Northern region of Thailand.

CHAPTER V

CONCLUSION AND RECOMMENDATIONS

Under this chapter, two main results which were reported according to objectives in the study including (1) to identify an optimal top three spectral indices for burned area evaluation and (2) to identify the algorithms for burned area and fire detection using MODIS and Landsat data are here separately concluded and recommended for future research and development.

5.1 Conclusions

5.1.1 Optimal top three spectral indices for burned area evaluation

To identify an optimal top three spectral indices for burned area evaluation, MODIS data were firstly used to calculate spectral indices, (NDVI, MSAVI, BAI, BAIM, NBR, GEMI, MIRBI, NDSWIR, NDWI, NMDI, SMI, and CSI) and their values were then compared with the extracted burned area and its severity from Landsat data using deviance value of the ordinal logistics regression. The study found that optimal top three of MODIS spectral indices for burned area detection were CSI, BAI, and NDSWIR. These spectral indices from MODIS Level 1B data show top three best goodness of fit with burn severity classes deriving from 12 scenes of Landsat 5 and 8 data.

5.1.2 Optimal burned area detection algorithm identification

For optimal burned area detection algorithm identification, MODIS data in 2014 were firstly used to extract burned area using threshold technique and decision tree classification with top three MODIS spectral indices and to assess accuracy with the burned areas from Landsat data extraction using BAMS. Using thresholding technique, BAI spectral index of MODIS Level 1B data (Scene 2014064) with threshold value between 104.7674 and 124.7674 can provide the best result for burned area extraction with overall accuracy between 97.8855% and 98.1059%, Kappa hat coefficient between 22.7512% and 20.9283%, burned area detection rate between 18.3929% and 14.6429%, and false alarm rate between 0.6667% and 0.3740%. Meanwhile, decision tree classification with combination BAI and CSI spectral indices can provide the best result for burned area extraction with overall accuracy at 98.3390%, Kappa hat coefficient at 23.6969%, burn detection rate at 14.8214%, and false alarm rate at 0.1399%. In addition, result of pairwise Z-test between Kappa hat coefficient between thresholding technique and decision tree classification showed statistically significantly at 90, 95, and 100% of confidence level.

Furthermore, the derived threshold value of thresholding technique and criteria of decision tree classification were reapplied for algorithm validation with other MODIS Level 1B data (Scene 2014080). It was found that thresholding technique provided overall accuracy at 97.2945%, burned area detection rate at 30.8458%, false alarm rate at 1.8411%, and Kappa hat coefficient at 21.3704%. At the same time, decision tree classification provided overall accuracy at 98.7479%, burned area detection rate at 11.9403%, false alarm rate at 0.1230%, and Kappa hat coefficient at 19.3069%.

As results of accuracy assessment and validation, it can be concluded that thresholding technique with BAI of MODIS Level 1B spectral index was an optimum algorithm of burned area detection.

5.1.3 Optimal fire detection algorithm identification

For identify an optimal fire detection algorithm, MODIS hotspot data in 2014 and the MODIS hotspot data with decision tree classification with 13 factors were here examined and evaluated accuracy. The results showed that overall accuracy of MODIS hotspot with original algorithm over Landsat scene LC81300472014088 and LC81310472014079 were 98.07% and 97.49%, respectively. Meanwhile, MODIS hotspot with the best decision tree classification using three criteria (distance from fire ground survey, elevation, and slope) over two Landsat scene (LC81300472014088 and LC81310472014079) can provide overall accuracy between 62.47 and 63.84%. Therefore, it can be concluded that hotspot (MOD14/MYD14 algorithm) of MODIS was an optimal fire detection algorithm.

In conclusion, BAI of MODIS Level 1B spectral index can be used to estimate burned area while MODIS hotspot data can be daily applied to monitor forest fire occurrence as routine work of the concerned agencies.

5.2 Recommendations

Even though this study had been fulfilled the objectives of the study as presented, the possibly expected recommendations could be made for further studies as follows:

(1) The burned area extraction by BAMS, which is firstly extract decision tree structure for burned area from pre- and post- fire Landsat data with “AND” logical operation based on spectral indices (BAIM, GEMI, MIRBI, NBR, and NDVI) from training area, can provide acceptable results in this study. According to RFD ground fire records during fire season beween February and April 2014, percentage of true hit ground fire survey points over burned areas of all Landsat scenes varied between 79.58% and 94.06%. Therefore, burned area extraction using BAMS should be annually implemented to assess effected forest fire on natural forest of the whole country by responsible agencies (DNP and RFD).

(2) Optimum top three MODIS spectral indices were identified based on deviance values using ordinal logistics regression between burn severity classes as dependent variable and the selected 12 MODIS spectral indices as independent variables in this study. Herein, burn severity classes was systematic assigned based burned area extraction from Landsat data using BAMS due to the limitation of ground based burn severity classes. Therefore, new approach on optimum top three MODIS spectral indices identification for burned area extraction should be investigated and examined in the near future, such as separability index suggested by Kaufman and Remer (1994).

(3) An optimum burned area detection algorithm using thresholding technique with BAI of MODIS Level 1B spectral index should be examined in another area or region for verification and validation its algorithm. The derived result will be useful to extract burned area at low spatial resolution and very high temporal resolution of the whole country.

(4) In this study, it was found that MODIS hotspot with MOD14/MYD14 algorithm can provide overall accuracy more than 97.49%. Consequently, MODIS hotspot data can be efficiently used as dependent variable to integrate with influential factor on forest fire as independent variables and geospatial model to predict forest fire susceptibility/hazard/risk for forest fire management, mitigation and prevention at provincial level in the near future. The recommended geospatial model might be included Binary logistics model, Frequency ratio model, etc.

REFERENCES

REFERENCES

Akaakara, S. (2000). **Forest Fire Control in Thailand.** Bangkok, Thailand: Forest Fire Control Office, Royal Forest Department.

Aragao, L., and Shimabukuro, Y. (2010) The Incidence of Fire in Amazonian Forests with Implications for REDD. **Science.** 328: 1275-1278. (Quoted by Müller and Suess, 2011)

Barbosa, P., Kucera, J., Strobl, P., Vogt, P., Camia, A., and San-Miguel-Ayanz, J. (2006). European Forest Fire Information System (EFFIS)—rapid damage assessment: Appraisal of burnt area maps in southern Europe using MODIS data (2003-2005). **Forest Ecology and Management.** 234: S218. doi: 10.1016/j.foreco.2006. 08.245.

Bastarrika, A. (2014). **Burned Area Mapping Software (BAMS) preliminary documentation.** University of Basque Country.

Bastarrika, A., Alvarado, M., Artano, K., Martinez, Mesanza, M., Torre, L., Ramo, R., and Chuvieco, E. (2014). BAMS: A Tool for Supervised Burned Area Mapping Using Landsat Data. **Remote Sensing of Environment.** 6(12): 12360-12380. doi:10.3390/rs61212360.

Chuvieco, E., Englefield, P., Trishchenko, A. P., and Luo, Y. (2008). Generation of long time series of burn area maps of the boreal forest from NOAA-AVHRR composite data. **Remote Sensing of Environment.** 112(5): 2381-2396. doi: 10.101 6/j.rse.2007.11.007.

Chuvieco, E., Martín, M. P., and Palacios, A. (2002). Assessment of different spectral indices in the red-near-infrared spectral domain for burned land discrimination. **International Journal of Remote Sensing.** 23(23): 5103-5110. doi: 10.1080/ 01431160210153129.

Congalton, R. G., and Green, K. (2008). **Assessing the Accuracy of Remotely Sensed Data: Principles and Practices.** (2 ed.). Boca Raton, FL: RC Press, Taylor and Francis Group.

Davies, D. K., Ilavajhala, S., Wong, M. M., and Justice, C. O. (2009). Fire Information for Resource Management System: Archiving and Distributing MODIS Active Fire Data. **IEEE Transactions on Geoscience and Remote Sensing.** 47(1): 72-79.

Department of National Park Wildlife and Plant Conservation: DNP. (2015). **Statistics of forest fires in Thailand from 2010 to 2014.** (online). Available : http://www.dnp.go.th/forestfire/2557/Stat2553-2557.xls.

Department of Provincial Administration. (2014). **Demographics and household in 2013 to 2014.** (online). Available : http://stat.dopa.go.th/stat/statnew/upstat_age.php.

Gao, B. (1996). NDWI-a normalized difference water index for remote sensing of vegetation liquid water from space. **Remote Sensing of Environment.** 58(3): 257-266.

Gerard, F., Plummer, S., Wadsworth, R., Sanfeliu, A. F., Iliffe, L., and Balzter, H., (2003). Forest fire scar detection in the boreal forest with multitemporal SPOT-VEGETATION data. **IEEE Transactions on Geoscience and Remote Sensing.** 41(11): 2575−2585. (Quoted by George et al., 2006)

George, C., Rowland, C., Gerard, F., and Balzter, H. (2006). Retrospective mapping of burnt areas in Central Siberia using a modification of the normalised difference water index. **Remote Sensing of Environment.** 104(3): 346-359. doi: 10.1016/j.rse.2006.05.015.

Giglio, L. (2010). **MODIS Collection 5 Active Fire Product User's Guide Version 2.4: Science Systems and Applications.** University of Maryland, Department of Geography.

Giglio, L., Csiszar, I., and Justice, C. O. (2006). Global distribution and seasonality of active fires as observed with the Terra and Aqua Moderate Resolution Imaging Spectroradiometer (MODIS) sensors. **Journal of Geophysical Research.** 111(G2): doi: 10.1029/2005jg000142.

Giglio, L., Descloitres, J., Justice, C. O. and Kaufman, Y. (2003). An Enhanced Contextual Fire Detection Algorithm for MODIS. **Remote Sensing of Environment.** 87(2-3): 273-282. doi: 10.1016/s0034-4257(03)00184-6.

Giglio, L., Werf, G. R. v. d., Randerson, J. T., Collatz, G. J., and Kasibhatla, P. (2006). Global estimation of burned area using MODIS active fire observations. **Atmospheric Chemistry and Physics.** 6: 957-974.

Gomarasca, M. A. (2004). **Basics of Geomatics.** Italy: Associazione Italiana di Telerilevamento.

Harris, S., Veraverbeke, S., and Hook, S. (2011). Evaluating Spectral Indices for Assessing Fire Severity in Chaparral Ecosystems (Southern California) Using MODIS/ASTER (MASTER) Airborne Simulator Data. **Remote Sensing.** 3(11): 2403-2419. doi: 10.3390/rs3112403.

Hawbaker, T. J., Radeloff, V. C., Syphard, A. D., Zhu, Z., and Stewart, S. I. (2008). Detection rates of the MODIS active fire product in the United States. **Remote Sensing of Environment.** 112(5): 2656-2664. doi: 10.1016/j.rse.2007.12.008.

Holden, Z. A., Smith, A. M. S., Morgan, P., Rollins, M. G., and Gessler, P. E. (2005). Evaluation of novel thermally enhanced spectral indices for mapping fire perimeters and comparisons with fire atlas data. **International Journal of Remote Sensing.** 26(21): 4801-4808. doi: 10.1080/01431160 500239008.

Hosmer, D., and Lemeshow, S. (2000). **Applied Logistic Regression.** New York, USA: Wiley.

Huete, A. R. (1988). A soil-adjusted vegetation index (SAVI). **Remote Sensing of Environment.** 25(3): 295-309. doi: 10.1016/0034-4257(88)90106-x.

Huete, A. R., Didan, K., Miura, T., Rodriguez, E. P., Gao, X., and Ferreira, L. G. (2002). Overview of the radiometric and biophysical performance of the MODIS vegetation indices. **Remote Sensing of Environment**. 83: 195-213.

Jacob, D. J. (1999): **Introduction to atmospheric chemistry.** (Princeton University Press: Princeton). (Quoted by Pereira et al., 2011)

Jiang, Z., Huete, A., Didan, K., and Miura, T. (2008). Development of a two-band enhanced vegetation index without a blue band. **Remote Sensing of Environment.** 112(10): 3833-3845. doi: 10.1016/j.rse. 2008.06.006.

Justice, C. O., Giglio, L., Boschetti, L., Roy, D., Csiszar, I., Morisette, J., and Kaufman, Y. (2006). **Algorithm Technical Background Document: MODIS fire product.** (online). Available : http://modis.gsfc.nasa.gov/data/ atbd/atbd_ mod14.pdf.

Justice, C. O., Giglio, L., Korontzi, S., Owensa, J., Morisette, J. T., Roy, D., Descloitres, J., Alleaume, S., Petitcolin, F., and Kaufman, Y. (2002). The MODIS fire products. **Remote Sensing of Environment.** 83: 244-262.

Kaufman, Y., and Remer, L. (1994). Detection of forests using Mid-IR reflectance: An application for aerosol studies. **IEEE Transactions on Geoscience and Remote Sensing.** 32: 672-683.

Kaufman, Y., Justice, C., Flynn, L., Kendall, J., Prins, E., Ward, D. E., Menzel, P., and Setzer, A. (1998). Monitoring Global Fires from EOS-MODIS. **Journal of Geophysical Research.** 103: 32215-32338.

Key, C., and Benson, N. (2005). Landscape assessment: Ground measure of severity; The Composite Burn Index, and remote sensing of severity, the Normalized Burn Index. In D. Lutes, R. Keane, J. Caratti, C. Key, N. Benson, S. Sutherland and L. Gangi (Eds.), **FIREMON: Fire Effects Monitoring and Inventory System.** USA: Rocky Mountains Research Station, USDA Forest Service: Fort Collins.

Koutsias, N., Pleniou, M., Nioti, F., and Mallinis, G. (2010). Spectral signatures of burned surfaces: evidence from Hyperspectral Remote Sensing data. **Hyperspectral 2010 Workshop.** Frascat. Italy. (online). Available : earth.esa. int/workshops/hyperspectral.../p_koutsi.pdf.

Langner, A., and Siegert, F. (2009). Spatiotemporal fire occurrence in Borneo over a period of 10 years. **Global Change Biology.** 15(1): 48-62. doi: 10.1111/j. 1365-2486.2008.01828.x.

Lobert, J. M., and Warnatz, J. (1993). Fires Emissions from the combustion process in vegetation. In Crutzen and J. Goldammer (Eds.), **Fire in the Environment: the Ecological, Atmospheric, and Climatic Importance of Vegetation.** UK: John Wiley and Sons.

Maeda, E. E., Formaggio, A. R., Shimabukuro, Y. E., Arcoverde, G. F. B., and Hansen, M. C. (2009). Predicting forest fire in the Brazilian Amazon using MODIS imagery and artificial neural networks. **International Journal of Applied Earth Observation and Geoinformation.** 11(4): 265-272. doi: 10.1016/j.jag.2009. 03.003.

Martin, M. P. (1998). **Cartografía e inventario de incendios forestales en la Península Ibérica a partir de imágenes NOAA-AVHRR Departamento de Geografía.** Universidad de Alcalá. (Quoted by Chuvieco et al., 2008)

Martin, P., Gómez, I., and Chuvieco, E. (2005). **Performance of a burned-area index (BAIM) for mapping Mediterranean burned scars from MODIS data.** Paper presented at the Proceedings of the 5th International Workshop on Remote Sensing and GIS Applications to Forest Fire Management: Fire Effects Assessment, Universidad de Zaragoza.

Miettinen, J., Langner, A., and Siegert, F. (2007) Burnt area estimation for the year 2005 in Borneo using multi-resolution satellite imagery. **International Journal of Wildland Fire.** 16: 45-53. (Quoted by Müller and Suess, 2011)

Müller, D., and Suess, S. (2011). **Can the MODIS active fire hotspots be used to monitor vegetation fires in the Lao PDR?** Climate Protection through Avoided Deforestation (CliPAD) programme, Deutsche Gesellschaft für Internationale Zusammenarbeit (GIZ).

NASA. (2012). **MODIS specifications.** (online). Available : http://modis.gsfc.nasa.gov/about/specifi cations.php.

NASA. (2013). **What does a MODIS hotspot/active fire detection mean on the ground?** (online). Available : https://earthdata.nasa.gov/faq.

NASA FIRMS. (2015). **MODIS Active Fire Detections Data set.** (online). Available : http://earthdata.nasa.gov/firms.

National Statistical Office. (2014). **Statistics of Meteorological Department 2014,** (online). Available : https://www.m-society.go.th/ewt_news.php?nid=14571.

Pereira, J. M. C. (1999). A comparative evaluation of NOAA-AVHRR Vegetation Indexes for burned surface detection and mapping. **IEEE Transactions on Geoscience and Remote Sensing.** 37: 217-226.

Pereira, J. M. C., Mota, B., Calado, T., Oliva, P., and González-Alonso, F. (2011). **Algorithm Theoretical Basis Document Volume II-BA Algorithm Development.** (online). Available : http://www.esa-fire-cci.org/webfm_send/158.

Pinty, B., and Verstraete, M. (1992). GEMI-A nonlinear index to monitor global vegetation from satellites. **Vegetatio.** 101: 15-20.

Qi, J., Chehbounidi, A., Huete, A., Kerr, Y., and Sorooshian, S. (1994). A modified soil adjusted vegetation index. **Remote Sensing of Environment.** 48: 119-126.

Qian, Y., Yan, G., Duan, S., and Kong, X. (2009). A Contextual Fire Detection Algorithm for Simulated HJ-1B Imagery. **Sensors (Basel).** 9(2): 961-979. doi: 10.3390/s90200961.

Roy, D. P., Jin, Y., Lewis, P. E., Justice, C. O. (2005). Prototyping a global algorithm for systematic fire-affected area mapping using MODIS time series data. **Remote Sensing of Environment.** 97: 137-162.

Ruthamnong, S. (2010). **Algorithm Development for Identifying False Hotspot.** Master of Sciences, Narasuan University, Thailand.

Schepers, L., Haest, B., Veraverbeke, S., Spanhove, T., Borre. J. V., Goossens, R., (2014). Burned Area Detection and Burn Severity Assessment of a Heathland Fire in Belgium Using Airborne Imaging Spectroscopy (APEX). **Remote Sensing of Environment.** 6: 1803-1826. doi: 10.3390/rs6031803.

Schroeder, W., Prins, E., Giglio, L., Csiszar, I., Schmidt, C., Morisette, J., and Morton, D. (2008). Validation of GOES and MODIS active fire detection products using ASTER and ETM+ data. **Remote Sensing of Environment.** 112(5): 2711-2726. doi: 10.1016/j.rse.2008.01.005.

Smith, A. M. S., Drake, N. A., Wooster, M. J., Hudak, A. T., Holden, Z. A., and Gibbons, C. J. (2007). Production of Landsat ETM+ reference imagery of burned areas within Southern African savannahs: comparison of methods and application to MODIS. **International Journal of Remote Sensing.** 28(12): 2753-2775. doi: 10.1080/01431160600954704.

Tanpipat, V., Honda, K., and Nuchaiya, P. (2009). MODIS Hotspot Validation over Thailand. **Remote Sensing.** 1(4): 1043-1054. doi: 10.3390/rs1041043.

Trigg, S., and Flasse, S. (2001). An evaluation of different bi-spectral spaces for discriminating burned shrub-savannah. **International Journal of Remote Sensing.** 22(13): 2641-2647. doi: 10.1080/ 01431160110053185.

Tucker, C. (1979). Red and photographic infrared linear combinations for monitoring vegetation. **Remote Sensing of Environment.** 8: 127-150.

Veraverbeke, S., Harris, S., and Hook, S. (2011). Evaluating spectral indices for burned area discrimination using MODIS/ASTER (MASTER) airborne simulator data. **Remote Sensing of Environment.** 115(10): 2702-2709. doi: 10.1016/j.rse.2011. 06.010.

Veraverbeke, S., Hook, S., and Hulley, G. (2012). An alternative spectral index for rapid fire severity assessments. **Remote Sensing of Environment.** 123: 72-80. doi: 10.1016/j.rse.2012.02.025.

Wang, L., Qu, J. J., and Hao, X. (2008). Forest fire detection using the normalized multi-band drought index (NMDI) with satellite measurements. **Agricultural and Forest Meteorology.** 148(11): 1767-1776. doi:10.1016/j.agrformet.2008. 06.005.

Wang, S. D., Miao, L. L., and Peng, G. X. (2012). An Improved Algorithm for Forest Fire Detection Using HJ Data. **Procedia Environmental Sciences.** 13: 140-150. doi:10.1016/j.proenv.2012.01.014.

Wikipedia. (2014). **Northern Thailand.** (online). Available : https://en.wikipedia. org/wiki/Northern_Thailand.

Yang, Skidmore, A. K., David R., Melick, Zhou, and Xu. (2006). Mapping non-wood forest product (matsutake mushrooms) using logistic regression and a GIS expert system. **Ecological Modeling**. 198(1-2): 208-218. doi:10.1016/j.ecol model.2006.04.01.

CURRICULUM VITAE

Name Suphatphong Ruthamnong

Date of Birth November 17, 1982

Place of Birth Chiang Rai, Thailand

Education

2007-2010 Master of Science (Space technology and Geo-informatics)

Naresuan University, Phitsanulok, Thailand

2001-2004 Bachelor of Science (Geography)

Chiang Mai University, Chiang Mai, Thailand

Working experiences

2006-present Lecturer at Kamphaeng Phet Rajabhat University.

2004-2006 GIS Analyst at Mappoint Asia (Thailand) Co Ltd.